Chapter 4
Modulation and Power Spectrum

Modulation is the process whereby message information is embedded into a radio frequency carrier. Such information can be transmitted in either the amplitude, frequency, or phase of the carrier, or a combination thereof, in either analog or digital format. Analog modulation schemes include amplitude modulation (AM) and frequency modulation (FM). Analog modulation schemes are still used today for legacy broadcast AM/FM radio and citizens band (CB) radio, but all other communication and broadcast systems now use digital modulation. Digital modulation schemes transmit information using a finite set of waveforms and have a number of advantages over their analog counterparts. Digital modulation is a natural choice for digital sources, e.g., computer communications. Source encoding or data compression techniques can reduce the required transmission bandwidth with a controlled amount of signal distortion. Digitally modulated waveforms are also more robust to channel impairments such as delay and Doppler spread, and co-channel and adjacent channel interference. Finally, encryption and multiplexing is easier with digital modulation schemes.

To achieve high spectral efficiency in wireless systems, signaling schemes are sought that provide power and bandwidth efficient communication. In an information theoretic sense, it is desirable to operate close to the Shannon capacity limit of a channel. This generally requires the use of error control coding along with a jointly designed encoder and modulator. However, this chapter only considers modulation schemes, while the subject of coding and coded modulation is considered in Chap. 8. The bandwidth efficiency of a modulation scheme indicates how much information is transmitted per channel use and is measured in units of bits per second per Hertz of bandwidth (bits/s/Hz). The power efficiency can be measured by the received signal-to-interference-plus-noise ratio (SINR) that is required to achieve reliable communication with a specified bandwidth efficiency in the presence of channel impairments such as delay spread and Doppler spread. In general, modulation techniques for spectrally efficient wireless systems should have the following properties:

- *Compact Power Density Spectrum:* To minimize the effect of adjacent channel interference, the power radiated into the adjacent band is often limited to be 60–80 dB below that in the desired band. This requires modulation techniques having a power spectrum characterized by a narrow main lobe and fast roll-off of side lobes.
- *Robust Communication:* Reliable communication must be achieved in the presence of delay and Doppler spread, adjacent and co-channel interference, and thermal noise. Modulation schemes that promote good power efficiency in the presence of channel impairments are desirable.
- *Envelope Properties:* Portable and mobile devices often employ power efficient nonlinear (Class-C) power amplifiers to minimize battery drain. However, amplifier nonlinearities will degrade the performance of modulation schemes that transmit information in the amplitude of the carrier and/or have a non-constant envelope. To obtain suitable performance, such modulation schemes require a less power efficient linear or a linearized power amplifier. Also, spectral shaping is usually performed prior to up-conversion and nonlinear amplification. To prevent the regrowth of spectral side lobes during nonlinear amplification, modulation schemes having a relatively constant envelope are desirable.

This chapter considers digital modulation techniques that are commonly found in wireless communication systems. Section 4.1 begins the chapter with a mathematical framework for bandpass modulated signals. Section 4.2 discusses Nyquist pulse shaping for ISI-free transmission. Sections 4.3, 4.4, 4.5, 4.6, 4.7, and 4.8 provide a detailed treatment of the various linear and nonlinear digital modulations techniques that are found in wireless systems, including QAM, PSK, $\pi/4$-DQPSK, orthogonal modulation, OFDM, CPM, GMSK, and others. Finally, Sect. 4.9 considers the power spectrum of digitally modulated signals.

G.L. Stüber, *Principles of Mobile Communication*, DOI 10.1007/978-3-319-55615-4_4

4.1 Representation of Bandpass Modulated Signals

Bandpass modulation schemes refer to modulation schemes that transmit information by using carrier modulation, such that the signal bandwidth is much less than the carrier frequency. A bandpass waveform $s(t)$ can be expressed in terms of its complex envelope as

$$s(t) = \text{Re}\left\{\tilde{s}(t)e^{j2\pi f_c t}\right\}, \tag{4.1}$$

where

$$\tilde{s}(t) = \tilde{s}_I(t) + j\tilde{s}_Q(t) \tag{4.2}$$

is the complex envelope and f_c is the carrier frequency. For any digital modulation scheme, the complex envelope can be written in the standard form

$$\tilde{s}(t) = A\sum_n b(t - nT, \mathbf{x}_n) \tag{4.3}$$

$$\mathbf{x}_n = (x_n,\ x_{n-1},\ \ldots,\ x_{n-K}), \tag{4.4}$$

where A is the amplitude and $\{x_n\}$ is the sequence of complex data symbols that are chosen from a finite alphabet, and K is the modulator memory order which may be finite or infinite. One data symbol is transmitted every T seconds, so that the baud rate is $R = 1/T$ symbols/s. The function $b(t, \mathbf{x}_i)$ is a *generalized shaping function* whose exact form depends on the type of modulation that is employed. For example, binary phase shift keying (BPSK) with rectangular amplitude pulse shaping has

$$b(t, \mathbf{x}_n) = x_n u_T(t) \tag{4.5}$$

where

$$x_n \in \{-1, +1\} \text{ is the data symbol transmitted at epoch } n$$
$$u_T(t) = u(t) - u(t - T) \text{ is a unit amplitude rectangular pulse of length } T$$

and $u(t)$ is the unit step function. Many types of modulation are considered in this chapter, where information is transmitted in the amplitude, phase, and/or frequency of the carrier. In each case, the modulated signal will be represented in the standard form in (4.3). This is done to streamline the task of finding their power spectra.

By expanding (4.1), the bandpass waveform can also be expressed in the quadrature form

$$s(t) = \tilde{s}_I(t)\cos(2\pi f_c t) - \tilde{s}_Q(t)\sin(2\pi f_c t). \tag{4.6}$$

The waveforms $\tilde{s}_I(t)$ and $\tilde{s}_Q(t)$ are known as the quadrature components $s(t)$, because they modulate the quadrature components of the carrier, $\cos 2\pi f_c t$ and $\sin 2\pi f_c t$, respectively.

Finally $s(t)$ can be expressed in the amplitude-phase form

$$s(t) = a(t)\cos(2\pi f_c t + \phi(t)), \tag{4.7}$$

where

$$a(t) = |\tilde{s}(t)| = \sqrt{\tilde{s}_I^2(t) + \tilde{s}_Q^2(t)} \tag{4.8}$$

$$\phi(t) = \text{Tan}^{-1}\left[\frac{\tilde{s}_Q(t)}{\tilde{s}_I(t)}\right], \tag{4.9}$$

and where $a(t)$ is the amplitude and $\phi(t)$ is the excess phase. The three representations in (4.1), (4.6), and (4.7) are equivalent, but sometimes one representation is more handy than the other two depending on the particular task at hand.

4.1.1 Vector Space Representations

For digital modulation schemes, the bandpass signal that is transmitted at each baud epoch will belong to a finite set of finite energy waveforms with a few exceptions. Let $\{s_1(t), s_2(t), \ldots, s_M(t)\}$ be the set of bandpass waveforms, where M denotes the size of the signal set. The corresponding complex envelopes are denoted by $\{\tilde{s}_1(t), \tilde{s}_2(t), \ldots, \tilde{s}_M(t)\}$. For now, the development will proceed using the complex envelopes, and the bandpass waveforms will be treated later.

An N-dimensional complex vector space can be defined by a set of N complex orthonormal basis functions $\{\varphi_1(t), \varphi_1(t), \ldots, \varphi_N(t)\}$, where

$$\int_{-\infty}^{\infty} \varphi_i(t)\varphi_j^*(t)\mathrm{d}t = \delta_{ij} \tag{4.10}$$

and

$$\delta_{ij} = \begin{cases} 1\ , i = j \\ 0\ , i \neq j \end{cases}. \tag{4.11}$$

Each waveform $\tilde{s}_m(t)$ in the signal set can be projected onto the set of basis functions to yield a signal vector

$$\tilde{\mathbf{s}}_m = (\tilde{s}_{m_1},\ \tilde{s}_{m_2},\ \ldots,\ \tilde{s}_{m_N})\ ,\ \ m = 1, \ldots, M, \tag{4.12}$$

where

$$\tilde{s}_{m_i} = \int_{-\infty}^{\infty} \tilde{s}_m(t)\varphi_i^*(t)\mathrm{d}t,\ \ i = 1,\ \ldots,\ N. \tag{4.13}$$

The collection of N basis functions is said to constitute a *complete set*, if each waveform in the set $\{\tilde{s}_1(t), \tilde{s}_2(t), \ldots, \tilde{s}_M(t)\}$ can be expressed *exactly* as a linear combination of the basis functions. That is,

$$\tilde{s}_m(t) = \sum_{i=1}^{N} \tilde{s}_{m_i}\varphi_i(t),\ \ m = 1,\ \ldots,\ M. \tag{4.14}$$

A systematic procedure for constructing a complete set of basis functions from the set of signal waveforms $\{\tilde{s}_1(t), \tilde{s}_2(t), \ldots, \tilde{s}_M(t)\}$ is now described.

4.1.2 Gram–Schmidt Orthonormalization Procedure

Define the inner product between two complex-valued waveforms $u(t)$ and $v(t)$ as

$$(u, v) \stackrel{\Delta}{=} \int_{-\infty}^{\infty} u(t)v^*(t)\mathrm{d}t \tag{4.15}$$

and define the norm of the waveform $u(t)$ as

$$\|u\| \stackrel{\Delta}{=} \sqrt{(u, u)}. \tag{4.16}$$

Note that the squared-norm

$$\|u\|^2 \stackrel{\Delta}{=} (u, u) = \int_{-\infty}^{\infty} |u(t)|^2\mathrm{d}t \tag{4.17}$$

is the energy contained in the complex-valued waveform $u(t)$.

Given the finite set of finite energy signals $\{\tilde{s}_1(t), \tilde{s}_2(t), \ldots, \tilde{s}_M(t)\}$, a complete set of orthonormal basis functions $\{\varphi_1(t), \varphi_2(t), \ldots, \varphi_N(t)\}$ can be constructed by using the following systematic procedure, known as the Gram–Schmidt orthonormalization procedure:

1: Using $\tilde{s}_1(t)$, let

$$g_1(t) = \tilde{s}_1(t)$$

and define

$$\varphi_1(t) = \frac{g_1(t)}{\|g_1\|}. \tag{4.18}$$

2: Using $\tilde{s}_2(t)$, let

$$g_2(t) = \tilde{s}_2(t) - \tilde{s}_{21}\varphi_1(t)$$

where

$$\tilde{s}_{21} = (\tilde{s}_2, \varphi_1)$$

and define

$$\varphi_2(t) = \frac{g_2(t)}{\|g_2\|}. \tag{4.19}$$

3: Using $\tilde{s}_i(t)$, let

$$g_i(t) = \tilde{s}_i(t) - \sum_{j=0}^{i-1} \tilde{s}_{ij}\varphi_j(t)$$

where

$$\tilde{s}_{ij} = (\tilde{s}_i, \varphi_j)$$

and define

$$\varphi_i(t) = \frac{g_i(t)}{\|g_i\|}. \tag{4.20}$$

4: Repeat Step 3 in a recursive fashion until all elements of the waveform set $\{\tilde{s}_1(t), \tilde{s}_2(t), \ldots, \tilde{s}_M(t)\}$ have been used.

If one or more steps in the above recursion yields $g_i(t) = 0$, then the corresponding waveform $\tilde{s}_i(t)$ can already be expressed exactly in terms of the basis functions already generated. Consequently, the waveform $\tilde{s}_i(t)$ will not yield an additional basis function and the procedure continues to the next waveform in the set, $\tilde{s}_{i+1}(t)$. In the end, a complete set of N, $1 \leq N \leq M$ complex orthonormal basis functions $\{\varphi_1(t), \varphi_2(t), \ldots, \varphi_N(t)\}$ corresponding to the non-zero $g_i(t)$ will be obtained. The dimensionality of the complex vector space N is equal to M if and only if the original set of waveforms $\{\tilde{s}_1(t), \tilde{s}_2(t), \ldots, \tilde{s}_M(t)\}$ are linearly independent, i.e., none of the waveforms in the set is a linear combination of the other waveforms in the set.

Example 4.1. Construct an orthonormal basis set for the set of waveforms shown in Fig. 4.1.

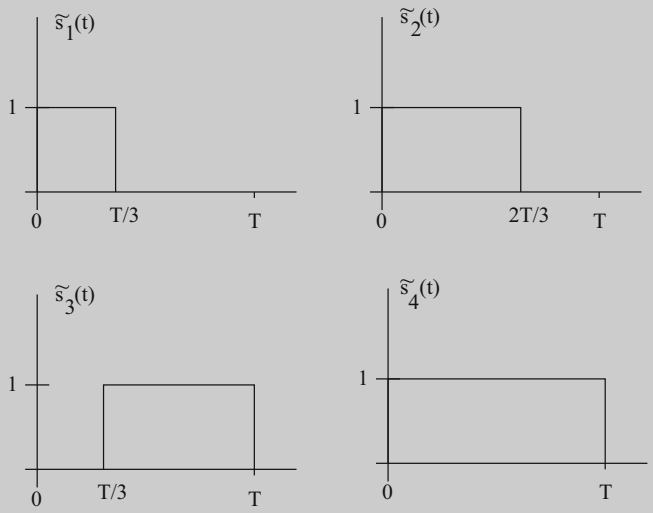

Fig. 4.1 Signal set $\{\tilde{s}_i(t)\}_{i=1}^4$ for Example 4.1

1: Let $g_1(t) = \tilde{s}_1(t)$. Then

$$\varphi_1(t) = \frac{g_1(t)}{\|g_1\|} = \begin{cases} \sqrt{3/T}\,, & 0 \le t \le T/3 \\ 0 \quad\;\; , & \text{else} \end{cases}.$$

2: Let $g_2(t) = \tilde{s}_2(t) - \tilde{s}_{21}\varphi_1(t)$, where

$$\tilde{s}_{21} = (\tilde{s}_2, \varphi_1) = \int_0^T \tilde{s}_2(t)\varphi_1^*(t)\mathrm{d}t = \sqrt{T/3}.$$

Then

$$\varphi_2(t) = \frac{g_2(t)}{\|g_2\|} = \begin{cases} \sqrt{3/T}\,, & T/3 \le t \le 2T/3 \\ 0 \quad\;\; , & \text{else} \end{cases}$$

3: Let $g_3(t) = \tilde{s}_3(t) - \tilde{s}_{31}\varphi_1(t) - \tilde{s}_{32}\varphi_2(t)$, where

$$\tilde{s}_{31} = (\tilde{s}_3, \varphi_1) = \int_0^T \tilde{s}_3(t)\varphi_1^*(t)\mathrm{d}t = 0$$

$$\tilde{s}_{32} = (\tilde{s}_3, \varphi_2) = \int_0^T \tilde{s}_3(t)\varphi_2^*(t)\mathrm{d}t = \sqrt{T/3}.$$

Then

$$\varphi_3(t) = \frac{g_3(t)}{\|g_3\|} = \begin{cases} \sqrt{3/T}\,, & 2T/3 \le t \le T \\ 0 \quad\;\; , & \text{else} \end{cases}.$$

4: Let $g_4(t) = \tilde{s}_4(t) - \tilde{s}_{41}\varphi_1(t) - \tilde{s}_{42}\varphi_2(t) - \tilde{s}_{43}\varphi_3(t)$, where

(continued)

Example 4.1 (continued)

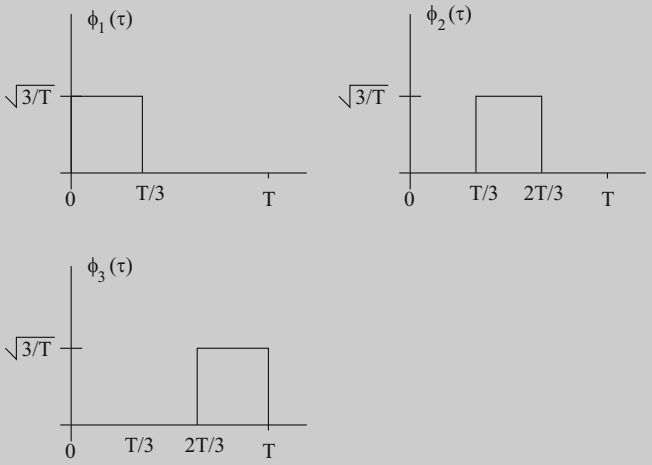

Fig. 4.2 Orthonormal basis functions $\{\varphi_i(t)\}_{i=1}^{3}$ for Example 4.1

$$\tilde{s}_{41} = (\tilde{s}_4, \varphi_1) = \int_0^T \tilde{s}_4(t)\varphi_1^*(t)\mathrm{d}t = \sqrt{T/3}$$
$$\tilde{s}_{42} = (\tilde{s}_4, \varphi_2) = \int_0^T \tilde{s}_4(t)\varphi_2^*(t)\mathrm{d}t = \sqrt{T/3}$$
$$\tilde{s}_{43} = (\tilde{s}_4, \varphi_3) = \int_0^T \tilde{s}_4(t)\varphi_3^*(t)\mathrm{d}t = \sqrt{T/3}.$$

But $g_4(t) = 0$, meaning that $\tilde{s}_4(t)$ is linearly dependent on $\{\tilde{s}_1(t), \tilde{s}_2(t), \tilde{s}_3(t)\}$, and $\tilde{s}_4(t)$ does not yield an additional basis function.

The set of orthonormal basis functions obtained from the above procedure is shown in Fig. 4.2, and they define a 3-dimensional vector space.

Each $\tilde{s}_i(t)$ in the signal set can be expressed as a linear combination of the basis functions, according to (4.14), and the corresponding signal vectors in (4.12) can be constructed. For this example, the signal vectors are

$$\tilde{\mathbf{s}}_1 = (\sqrt{T/3}, 0, 0)$$
$$\tilde{\mathbf{s}}_2 = (\sqrt{T/3}, \sqrt{T/3}, 0)$$
$$\tilde{\mathbf{s}}_3 = (0, \sqrt{T/3}, \sqrt{T/3})$$
$$\tilde{\mathbf{s}}_4 = (\sqrt{T/3}, \sqrt{T/3}, \sqrt{T/3}).$$

The set of signal vectors $\{\tilde{\mathbf{s}}_i\}$ can be plotted in the 3-D vector space defined by the set of orthonormal basis functions $\{\varphi_i(t)\}$ as shown in Fig. 4.3. The plotted set of signal vectors is sometimes called a signal constellation.

(continued)

Example 4.1 (continued)

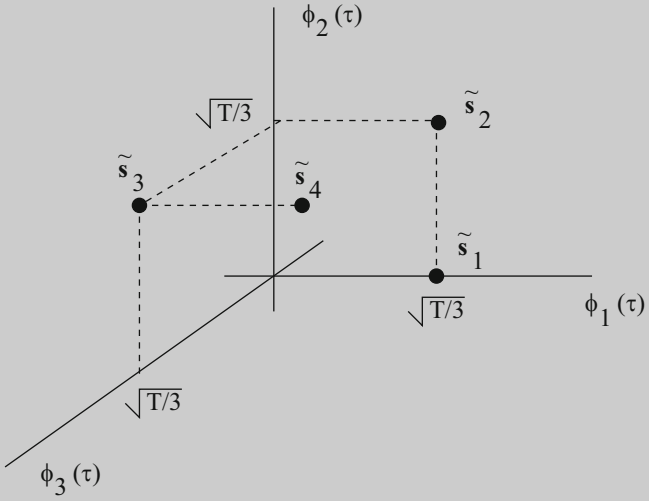

Fig. 4.3 Signal constellation for Example 4.1

In the above development, the Gram–Schmidt orthonormalization procedure was applied to the set of complex envelopes $\{\tilde{s}_1(t), \tilde{s}_2(t), \ldots, \tilde{s}_M(t)\}$ to produce a complete set of $N \leq M$ *complex* basis functions $\{\varphi_1(t), \varphi_2(t), \ldots, \varphi_N(t)\}$, where N is the dimension of the *complex* vector space. By using the exact same Gram–Schmidt orthonormalization procedure, a complete set of N real-valued orthonormal basis functions $\{\varphi_1(t), \varphi_2(t), \ldots, \varphi_N(t)\}$ can be obtained from the real-valued bandpass waveforms $\{s_1(t), s_2(t), \ldots, s_M(t)\}$, expressed in quadrature representation (4.6), and where N is the dimension of the *real* vector space. In this case, the complex conjugates in (4.10) and (4.13) may be omitted since all waveforms are real-valued. By using the real-valued basis functions, each bandpass waveform $s_m(t)$ can be projected onto the set of real-valued basis functions to yield the set of signal vectors

$$\mathbf{s}_m = (s_{m_1},\ s_{m_2},\ \ldots,\ s_{m_N})\ ,\quad m = 1, \ldots, M, \tag{4.21}$$

where

$$s_{m_i} = \int_{-\infty}^{\infty} s_m(t)\varphi_i(t)\mathrm{d}t,\quad i = 1,\ \ldots,\ N, \tag{4.22}$$

and

$$s_m(t) = \sum_{i=1}^{N} s_{m_i}\varphi_i(t),\quad m = 1,\ \ldots,\ M. \tag{4.23}$$

Note that the set of orthonormal basis functions and the dimensionality of the vector space needed to represent the bandpass waveforms and their corresponding complex envelopes are related. The complex-valued basis functions each define a 2-dimensional complex plane. So for one-dimensional complex-valued or two-dimensional real-valued signal constellations each complex basis function will yield two orthogonal real-valued basis functions. If the complex envelopes happen to be real-valued, then just a single real-valued basis function, different in each case, is required to represent both the real-valued bandpass waveforms and their complex envelopes.

4.1.3 Signal Energy and Correlations

Define the inner (dot) product between two length-N complex vectors $\mathbf{u}$ and $\mathbf{v}$ as

$$\mathbf{u} \cdot \mathbf{v}^* \triangleq \sum_{i=1}^{N} u_i v_i^* \tag{4.24}$$

and the norm (length) of the vector $\mathbf{u}$ as

$$\|\mathbf{u}\| \triangleq \sqrt{\mathbf{u} \cdot \mathbf{u}^*} = \sqrt{\sum_{i=1}^{N} |u_i|^2}. \tag{4.25}$$

If the vectors happen to be real, the complex conjugates and absolute values can be neglected.

Consider the set of bandpass waveforms

$$s_m(t) = \text{Re}\left\{\tilde{s}_m(t) e^{j2\pi f_c t}\right\}, \quad m = 1, \ldots, M. \tag{4.26}$$

The energy in the bandpass waveform $s_m(t)$ is

$$E_m = (s_m, s_m) = \int_{-\infty}^{\infty} s_m^2(t) \mathrm{d}t. \tag{4.27}$$

Using the amplitude-phase representation of a bandpass waveform in (4.7), and the trig identity $\cos^2(x) = \frac{1}{2}(1 + \cos(2x))$, gives

$$\begin{aligned} E_m &= \int_{-\infty}^{\infty} \left(|\tilde{s}_m(t)| \cos(2\pi f_c t + \phi_m(t))\right)^2 \mathrm{d}t \\ &= \frac{1}{2} \int_{-\infty}^{\infty} |\tilde{s}_m(t)|^2 \mathrm{d}t + \frac{1}{2} \int_{-\infty}^{\infty} |\tilde{s}_m(t)|^2 \cos(4\pi f_c t + 2\phi_m(t)) \mathrm{d}t \\ &\approx \frac{1}{2} \int_{-\infty}^{\infty} |\tilde{s}_m(t)|^2 \mathrm{d}t \\ &= \frac{1}{2} (\tilde{s}_m, \tilde{s}_m). \end{aligned} \tag{4.28}$$

where $\phi_m(t) = \text{Tan}^{-1}\left[\tilde{s}_{m,Q}(t)/\tilde{s}_{m,I}(t)\right]$. The above approximation is valid when the bandwidth of the complex envelope is much less than the carrier frequency so that the double frequency term can be neglected. For digital bandpass modulated signals, this condition is equivalent to $f_c T \gg 1$ so that there are many cycles of the carrier in the baud period T. This condition is satisfied in most wireless systems.

By using the vector representation of the bandpass waveforms in (4.21)–(4.23), it follows that the energy in the bandpass waveform $s_m(t)$ is

$$E_m = \int_{-\infty}^{\infty} \left(\sum_{i=1}^{N} s_{m_i} \varphi_i(t) \right)^2 \mathrm{d}t = \sum_{i=1}^{N} s_{m_i}^2 = \|\mathbf{s}_m\|^2, \tag{4.29}$$

where the second equality follows from the orthonormal property of the basis functions in (4.10). Notice that the energy in $s_m(t)$ is equal to the squared-norm (length) of the corresponding signal vector $\mathbf{s}_m$. Likewise, by using the vector representation of the corresponding complex envelope, the energy in the bandpass waveform $s_m(t)$ is also equal to

$$E_m = \frac{1}{2} \int_{-\infty}^{\infty} \left| \sum_{i=1}^{N} \tilde{s}_{m_i} \varphi_i(t) \right|^2 \mathrm{d}t = \frac{1}{2} \sum_{i=1}^{N} |\tilde{s}_{m_i}|^2 = \frac{1}{2} \|\tilde{\mathbf{s}}_m\|^2. \tag{4.30}$$

Note that the energy in the bandpass waveform is one-half the energy in its complex envelope. This is due to the carrier modulation.

The correlation between the bandpass waveforms $s_m(t)$ and $s_k(t)$ is defined as

$$\begin{aligned}\rho_{km} &= \frac{1}{\sqrt{E_k E_m}} \int_{-\infty}^{\infty} s_m(t) s_k(t) \mathrm{d}t \\ &= \frac{\mathbf{s}_m \cdot \mathbf{s}_k}{\|\mathbf{s}_m\| \|\mathbf{s}_k\|} \\ &= \mathrm{Re}\left\{ \frac{\tilde{\mathbf{s}}_m \cdot \tilde{\mathbf{s}}_k^*}{\|\tilde{\mathbf{s}}_m\| \|\tilde{\mathbf{s}}_k\|} \right\}. \end{aligned} \tag{4.31}$$

Finally, the squared Euclidean distance between the bandpass waveforms $s_k(t)$ and $s_m(t)$ is

$$\begin{aligned} d_{km}^2 &= \int_{-\infty}^{\infty} (s_m(t) - s_k(t))^2 \, \mathrm{d}t \\ &= \|\mathbf{s}_m - \mathbf{s}_k\|^2 \\ &= \frac{1}{2} \|\tilde{\mathbf{s}}_m - \tilde{\mathbf{s}}_k\|^2. \end{aligned} \tag{4.32}$$

The results in (4.31) and (4.32) may be obtained using (4.14) and (4.23) along with the orthonormal property of the basis functions.

4.2 Nyquist Pulse Shaping

Consider a modulation scheme where the transmitted complex envelope has the

$$\tilde{s}(t) = A \sum_n x_n h_a(t - nT) \tag{4.33}$$

where $h_a(t)$ is a real-valued amplitude shaping pulse, $\{x_n\}$ is a complex data symbol sequence, and T is the baud period. As will be discussed in Chap. 5, the receiver usually employs a filter that is *matched* to the transmitted pulse, having the form $h_r(t) = h_a(T_o - t)$, where T_o is the duration of the amplitude shaping pulse $h_a(t)$. An overall pulse can be defined that is the cascade of the transmitted pulse $h_a(t)$ and the receiver matched filter $h_r(t)$ as $p(t) = h_a(t) * h_a(T_o - t)$, where $*$ denotes the operation of convolution.

For the time being, consider an ideal channel having impulse response $g(t, \tau) = \delta(\tau)$. In the absence of thermal noise in the receiver, the waveform at the output of the receiver matched filter is

$$\tilde{y}(t) = A \sum_n x_n p(t - nT). \tag{4.34}$$

Now suppose the received complex envelope $\tilde{y}(t)$ is sampled once every T seconds to yield the sample sequence $\{\tilde{y}_k\}$, where

$$\tilde{y}_k = \tilde{y}(kT + t_o) = A \sum_n x_n p(kT + t_o - nT) \tag{4.35}$$

and t_o is a timing offset assumed to lie in the interval $[0, T)$. First consider the case when $t_o = 0$; the effect of having a non-zero timing offset will be treated later. When $t_o = 0$

$$\tilde{y}_k = A \sum_n x_n p_{k-n} = A x_k p_0 + A \sum_{n \neq k} x_n p_{k-n}, \tag{4.36}$$

where $p_m = p(mT)$ is the sampled overall pulse. The first term in (4.36) is equal to the data symbol transmitted at the kth baud epoch, scaled by the factor Ap_0. The second term is the contribution of all other data symbols on the sample $\tilde{y}_k$. This term is called intersymbol interference (ISI). To avoid the appearance of ISI, the sampled pulse response $\{p_k\}$ must satisfy the condition

$$p_k = \delta_{k0} p_0, \tag{4.37}$$

where δ_{jk} is the Dirac delta function defined in (4.11). This requirement is known as the (first) Nyquist criterion. Under this condition,

$$\tilde{y}_k = Ax_k p_0. \tag{4.38}$$

An equivalent frequency domain requirement is now derived by showing that the continuous-time pulse $p(t)$ satisfies the condition $p_k = \delta_{k0} p_0$ if and only if

$$P_\Sigma(f) \triangleq \frac{1}{T} \sum_{n=-\infty}^{\infty} P\left(f + \frac{n}{T}\right) = p_0. \tag{4.39}$$

The function $P_\Sigma(f)$ is called the folded spectrum, and ISI is avoided if and only if the folded spectrum is *flat*, i.e., it assumes a constant value. To prove the above property, the inverse Fourier transform can be used to write

$$\begin{aligned} p_k &= \int_{-\infty}^{\infty} P(f) \mathrm{e}^{j2\pi fkT} \mathrm{d}f \\ &= \sum_{n=-\infty}^{\infty} \int_{(2n-1)/2T}^{(2n+1)/2T} P(f) \mathrm{e}^{j2\pi kfT} \mathrm{d}f \\ &= \sum_{n=-\infty}^{\infty} \int_{-1/2T}^{1/2T} P\left(f' + \frac{n}{T}\right) \mathrm{e}^{j2\pi k\left(f' + \frac{n}{T}\right)T} \mathrm{d}f' \\ &= \int_{-1/2T}^{1/2T} \left[\sum_{n=-\infty}^{\infty} P\left(f + \frac{n}{T}\right) \right] \mathrm{e}^{j2\pi fkT} \mathrm{d}f \\ &= T \int_{-1/2T}^{1/2T} P_\Sigma(f) \mathrm{e}^{j2\pi fkT} \mathrm{d}f. \end{aligned} \tag{4.40}$$

Since $P_\Sigma(f)$ is periodic with period $1/T$, it follows that the last line in (4.40) represents a Fourier series analysis equation except for the sign of the exponential term. Therefore, $\{p_{-k}\}$ and $P_\Sigma(f)$ are a Fourier series pair, and $P_\Sigma(f)$ can be constructed from $\{p_{-k}\}$ by using the Fourier series synthesis equation, viz.,

$$P_\Sigma(f) = \sum_{k=-\infty}^{\infty} p_{-k} \mathrm{e}^{j2\pi kfT} = \sum_{k=-\infty}^{\infty} p_k \mathrm{e}^{-j2\pi kfT}. \tag{4.41}$$

To prove that (4.39) is a sufficient condition for ISI-free transmission, suppose that (4.39) holds true. Then $P_\Sigma(f) = p_0 T$ and from the last line of (4.40)

$$p_k = \int_{-1/2T}^{1/2T} \mathrm{e}^{j2\pi fkT} p_0 T \mathrm{d}f = \frac{\sin \pi k}{\pi k} p_0 = \delta_{k0} p_0. \tag{4.42}$$

To prove that (4.39) is a necessary condition for ISI-free transmission, suppose that $p_k = p_0 \delta_{k0}$ holds true. Then from (4.41) $P_\Sigma(f) = p_0$, and the folded spectrum must be flat.

The requirement on the folded spectrum in (4.39) allows us to design pulses in the frequency domain that will admit ISI-free transmission. First consider a pulse having the Fourier transform

$$P_N(f) = T\mathrm{rect}(fT), \tag{4.43}$$

where

$$\mathrm{rect}(fT) = \begin{cases} 1, & |f| \le \frac{1}{2T} \\ 0, & \text{elsewhere} \end{cases}. \tag{4.44}$$

This pulse has a flat folded spectrum. The corresponding time domain pulse

$$p_N(t) = \mathrm{sinc}(t/T) \tag{4.45}$$

satisfies the first Nyquist criterion because it has equally spaced zero crossings at T second intervals. Furthermore, from the requirement of a flat folded spectrum, it achieves zero ISI while occupying the smallest possible bandwidth. Hence, it is called an *ideal* Nyquist pulse. The edge frequency $f = 1/2T$ is called the Nyquist frequency.

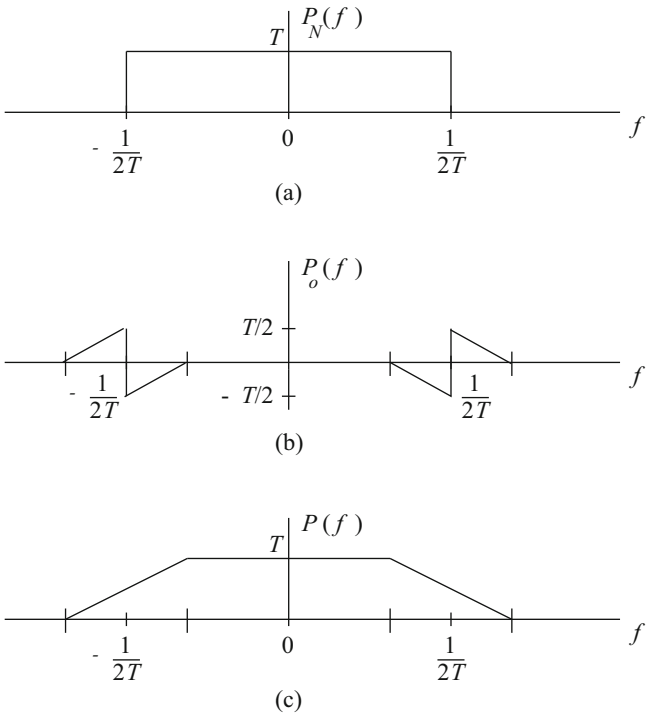

Fig. 4.4 Construction of pulses satisfying the (first) Nyquist criterion

The effect of the sampling or timing offset t_o is now examined with the aid of the ideal Nyquist pulse. With a timing offset

$$\begin{aligned}\tilde{y}_k &= A\sum_n x_n \text{sinc}((kT + t_o - nT)/T) \\ &= Ax_k \text{sinc}(t_o/T) + A\sum_{n\neq k} x_n \text{sinc}((kT + t_o - nT)/T)\end{aligned} \tag{4.46}$$

Observe that the ISI term is non-zero when the timing offset is non-zero. In fact, with an ideal Nyquist pulse, the ISI term is not absolutely summable as shown in Problem 4.1. This is because the tails of the ideal Nyquist pulse in (4.45) decay in time as $1/t$. To reduce this sensitivity to symbol timing errors, pulses need to be designed that satisfy the first Nyquist criterion while having tails that decay faster than $1/t$.

The construction of other Nyquist pulses starts with the ideal Nyquist pulse, $P_N(f)$, shown in Fig. 4.4a. To the pulse $P_N(f)$, a "transmittance" function $P_o(f)$ is added as shown in Fig. 4.4b. The transmittance function must have *skew* symmetry about the Nyquist frequency $1/2T$, and any skew symmetric function will do. The resulting Nyquist pulse $P(f)$ is shown in Fig. 4.4c. Clearly, the folded spectrum $P_\Sigma(f)$ is flat if the transmittance function is skew symmetric about the Nyquist frequency $1/2T$. The corresponding time domain pulse $p(t)$ can be obtained from the inverse Fourier transform of resulting $P(f)$. Notice that the pulse $P(f)$ takes up additional bandwidth, but the bandwidth expansion will result in a time domain pulse $p(t)$ having tails that decay faster in time than the ideal Nyquist pulse.

4.2.1 Raised Cosine and Root Raised Cosine Pulse

The raised cosine pulse is defined in the frequency domain by

$$P(f) = \begin{cases} T & , \ 0 \le |f| \le (1-\beta)/2T \\ \frac{T}{2}\left[1 - \sin\left(\frac{\pi|f|T}{\beta} - \frac{\pi}{2\beta}\right)\right] & , \ (1-\beta)/2T \le |f| \le (1+\beta)/2T \\ 0 & , \ |f| \ge (1+\beta)/2T \end{cases}. \tag{4.47}$$

The bandwidth of the raised cosine pulse is $(1+\beta)/2T$, where the parameter $\beta, 0 \le \beta \le 1$ is called the roll-off factor and controls the bandwidth expansion. The term "raised cosine" comes from the fact that pulse spectrum $P(f)$ with $\beta = 1$ has a "raised cosine" shape, i.e., with $\beta = 1$

$$P(f) = \frac{T}{2}\left[1 + \cos(\pi f T)\right], \quad 0 \le |f| \le 1/T. \tag{4.48}$$

The inverse Fourier transform of $P(f)$ in (4.47) gives the corresponding time domain pulse

$$p(t) = \frac{\sin(\pi t/T)}{\pi t/T}\,\frac{\cos(\beta\pi t/T)}{1-(2\beta t/T)^2}. \tag{4.49}$$

For $\beta = 0$, $p(t)$ reduces to the ideal Nyquist pulse in (4.45). Notice that the tails of the raised cosine pulse decay as $1/t^3$.

As mentioned before, the overall pulse produced by the cascade of the transmitter and receiver matched filters is $p(t) = h_a(t) * h_a(T_o - t)$. It follows that the Fourier transform of $p(t)$ is $P(f) = H_a(f)H_a^*(f)\mathrm{e}^{-j2\pi f T_o} = |H_a(f)|^2\mathrm{e}^{-j2\pi f T_o}$. Hence, both the transmitted pulse and receiver matched filter have the same magnitude response $|H_a(f)| = |P(f)|^{1/2}$, where $P(f)$ is defined in (4.47). If the overall pulse $p(t)$ is a raised cosine pulse with $P(f)$ defined in (4.47), then the pulse $h_a(t)$ is said to be a root raised cosine pulse. Taking the inverse Fourier transform of $|H_a(f)| = \sqrt{T}|P(f)|^{1/2}$ gives the root raised cosine pulse

$$h_a(t) = \begin{cases} 1-\beta+4\beta/\pi & , \ t = 0 \\ (\beta/\sqrt{2})\left((1+2/\pi)\sin(\pi/4\beta) + (1-2/\pi)\cos(\pi/4\beta)\right) & , \ t = \pm T/4\beta \\ \frac{4\beta(t/T)\cos((1+\beta)\pi t/T)+\sin((1-\beta)\pi t/T)}{\pi(t/T)(1-(4\beta t/T)^2)} & , \ \text{elsewhere} \end{cases} \tag{4.50}$$

For $\beta = 0$, the root raised cosine pulse reduces to the sinc pulse

$$h_a(t) = \mathrm{sinc}(t/T). \tag{4.51}$$

The raised cosine and root raised cosine pulses corresponding to $\beta = 0.5$ are shown in Fig. 4.5. Strictly speaking, the root-raised cosine pulse in (4.50) is non-causal. Therefore, in practice, a truncated and time shifted approximation of the pulse must be used. For example, in Fig. 4.5 the pulse is truncated to length $6T$ and right time-shifted by $3T$ seconds to yield a causal pulse. The time-shifting makes the pulse have a linear phase response, while the pulse truncation will result in a pulse that is no longer strictly bandlimited. Finally, the raised cosine pulse is a Nyquist pulse having equally spaced zero crossings at the baud period T, while the root-raised cosine pulse by itself is not a Nyquist pulse and does not have equally spaced zero crossings.

4.3 Quadrature Amplitude Modulation

Quadrature amplitude modulation (QAM) is a bandwidth efficient modulation scheme that is used in numerous wireless standards. With QAM, the complex envelope of the transmitted waveform is

$$\tilde{s}(t) = A\sum_n b(t-nT, \mathbf{x}_n) \tag{4.52}$$

where

$$b(t, \mathbf{x}_n) = x_n h_a(t) \tag{4.53}$$

$h_a(t)$ is the amplitude shaping pulse (very often chosen as a root-raised cosine pulse), and $x_n = x_{I,n} + jx_{Q,n}$ is the complex-valued data symbol that is transmitted at baud epoch n. It is apparent that both the amplitude and the excess phase of a QAM waveform depend on the complex data symbols. QAM has the advantage of high bandwidth efficiency, but amplifier nonlinearities will degrade its performance due to the non-constant envelope.

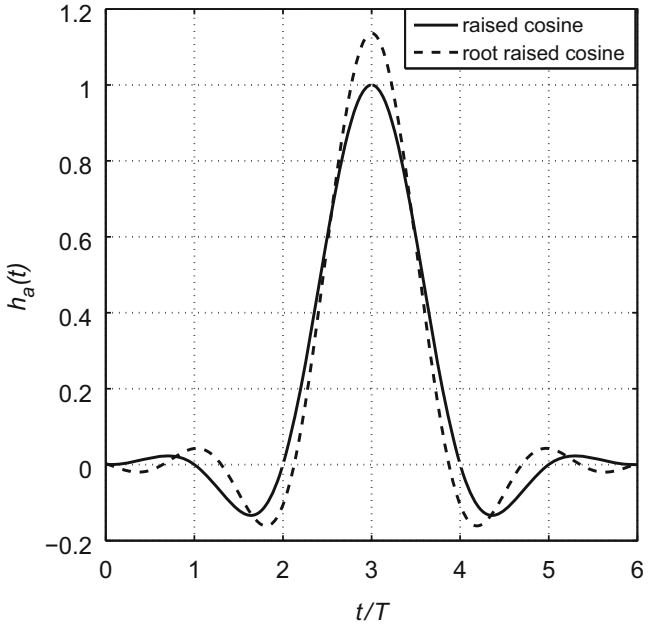

Fig. 4.5 Raised cosine and root raised cosine pulses with roll-off factor $\beta = 0.5$. The pulses are truncated to length $6T$ and right time shifted by $3T$ seconds to yield causal pulses

The set of possible QAM waveforms that are transmitted at each baud epoch have the complex envelopes

$$\tilde{s}_m(t) = Ax_m h_a(t) \quad m = 1, 2, \ldots, M. \tag{4.54}$$

To obtain the vector representation of the complex envelopes $\tilde{s}_m(t), m = 1, 2, \ldots, M$, the basis function

$$\varphi_1(t) = \sqrt{\frac{A^2}{2E_h}} h_a(t) \tag{4.55}$$

can be used, where

$$E_h = \frac{A^2}{2} \int_{-\infty}^{\infty} h_a^2(t) dt \tag{4.56}$$

is the energy in the bandpass pulse $Ah_a(t) \cos 2\pi f_c t$ under the condition $f_c T \gg 1$. Using this basis function

$$\tilde{s}_m(t) = \sqrt{2E_h}\, x_m\, \varphi_1(t), \tag{4.57}$$

and the QAM complex signal vectors are the complex-valued scalars[1]

$$\tilde{s}_m = \sqrt{2E_h}\, x_m\,, \quad m = 1, 2, \ldots, M. \tag{4.58}$$

4.3.1 QAM Signal Constellations

A variety of QAM signal constellations may be constructed. Square QAM constellations can be constructed when M is an even power of 2 by choosing $x_{I,m}, x_{Q,m} \in \{\pm 1, \pm 3, \ldots, \pm(\hat{M} - 1)\}$, where $\hat{M} = \sqrt{M}$. The complex signal-space diagram for the square 4-, 16, and 64-QAM constellations is shown in Fig. 4.6. Notice that the minimum Euclidean distance between any two signal vectors is $2\sqrt{2E_h}$. When M is an odd power of 2, the QAM signal constellation is not square. In this case,

[1]Note that the dimensionality of the complex signal-space is $N = 1$.

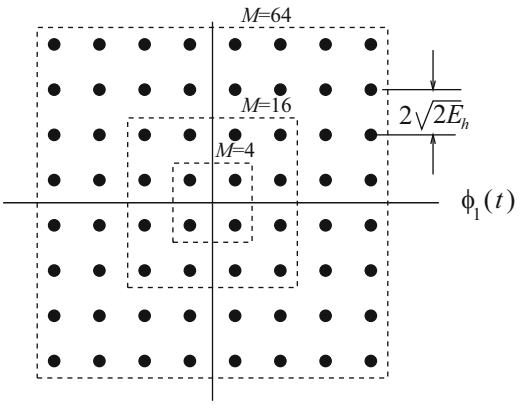

Fig. 4.6 Complex signal-space diagram for square QAM constellations

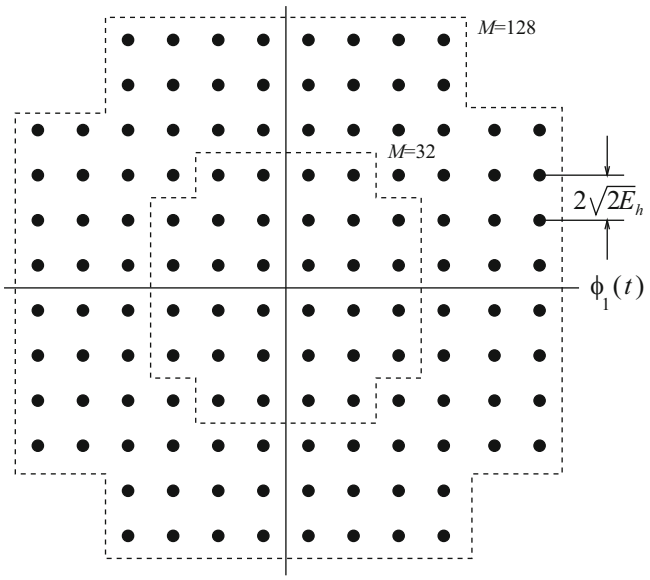

Fig. 4.7 Complex signal-space diagram for cross QAM constellations

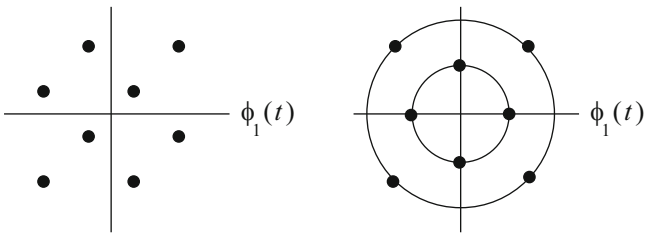

Fig. 4.8 Complex signal-space diagrams for 8-QAM constellations

the constellation assumes the shape of a cross in an attempt to minimize the average energy in the constellation for a given minimum Euclidean distance between signal vectors. Examples of QAM "cross constellations" are shown in Fig. 4.7. Other types of QAM constellations are possible as well. Figure 4.8 shows two different 8-QAM constellations.

4.3.2 PAM Signal Constellations

Pulse amplitude modulation (PAM) can be viewed as a special case of QAM, where information is transmitted only in the cosine component of the RF carrier. This can be accomplished by using real data symbols $x_m = x_{I,m}$, where

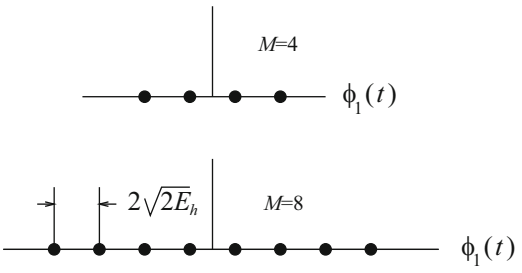

Fig. 4.9 Complex signal-space diagram for the 4- and 8-PAM constellations

$x_{I,m} \in \{\pm 1, \pm 3, \ldots, \pm(M-1)\}$. Equivalently, the set of data symbols can be generated according to $x_{I,m} \in \{2m - 1 - M : m = 1, 2, \ldots, M\}$. The PAM complex signal vectors are the real-valued scalars

$$\tilde{s}_m = \sqrt{2E_h}(2m - 1 - M) \ , \quad m = 1, 2, \ldots, M. \tag{4.59}$$

Typical 4- and 8-PAM signal constellations are shown in Fig. 4.9.

4.4 Phase Shift Keying

The complex envelope of a phase shift keying (PSK) signal has the form

$$\tilde{s}(t) = A \sum_n b(t - nT, \mathbf{x}_n), \tag{4.60}$$

where

$$b(t, \mathbf{x}_n) = x_n h_a(t), \tag{4.61}$$

$h_a(t)$ is the amplitude shaping pulse, $x_n = e^{j\theta_n}$ and the phases θ_n take on values from the set

$$\theta_n \in \left\{ \frac{2\pi}{M} n \ , \ \ n = 0, 1, \ \ldots, \ M - 1 \right\} , \tag{4.62}$$

The set of possible PSK waveforms that are transmitted at each baud epoch have the complex envelopes

$$\tilde{s}_m(t) = A h_a(t) e^{j\theta_m} \ , \ \ m = 1, 2, \ldots, M. \tag{4.63}$$

Using the basis function in (4.55)

$$\tilde{s}_m(t) = \sqrt{2E_h} e^{j\theta_m} \varphi_0(t) \ , \ \ m = 1, \ldots, M, \tag{4.64}$$

and the PSK complex signal vectors are the complex-valued scalars

$$\tilde{s}_m = \sqrt{2E_h} e^{j\theta_m} \ , \ \ m = 1, 2, \ldots, M. \tag{4.65}$$

The complex signal-space diagram for 8-PSK is shown in Fig. 4.10. Recall the energy in a PSK bandpass waveform is equal to one-half the squared length of its complex signal vector. It follows that the PSK bandpass waveforms all have equal energy E_h.

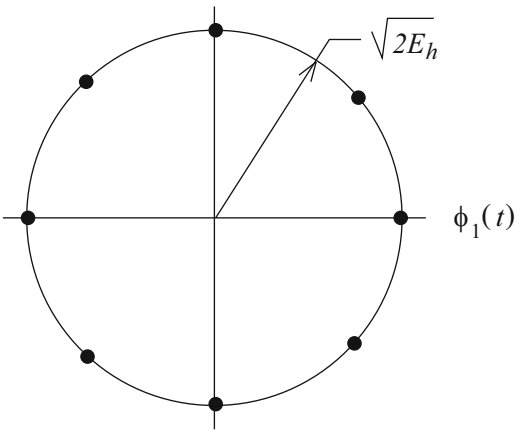

Fig. 4.10 Complex signal-space diagram for the 8-PSK constellation

4.4.1 Offset QPSK (OQPSK)

QPSK or 4-PSK is equivalent to 4-QAM, where $x_n = x_{I,n} + jx_{Q,n}$ and $x_{I,n}, x_{Q,n} \in \{-1/\sqrt{2}, +1/\sqrt{2}\}$. The QPSK signal can have either $\pm 90°$ or $180°$ shifts of the excess phase from one baud interval to the next. With offset (or staggered) QPSK (OQPSK), the complex envelope is

$$\tilde{s}(t) = A \sum_n b(t - nT, \mathbf{x}_n) \tag{4.66}$$

where

$$b(t, \mathbf{x}_n) = x_{I,n} h_a(t) + jx_{Q,n} h_a(t - T_b) \tag{4.67}$$

and $T_b = T/2$ is the bit interval. With OQPSK signals, the possibility of $180°$ shifts of the excess phase is eliminated. In fact, the excess phase can only change by $\pm 90°$ every T_b seconds. With OQPSK, the amplitude shaping pulse $h_a(t)$ is often chosen to be the root-raised cosine pulse in (4.50) to yield a compact power spectrum.

The signal-space diagrams for QPSK and OQPSK are shown in Fig. 4.11, where E_h is the symbol energy. The dotted lines in Fig. 4.11 show the allowable excess phase transitions. The exact excess phase trajectories depend on the amplitude shaping function. Note that the excess phase trajectories with OQPSK do not pass through the origin, while those with QPSK do. This property reduces the peak-to-average power ratio (PAPR) of the OQPSK waveform as compared to the QPSK waveform, where the PAPR is defined as

$$\text{PAPR} = \lim_{T \to \infty} \frac{\max_{0 \le t \le T} |\tilde{s}(t)|^2}{T^{-1} \int_0^T |\tilde{s}(t)|^2 dt}.$$

A lower PAPR makes the OQPSK waveform less sensitive to power amplifier nonlinearities than the QPSK waveform. For this reason OQPSK waveforms have been used for satellite communication links, where the satellite transponders use power efficient nonlinear amplifiers.

4.4.2 $\pi/4$-DQPSK

The $\pi/4$ phase-shifted differential quadrature phase shift keyed ($\pi/4$-DQPSK) modulation scheme was used in some types of now extinct second generation cellular telephone systems. Similar to QPSK and OQPSK, $\pi/4$-DQPSK transmits 2 bits per modulated symbol. However, unlike QPSK and OQPSK where information is transmitted in the absolute excess phase, $\pi/4$-DQPSK transmits information in the differential excess phase, and one of 8 absolute excess phases are transmitted at each baud epoch.

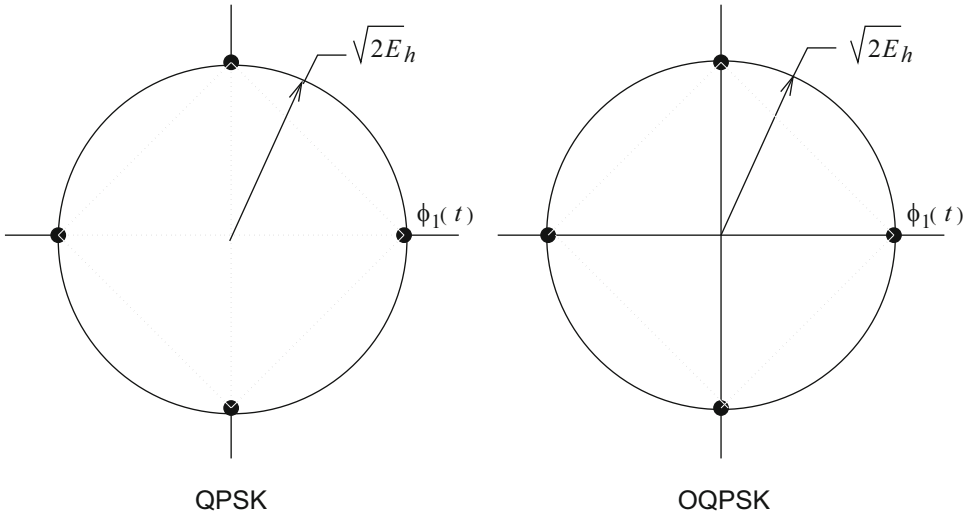

Fig. 4.11 Complex signal-space diagram QPSK and OQPSK signals

Let θ_n be the absolute excess phase for the nth data symbol, and let $\Delta\theta_n = \theta_n - \theta_{n-1}$ be the differential excess phase. With $\pi/4$-DQPSK, the differential excess phase is related to the quaternary data sequence $\{x_n\}$, $x_n \in \{\pm 1, \pm 3\}$ through the mapping

$$\Delta\theta_n = x_n \frac{\pi}{4}. \tag{4.68}$$

Notice that the excess phase differences are $\pm\pi/4$ and $\pm 3\pi/4$. The complex envelope of the $\pi/4$-DQPSK signal is

$$\tilde{s}(t) = A \sum_n b(t - nT, \mathbf{x}_n), \tag{4.69}$$

where

$$\begin{aligned} b(t, \mathbf{x}_n) &= h_a(t) \exp\left\{ j\left(\theta_{n-1} + x_n \frac{\pi}{4}\right)\right\} \\ &= h_a(t) \exp\left\{ j\frac{\pi}{4}\left(\sum_{k=-\infty}^{n-1} x_k + x_n\right)\right\}. \end{aligned} \tag{4.70}$$

The summation in the exponent of (4.70) represents the accumulated excess phase, while the last term is the excess phase increment due to the nth data symbol. The absolute excess phase during the even and odd baud intervals belongs to the sets $\{0, \pi/2, \pi, 3\pi/2\}$ and $\{\pi/4, 3\pi/4, 5\pi/4, 7\pi/4\}$, respectively, or vice versa. With $\pi/4$-DQPSK the amplitude shaping pulse $h_a(t)$ is often chosen to be the root-raised cosine pulse in (4.50).

The signal-space diagrams for QPSK and $\pi/4$-DQPSK are shown in Fig. 4.12, where E_h is the symbol energy. The dotted lines in Fig. 4.12 show the allowable phase transitions. The phaser diagram for $\pi/4$-DQPSK with root-raised cosine amplitude pulse shaping is shown in Fig. 4.13. Note that the phase trajectories do not pass through the origin. Like OQPSK, this property reduces the PAPR of the complex envelope, making the $\pi/4$-DQPSK waveform less sensitive to power amplifier nonlinearities. Moreover, since the root-raised cosine pulse is not a Nyquist pulse, the phase trajectories do not go through the signal constellation points either. Finally, observe that the excess phase of $\pi/4$-DQPSK changes by $\pm\pi/4$ or $\pm 3\pi/4$ radians during *every* baud interval. This property makes symbol synchronization is easier with $\pi/4$-DQPSK as compared to QPSK.

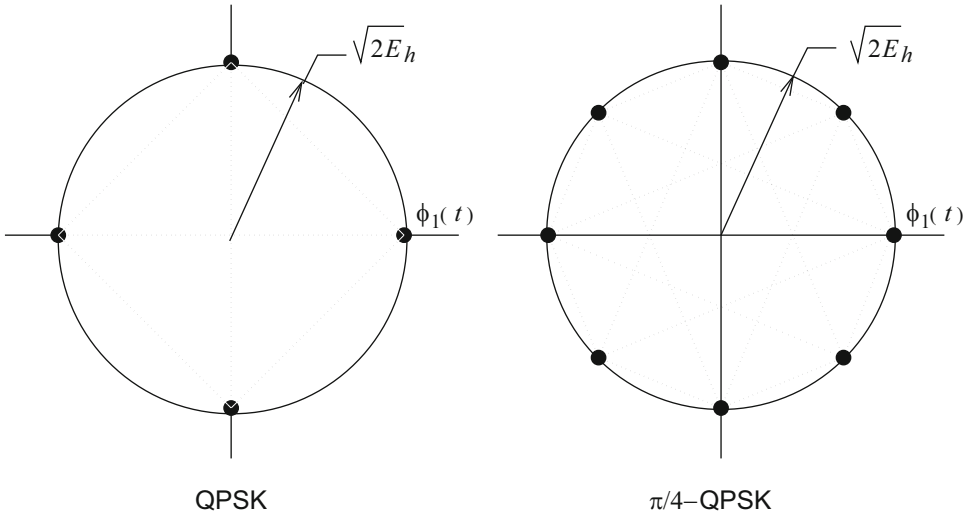

Fig. 4.12 Complex signal-space diagram QPSK and $\pi/4$-DQPSK signals

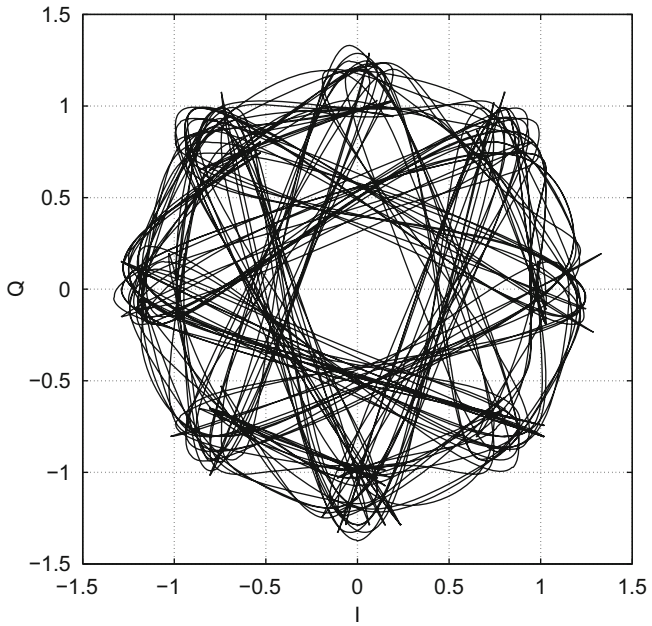

Fig. 4.13 Phaser diagram for $\pi/4$-DQPSK with root-raised cosine amplitude pulse shaping; $\beta = 0.5$

4.5 Orthogonal Modulation and Variants

Orthogonal modulation schemes transmit information by using a set of waveforms, that may overlap in frequency but are orthogonal in time. Many different types of orthogonal waveforms are possible and here a few methods are considered that are commonly used in wireless systems.

4.5.1 Orthogonal FSK Modulation

Orthogonal M-ary frequency shift keying (MFSK) uses a set of M waveforms that all have different frequencies. The MFSK complex envelope is

$$\tilde{s}(t) = A \sum_n b(t - nT, \mathbf{x}_n), \tag{4.71}$$

where

$$b(t, \mathbf{x}_n) = \exp\left\{ j \frac{x_n \pi \Delta_f}{2} t \right\} u_T(t) \tag{4.72}$$

and $x_n \in \{\pm 1, \pm 3, \ldots, \pm M - 1\}$. The set of MFSK waveforms that are transmitted at each baud epoch have the complex envelopes

$$\tilde{s}_m(t) = A \exp\left\{ j \frac{x_m \pi \Delta_f}{2} t \right\} u_T(t) \ , \quad m = 1, \ldots, M. \tag{4.73}$$

By choosing the frequency separation $\Delta_f = 1/2T$, all the $\tilde{s}_m(t), m = 1, \ldots, M$ are mutually orthogonal (see Problem 4.7). Since the $\tilde{s}_m(t)$ are mutually orthogonal, the MFSK signal vectors have dimension $N = M$. The appropriate set of basis functions is

$$\varphi_i(t) = \sqrt{\frac{1}{T}} \exp\left\{ j \frac{x_m \pi \Delta_f}{2} t \right\} u_T(t) \ , \quad i = 1, \ldots, M = N. \tag{4.74}$$

The MFSK complex signal vectors are

$$\tilde{\mathbf{s}}_m = \sqrt{2E_h} \mathbf{e}_m \ , \quad m = 1, \ldots, M, \tag{4.75}$$

where $\mathbf{e}_m = (e_1, e_2, \ldots, e_M)$, $e_j = \delta_{jm}$, is a length-M unit basis vector with a "1" in the mth coordinate.

4.5.2 Binary Orthogonal Codes

Another set of mutually orthogonal waveforms can be obtained from the rows of a Hadamard matrix. A Hadamard matrix, $\mathbf{H}_M$, is generated recursively according to

$$\mathbf{H}_M = \begin{bmatrix} \mathbf{H}_{M/2} & \mathbf{H}_{M/2} \\ \mathbf{H}_{M/2} & -\mathbf{H}_{M/2} \end{bmatrix}.$$

where $\mathbf{H}_1 = [1]$. For example, the 8×8 Hadamard matrix obtained from the above recursive procedure is

$$\mathbf{H}_8 = \begin{bmatrix} +1 & +1 & +1 & +1 & +1 & +1 & +1 & +1 \\ +1 & -1 & +1 & -1 & +1 & -1 & +1 & -1 \\ +1 & +1 & -1 & -1 & +1 & +1 & -1 & -1 \\ +1 & -1 & -1 & +1 & +1 & -1 & -1 & +1 \\ +1 & +1 & +1 & +1 & -1 & -1 & -1 & -1 \\ +1 & -1 & +1 & -1 & -1 & +1 & -1 & +1 \\ +1 & +1 & -1 & -1 & -1 & -1 & +1 & +1 \\ +1 & -1 & -1 & +1 & -1 & +1 & +1 & -1 \end{bmatrix}. \tag{4.76}$$

The rows of the Hadamard matrix are mutually orthogonal. A set of M equal energy orthogonal waveforms can be constructed according to

$$\tilde{s}_m(t) = A \sum_{k=1}^{M} h_{m_k} h_c(t - kT_c) \ , \quad m = 1, \ldots, M, \tag{4.77}$$

where h_{m_k} is the kth co-ordinate in the mth row of the Hadamard matrix, $T = MT_c$ is the symbol duration, and $h_c(t)$ is a root Nyquist shaping pulse with a Nyquist frequency of $1/(2T_c)$. Sometimes the above waveforms are called Walsh codes, and find application in the forward link of some cellular code division multiple access (CDMA) systems, such as IS-95A/B and cdma2000.

The bandpass waveforms, $s_m(t)$, all have energy

$$E_h = \frac{MA^2}{2} \int_{-\infty}^{\infty} h_c^2(t)dt. \tag{4.78}$$

To construct signal vectors, the appropriate choice of basis function is

$$\varphi_i(t) = \frac{A}{\sqrt{2E_h}} \sum_{k=1}^{M} h_{i_k} h_c(t - kT_c) \ , \quad i = 1, \ldots, M \tag{4.79}$$

and once again the signal vectors are

$$\tilde{\mathbf{s}}_m = \sqrt{2E_h}\mathbf{e}_m \ , \quad m = 1, \ldots, M. \tag{4.80}$$

4.5.3 Biorthogonal Signals

A set of M biorthogonal waveforms can be constructed from a set of $M/2$ orthogonal waveforms. The M-ary biorthogonal waveforms have complex signal vectors

$$\tilde{\mathbf{s}}_i = \begin{cases} \sqrt{2E_h}\mathbf{e}_i \ , & i = 1, \ldots, M/2 \\ -\tilde{\mathbf{s}}_{i-M/2} \ , & i = M/2 + 1, \ldots, M \end{cases}, \tag{4.81}$$

where the unit basis vectors $\mathbf{e}_i$ have length $N = M/2$. By using an appropriate set of basis functions, for example in (4.74) or (4.79), the complex envelopes of the biorthogonal waveforms can be synthesized.

4.5.4 Orthogonal Multipulse Modulation

With binary orthogonal codes only $k = \log_2 M$ bits are transmitted at each baud epoch. A much more bandwidth efficient scheme can be obtained by using the rows of the Hadamard matrix $\mathbf{H}_N$ to define N orthogonal amplitude shaping pulses

$$h_i(t) = \sum_{k=0}^{N-1} h_{ik} h_c(t - kT_c) \ , \quad i = 1, \ldots, N \tag{4.82}$$

each having duration $T = NT_c$. With orthogonal multipulse modulation, a block of $M = N$ data symbols are transmitted in parallel every T seconds by using the N orthogonal amplitude shaping pulses in (4.82). The transmitted complex envelope is

$$\tilde{s}(t) = A \sum_n b(t - nT, \mathbf{x}_n), \tag{4.83}$$

where

$$b(t, \mathbf{x}_n) = \sum_{k=0}^{N-1} x_{n_k} h_k(t) \tag{4.84}$$

$T = NT_c$, and $\mathbf{x}_n = (x_{n_1}, x_{n_2}, \ldots, x_{n_N})$ is the block of $M = N$ data symbols transmitted at epoch n.

4.6 Orthogonal Frequency Division Multiplexing

All of the modulation techniques discussed so far are *single-carrier* modulation techniques that employ a single RF carrier. Another possibility is to use *multi-carrier* modulation techniques where information is transmitted in parallel by using multiple subcarriers. Orthogonal frequency division multiplexing (OFDM) is perhaps the most popular multi-carrier modulation technique. OFDM was first introduced in the 1960s [55], but it was perhaps the efficient DFT implementation of OFDM developed by Weinstein and Ebert [348] that has led to its popularity and widespread use. OFDM was first suggested for use cellular land mobile radio by Cimini [66] and later implemented in the Motorola IDEN (Integrated Digital Enhanced Network) standard [44]. OFDM is now used in a large number of standards for broadcasting (DVB-T, DVB-H, MediaFLO, and others), wireless LAN or WiFi (IEEE 802.11a/g/n/p), wireless MAN or WiMAX (IEEE 802.16), mobile broadband wireless access (MBWA) (IEEE 802.16e mobile WiMAX), wireless regional area networks (WRAN) (IEEE 802.22), and the cellular land mobile radio [3GPP Long Term Evolution (LTE) air interface named High Speed OFDM Packet Access (HSOPA)], among others.

OFDM is a block modulation scheme where data symbols are transmitted in parallel on orthogonal subcarriers. A block of N data symbols, with symbol period T_s, is converted into a block of N parallel data symbols, each of duration $T = NT_s$. The N parallel data symbols modulate N subcarriers that are spaced in frequency $1/T$ Hz apart. The OFDM complex envelope is given by

$$\tilde{s}(t) = A \sum_n b(t - nT, \mathbf{x}_n), \tag{4.85}$$

where

$$b(t, \mathbf{x}_n) = u_T(t) \sum_{k=0}^{N-1} x_{n,k} e^{j\frac{2\pi kt}{T}} \tag{4.86}$$

n is the block index, k is the subcarrier index, N is the number of subcarriers, and $\mathbf{x}_n = \{x_{n,0},\ x_{n,1},\ \ldots,\ x_{n,N-1}\}$ is the data symbol block at epoch n.

The data symbols $x_{n,k}$ are usually chosen from a QAM or PSK signal constellation, although any 2-D signal constellation can be used. The $1/T$ Hz frequency separation of the subcarriers ensures that the corresponding waveforms transmitted on the N subcarriers are mutually orthogonal regardless of the random phases that are imparted by the random data symbols $x_{n,k}$ (see Problem 4.7).

A cyclic extension (or guard interval) is usually added to the OFDM waveform in (4.85) and (4.86) to combat intersymbol interference (ISI) as explained in Sect. 10.1 of Chap. 10. The cyclic extension can be in the form of either a cyclic prefix or a cyclic suffix. With a cyclic suffix, the OFDM complex envelope becomes

$$\tilde{s}_g(t) = \begin{cases} \tilde{s}(t) & ,\ 0 \le t < T \\ \tilde{s}(t-T) & ,\ T \le t < (1+\alpha_g)T \end{cases}, \tag{4.87}$$

where $\alpha_g T$ is the length of the guard interval and $\tilde{s}(t)$ is defined in (4.85) and (4.86). The OFDM waveform with cyclic suffix can be rewritten in the standard form

$$\tilde{s}_g(t) = A \sum_n b(t - nT_g, \mathbf{x}_n), \tag{4.88}$$

where

$$b(t, \mathbf{x}_n) = u_T(t) \sum_{k=0}^{N-1} x_{n,k} e^{j\frac{2\pi kt}{T}} + u_{\alpha_g T}(t - T) \sum_{k=0}^{N-1} x_{n,k} e^{j\frac{2\pi k(t-T)}{T}}, \tag{4.89}$$

and $T_g = (1 + \alpha_g)T$ is the OFDM symbol period with addition of the guard interval. Likewise, with a cyclic prefix, the OFDM complex envelope becomes

$$\tilde{s}_g(t) = \begin{cases} \tilde{s}(t+T) & , \ -\alpha_g T \le t < 0 \\ \tilde{s}(t) & , \ 0 \le t < T \end{cases}, \tag{4.90}$$

and

$$b(t, \mathbf{x}_n) = u_{\alpha_g T}(t + \alpha_g T) \sum_{k=0}^{N-1} x_{n,k} \mathrm{e}^{j\frac{2\pi k(t+T)}{T}} + u_T(t) \sum_{k=0}^{N-1} x_{n,k} \mathrm{e}^{j\frac{2\pi kt}{T}}. \tag{4.91}$$

4.6.1 DFT-Based OFDM Baseband Modulator

A key advantage of using OFDM is that the baseband modulator can be implemented by using an inverse discrete-time Fourier transform (IDFT). In practice, the computationally efficient inverse fast Fourier transform (IFFT) algorithm is used to implement the IDFT. Consider the OFDM complex envelope defined by (4.85) and (4.86). During the interval $nT \le t < (n+1)T$, the complex envelope has the form

$$\begin{aligned} \tilde{s}(t) &= A u_T(t - nT) \sum_{k=0}^{N-1} x_{n,k} \mathrm{e}^{\frac{j2\pi k(t-nT)}{T}} \\ &= A u_T(t - nT) \sum_{k=0}^{N-1} x_{n,k} \mathrm{e}^{\frac{j2\pi kt}{NT_s}}, \quad nT \le t < (n+1)T. \end{aligned} \tag{4.92}$$

Now suppose that the complex envelope in (4.92) is sampled at synchronized T_s second intervals beginning at time nT to yield the sample sequence

$$X_{n,m} = \tilde{s}(mT_s) = A \sum_{k=0}^{N-1} x_{n,k} \mathrm{e}^{\frac{j2\pi km}{N}}, \quad m = 0,\ 1,\ \ldots,\ N-1. \tag{4.93}$$

Observe that the vector $\mathbf{X}_n = \{X_{n,m}\}_{m=0}^{N-1}$ is the IDFT of the vector $A\mathbf{x}_n = A\{x_{n,k}\}_{k=0}^{N-1}$. Contrary to conventional notation, with OFDM it is customary that the lowercase vector $A\mathbf{x}_n$ represents the frequency domain coefficients, as the vector $\mathbf{x}_n$ is the vector of data symbols, while the uppercase vector $\mathbf{X}_n$ represents the IDFT time domain coefficients.

As mentioned earlier, a cyclic extension (or guard interval) is usually added to the OFDM waveform as described in (4.88) and (4.89) to combat ISI. When a cyclic suffix is used, the corresponding sample sequence is

$$X_{n,m}^g = X_{n,(m)_N} \tag{4.94}$$

$$= A \sum_{k=0}^{N-1} x_{n,k} \mathrm{e}^{\frac{j2\pi km}{N}}, \quad m = 0,\ 1,\ \ldots,\ N+G-1, \tag{4.95}$$

where G is the length of the guard interval in samples, and $(m)_N$ is the residue of m modulo N. This gives the vector $\mathbf{X}_n^g = \{X_{n,m}^g\}_{m=0}^{N+G-1}$, where the values in the first and last G coordinates of the vector $\mathbf{X}_n^g$ are the same. Likewise, when a cyclic prefix is used, the corresponding sample sequence is

$$X_{n,m}^g = X_{n,(m)_N} \tag{4.96}$$

$$= A \sum_{k=0}^{N-1} x_{n,k} \mathrm{e}^{\frac{j2\pi km}{N}}, \quad m = -G,\ \ldots, -1,\ 0,\ 1,\ \ldots,\ N-1. \tag{4.97}$$

This yields the vector $\mathbf{X}_n^g = \{X_{n,m}^g\}_{m=-G}^{N-1}$, where again the first and last G coordinates of the vector $\mathbf{X}_n^g$ are the same. The sample interval after insertion of the guard interval, T_s^g, is compressed in time such that $(N+G)T_s^g = NT_s$.

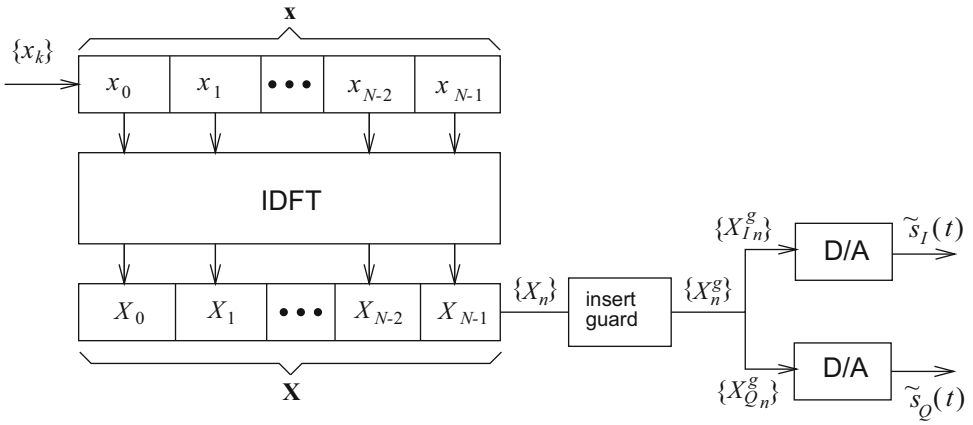

Fig. 4.14 Block diagram of IDFT-based baseband OFDM modulator with guard interval insertion and digital-to-analog conversion

The OFDM complex envelope can be generated by splitting the complex-valued output vector $\mathbf{X}_m$ into its real and imaginary parts, $\mathrm{Re}(\mathbf{X}_n)$ and $\mathrm{Im}(\mathbf{X}_n)$, respectively. The sequences $\{\mathrm{Re}(X_{n,m})\}$ and $\{\mathrm{Im}(X_{n,m})\}$ are then input to a pair of balanced digital-to-analog converters (DACs) to generate the real and imaginary components $\tilde{s}_I(t)$ and $\tilde{s}_Q(t)$, respectively, of the complex envelope $\tilde{s}(t)$, during the time interval $nT \leq t < (n+1)T$. As shown in Fig. 4.14, the OFDM baseband modulator consists of an IDFT operation, followed by guard interval insertion and digital-to-analog conversion.

It is instructive at this stage to note that the waveform generated by using the IDFT OFDM baseband modulator is *not exactly* the same as the waveform generated from the analog waveform definition of OFDM. Consider for example, the OFDM waveform without a cyclic guard in (4.85) and (4.86). The analog waveform definition uses the rectangular amplitude shaping pulse $u_T(t)$ that is strictly time-limited to T seconds. As shown in Sect. 4.9.6, the corresponding power spectrum has infinite bandwidth. Consequently, sampling the complex envelope with any finite sampling rate will lead to aliasing and imperfect reconstruction.

With the IDFT OFDM baseband modulator, the IDFT outputs are applied to a pair of balanced DACs as explained earlier. However, the ideal DAC is an ideal low pass filter with cutoff frequency $1/(2T_s)$, with a corresponding non-causal impulse response $h(t) = \mathrm{sinc}(t/T_s)$. Since the ideal DAC is non-realizable, a causal, finite-length reconstruction filter must be used instead. However, such a filter will necessarily generate a waveform that is not strictly bandlimited. In conclusion, the side lobe structure of the analog waveform definition of OFDM is inherent in the waveform due to rectangular amplitude pulse shaping, whereas the side lobe structure with the IDFT implementation is introduced by the non-ideal (practical) DAC.

Finally, non-rectangular amplitude pulse shaping can be used with OFDM and may yield a more compact power spectrum while still maintaining sub-channel orthogonality. However, such pulse shaping will require an extension of the OFDM symbol beyond T, or with guard interval T_g, seconds in the time domain. This will be discussed in more detail in Chap. 10.

4.6.2 Adaptive Bit Loading and Discrete Multitone Modulation

A wireless OFDM system generally operates over a frequency-selective fading channel with transfer function $T(t,f)$, such that the amplitude response $|T(t,f)|$ varies across the channel bandwidth W. The power spectral density of the additive noise impairment $S_{nn}(f)$ may vary with frequency as well due to the presence of interference. Consider a quasi-static fading channel, such that the channel remains constant over an OFDM block of duration T seconds. For convenience, the time variable t is suppressed with the understanding that $T(t,f) \equiv T(f)$ over an OFDM block, but the channel may change from block to block. Furthermore, knowledge of the channel is assumed to be available at the transmitter. Shannon [300] proved that the capacity of a frequency-selective channel with additive Gaussian noise is achieved when the transmitted power $\Omega_t(f)$ is adjusted across the bandwidth W_s according to

$$\Omega_t(f) = \begin{Bmatrix} K - S_{nn}(f)/|T(f)|^2\,, & f \in W_s \\ 0\,, & f \notin W_s \end{Bmatrix}, \tag{4.98}$$

where K is a constant chosen to satisfy the constraint

$$\int_{W_s} \Omega_t(f)\mathrm{d}f \leq \Omega_{\mathrm{av}}, \tag{4.99}$$

and Ω_{av} is the average available power to the transmitter. One method to achieve capacity is to divide the bandwidth W_s into N sub-bands of width W_s/Δ_f, where $\Delta_f = 1/T$ is chosen small enough so that $|T(f)|^2/S_{nn}(f)$ is approximately constant within each sub-band. The signals in each sub-band may then be transmitted with the optimum power allocation $\Omega_t(f)$, while being individually coded to achieve capacity.

It is clear from (4.86) that the data symbols $x_{n,k}$ for fixed n modulate the nth subcarrier. From (4.98), the transmitter power should be high when $|T(f)|^2/S_{nn}(f)$ is large and small when $T(f)/S_{nn}(f)$ is small. In a practical system, a higher transmit power admits the use of a larger size signal constellation in sub-bands where $|T(f)|^2/S_{nn}(f)$ is large, and vice versa. The technique whereby different sized signal constellations are used on the different OFDM subcarriers is sometimes called adaptive bit loading or discrete multitone modulation (DMT).

4.6.3 Multiresolution Modulation

In broadcasting applications, it is sometimes desirable to transmit video or audio information in frames that will simultaneously provide different resolutions, depending on the received signal-to-noise ratio. Low resolution information is typically of high priority (HP) and must be received with high reliability. High resolution information, on the other hand, is typically of low priority (LP) and may be received with a lower reliability. The solution is multi-resolution modulation (MRM), a class of modulation techniques that transmit multiple resolutions in a simultaneous or concurrent fashion, that differ in their bit rates and/or error probabilities. MRM can be implemented in OFDM schemes by using multiplexed, interleaved, embedded signal constellations, and others.

Multiplexed MRM divides the OFDM band into subsets of contiguous subcarriers, for example the upper half subcarriers may be used to transmit HP data symbols and the lower half subcarriers used to transmit an equal number of LP data symbols. The HP low resolution information can be transmitted by using a smaller signal constellation and/or higher transmit power for further robustness and reliability. Likewise, the LP high resolution information can be transmitted using a larger signal constellation and/or lower transmit power. Broadcast service contours can be established for either high definition (both the HP and LP data streams are decodable) or standard definition (only the HP data stream is decodable) reception.

Interleaved MRM interleaves the different resolutions onto the subcarriers in a cyclic fashion. If there are K different resolutions, then subcarriers $\ell, \ell + K, \ell + 2K, \ldots$, are assigned to the ℓth resolution. Each resolution is then transmitted by using a different sized signal constellation and/or transmit power level.

Embedded MRM is more subtle and relies upon the use of an asymmetric signal constellation and finds application in some broadcast video systems. Figure 4.15 shows an example of a 16-QAM embedded MRM signal constellation, that can be used to simultaneously transmit two different resolutions. In Fig. 4.15, two HP low resolution bits are used to select the quadrant of the transmitted signal point, while two low LP high resolution bits are used to select the signal point within the selected quadrant. The relative error probability or reliability between the two priorities is controlled by the parameter $\lambda = d^l/d^h, \lambda \leq 0.5$, where d^l is the distance between LP symbols and d^h is the distance between the centroids of the HP symbols. The upper limit on λ is due to the fact that the MRM constellation becomes a symmetric 16-QAM constellation when $\lambda = 0.5$. As λ becomes smaller than 0.5, more power is allocated to the HP low resolution bits than the LP high resolution bits. For broadcasting applications, this can be used to provide high definition reception over some adjustable fraction of the service area where standard definition service can be received. At $\lambda = 0.5$, both resolution classes are treated equally and the coverage areas for standard and high definition service are the same.

4.7 Continuous Phase Modulation

Continuous phase modulation (CPM) refers to a broad class of frequency modulation techniques where the carrier phase varies in a continuous manner. A comprehensive treatment of CPM is provided by Anderson et al. [17]. CPM schemes are attractive because they have constant envelope and excellent spectral characteristics, i.e., a narrow main lobe and fast roll-off of sidelobes. CPM waveforms find application in satellite communication systems, and cellular telephone systems notably GSM.

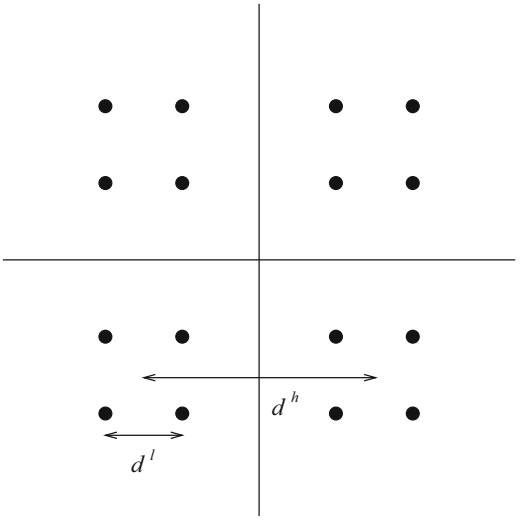

Fig. 4.15 16-QAM embedded MRM signal constellation with two resolutions

The complex envelope of a CPM waveform has the general form

$$\tilde{s}(t) = Ae^{j(\phi(t)+\theta_o)}, \tag{4.100}$$

where A is the amplitude, θ_o is the initial carrier phase at $t = 0$, and

$$\phi(t) = 2\pi h \int_0^t \sum_{k=0}^{\infty} x_k h_f(\tau - kT)\mathrm{d}\tau \tag{4.101}$$

is the excess phase, where h is the modulation index, $\{x_k\}$ is the data symbol sequence, $h_f(t)$ is the frequency shaping pulse, and T is the baud period. The CPM waveform can be written in the standard form

$$\tilde{s}(t) = A \sum_n b(t - nT, \mathbf{x}_n) \tag{4.102}$$

where

$$b(t, \mathbf{x}_n) = e^{j2\pi h \int_0^t \sum_{k=0}^{\infty} x_k h_f(\tau - kT)\mathrm{d}\tau} u_T(t) \tag{4.103}$$

where $\mathbf{x}_n = (x_n, x_{n-1}, \ldots, x_0)$, and an initial phase $\theta_o = 0$ at $t = 0$ is assumed. CPM waveforms have the following properties:

- The data symbols are chosen from the alphabet $\{\pm 1, \pm 3, \cdots, \pm(M-1)\}$, where M is the modulation alphabet size.
- h is the modulation index and is directly proportional to the peak and/or average frequency deviation from the carrier. The instantaneous frequency deviation from the carrier is

$$f_{\mathrm{dev}}(t) = \frac{1}{2\pi}\frac{\mathrm{d}\phi(t)}{\mathrm{d}t} = h\sum_{k=0}^{\infty} x_k h_f(t - kT). \tag{4.104}$$

- $h_f(t)$ is the frequency shaping function, that is zero for $t < 0$ and $t > LT$, and normalized to integrate to 1/2. Full response CPM has $L = 1$, while partial response CPM has $L > 1$. Some possible frequency shaping pulses are shown in Table 4.1. A more compact power density spectrum is usually obtained by using frequency shaping functions having continuous higher-order derivatives, such as the raised cosine pulse in Table 4.1. The excess phase is continuous provided that the frequency shaping function $h_f(t)$ does not contain impulses, which is true for all CPM waveforms. When describing CPM waveforms, it is useful to define the phase shaping function,

Table 4.1 CPM frequency shaping functions

Pulse type	$h_f(t)$
L-rectangular (LREC)	$\frac{1}{2LT} u_{LT}(t)$
L-raised cosine (LRC)	$\frac{1}{2LT}\left[1-\cos\left(\frac{2\pi t}{LT}\right)\right] u_{LT}(t)$
L-half sinusoid (LHS)	$\frac{\pi}{4LT}\sin(\pi t/LT) u_{LT}(t)$
L-triangular (LTR)	$\frac{1}{LT}\left(1-\frac{\lvert t-LT/2\rvert}{LT/2}\right) u_{LT}(t)$

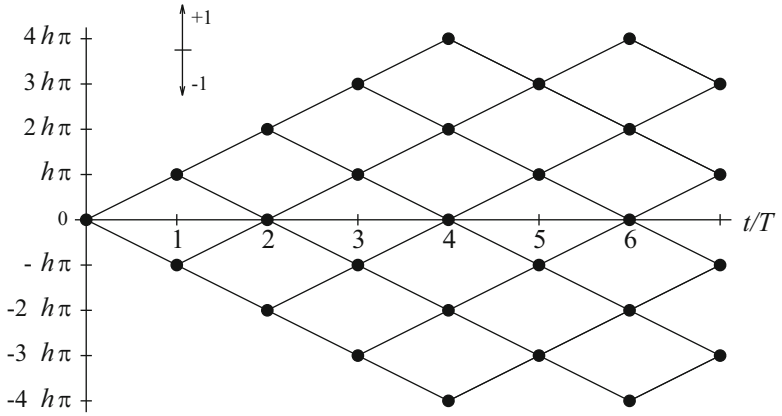

Fig. 4.16 Phase tree of binary CPFSK with an arbitrary modulation index. CPFSK is characterized by linear excess phase trajectories

$$\beta(t) = \begin{cases} 0 & , \ t < 0 \\ \int_0^t h_f(\tau)\mathrm{d}\tau & , \ 0 \le t \le LT \\ 1/2 & , \ t \ge LT \end{cases}, \tag{4.105}$$

which is the integral of the frequency shaping pulse. An infinite variety of CPM waveforms can be generated by choosing different frequency shaping pulses, modulation indices, and modulation alphabet sizes.

4.7.1 Full Response CPM

For a full response CPM waveform with $L = 1$, the shaping function in (4.103) has the form

$$b(t, \mathbf{x}_n) = \mathrm{e}^{j\left(\pi h \sum_{k=0}^{n-1} x_k + 2\pi h x_n \beta(t)\right)} u_T(t). \tag{4.106}$$

The first term in the exponent of (4.106) represents the accumulated excess phase up to time nT, while the second term represents the excess phase increment during the time interval $nT \le t < (n+1)T$.

Continuous phase frequency shift keying (CPFSK) is a special type of full response CPM characterized by the rectangular frequency shaping function LREC with $L = 1$. For CPFSK

$$\beta(t) = \begin{cases} 0 & , \ t < 0 \\ t/2T & , \ 0 \le t < T \\ 1/2 & , \ t \ge T \end{cases}. \tag{4.107}$$

CPM signals can be visualized by sketching the evolution of the excess phase $\phi(t)$ for all possible data sequences. This plot is called a phase tree, and a typical phase tree is shown in Fig. 4.16 for binary CPFSK. Since the CPFSK frequency shaping function is rectangular, the excess phase trajectories are linear as suggested by (4.107). In each baud interval, T, the excess phase increases by πh if the data symbol is $+1$ and decreases by πh if the data symbol is -1.

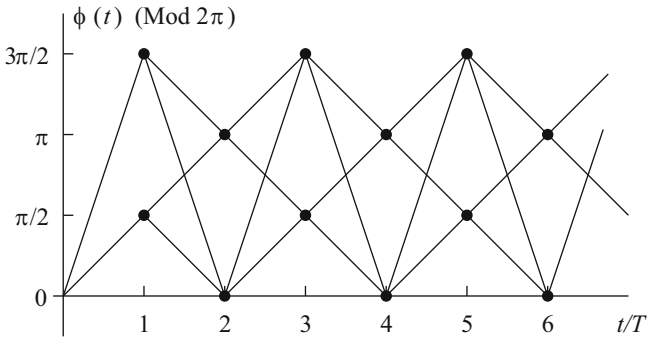

Fig. 4.17 Phase-trellis for MSK

4.7.1.1 Minimum Shift Keying

Minimum shift keying (MSK) is binary CPFSK with modulation index $h = 1/2$. In this case,

$$b(t, \mathbf{x}_n) = \mathrm{e}^{j\left(\frac{\pi}{2}\sum_{k=0}^{n-1} x_k + \frac{\pi}{2} x_n \frac{t}{T}\right)} u_T(t). \tag{4.108}$$

The MSK waveform can be described in terms of the phase tree as shown in Fig. 4.16 with $h = 1/2$. At the end of each symbol interval the excess phase $\phi(t)$ takes on values that are integer multiples of $\pi/2$. Since excess phases that differ by integer multiples of 2π are indistinguishable, the values taken by $\phi(t)$ at the end of each symbol interval belong to the finite set $\{0, \pi/2, \pi, 3\pi/2\}$. The MSK phase tree reduced modulo 2π yields the MSK phase trellis shown in Fig. 4.17.

An interesting property of MSK can be observed from the MSK bandpass waveform. The bandpass waveform on the interval $nT \le t < (n+1)T$ can be obtained from (4.108) as

$$\begin{aligned} s(t) &= A\cos\left(2\pi f_c t + \frac{\pi}{2}\sum_{k=0}^{n-1} x_k + \frac{\pi}{2} x_n \frac{t - nT}{T}\right) \\ &= A\cos\left(2\pi\left(f_c + \frac{x_n}{4T}\right)t + \frac{\pi}{2}\sum_{k=0}^{n-1} x_k - \frac{\pi n}{2} x_n\right). \end{aligned} \tag{4.109}$$

Observe that the MSK bandpass waveform has one of two possible frequencies in each baud interval, given by

$$f_L = f_c - \frac{1}{4T} \qquad \text{and} \qquad f_U = f_c + \frac{1}{4T} \tag{4.110}$$

depending on the data symbol x_n. The difference between these two frequencies is $f_U - f_L = 1/(2T)$. This is the minimum frequency separation to ensure orthogonality between two co-phased sinusoids of duration T (Problem 4.7) and, hence, the name *minimum* shift keying.

Another interesting representation for MSK waveforms can be obtained by using Laurent's decomposition [193] (detailed in Sect. 4.8.3) to express the MSK complex envelope in the quadrature form

$$\tilde{s}(t) = A\sum_n b(t - 2nT, \mathbf{x}_n), \tag{4.111}$$

where

$$b(t, \mathbf{x}_n) = \hat{x}_{2n+1} h_a(t - T) + j\hat{x}_{2n} h_a(t) \tag{4.112}$$

and where $\mathbf{x}_n = (\hat{x}_{2n+1}, \hat{x}_{2n})$,

$$\hat{x}_{2n} = \hat{x}_{2n-1} x_{2n} \tag{4.113}$$

$$\hat{x}_{2n+1} = -\hat{x}_{2n} x_{2n+1} \tag{4.114}$$

$$\hat{x}_{-1} = 1 \tag{4.115}$$

and

$$h_a(t) = \sin\left(\frac{\pi t}{2T}\right) u_{2T}(t). \tag{4.116}$$

The sequences, $\{\hat{x}_{2n}\}$ and $\{\hat{x}_{2n+1}\}$, are independent binary symbol sequences taking on elements from the set $\{-1, +1\}$. The symbols $\hat{x}_{2n}$ and $\hat{x}_{2n+1}$ are transmitted on the quadrature branches with a half-sinusoid (HS) amplitude shaping pulse of duration $2T$ seconds and an offset of T seconds. Hence, MSK is equivalent to offset quadrature amplitude shift keying (OQASK) with HS amplitude pulse shaping. This linear representation of MSK is useful in practice for simplified linear detection of MSK waveforms as discussed in Sect. 5.10.1 of Chap. 5.

4.8 Partial Response CPM

Partial response CPM signals have a frequency shaping pulse $h_f(t)$ with duration LT, where $L > 1$. Partial response CPM signals typically have better spectral characteristics than full response CPM signals, i.e., a narrower main lobe and faster roll-off of side lobes.

The partial response frequency shaping function can be written as

$$\begin{aligned} h_f(t) &= \sum_{k=0}^{L-1} h_f(t) u_T(t - kT) \\ &= \sum_{k=0}^{L-1} h_{f,k}(t - kT), \end{aligned} \tag{4.117}$$

where

$$h_{f,k}(t) = h_f(t + kT) u_T(t). \tag{4.118}$$

Likewise, the partial response phase shaping function can be written as

$$\beta(t) = \sum_{k=0}^{L-1} \beta_k(t - kT), \tag{4.119}$$

where

$$\beta_k(t) = \beta(t + kT) u_T(t). \tag{4.120}$$

Note that

$$\beta_k(t) = \begin{cases} 0 & , \ t < 0 \\ \int_0^t h_{f,k}(\tau) \mathrm{d}\tau & , \ 0 \le t < LT \\ \beta_k(T) & , \ t \ge T \end{cases} \tag{4.121}$$

and

$$\sum_{k=0}^{L-1} \beta_k(T) = \frac{1}{2}. \tag{4.122}$$

An equivalent frequency shaping function of duration T can be derived by noting that the CPM baseband modulating signal has the form

$$\begin{aligned} x(t) &= \sum_n x_n h_f(t - nT) \\ &= \sum_n \sum_{k=0}^{L-1} x_n h_{f,k}(t - (n+k)T) \\ &= \sum_m \sum_{k=0}^{L-1} x_{m-k} h_{f,k}(t - mT). \end{aligned} \tag{4.123}$$

It follows that

$$x(t) = \sum_m h_f(t - mT, \mathbf{x}_m), \tag{4.124}$$

where

$$h_f(t, \mathbf{x}_m) = \sum_{k=0}^{L-1} x_{m-k} h_{f,k}(t) \tag{4.125}$$

and

$$x(t) = \sum_m \beta(t - mT, \mathbf{x}_m), \tag{4.126}$$

where

$$\beta(t, \mathbf{x}_m) = \sum_{k=0}^{L-1} x_{m-k} \beta_k(t) \tag{4.127}$$

and

$$\mathbf{x}_m = (x_m,\ x_{m-1},\ \ldots,\ x_{m-L+1})\,. \tag{4.128}$$

Finally, the complex envelope of partial response CPM signal can be written in the standard form

$$\tilde{s}(t) = A \sum_n b(t - nT, \mathbf{x}_n) \tag{4.129}$$

where

$$b(t, \mathbf{x}_n) = \mathrm{e}^{j2\pi h\left(\sum_{i=0}^{n-1} \beta(T, \mathbf{x}_i) + \beta(t, \mathbf{x}_n)\right)} u_T(t) \tag{4.130}$$

and an initial excess phase of zero is assumed.

Example 4.2. Consider a partial response CPM waveform with an LREC frequency shaping function. In this case

$$h_f(t) = \frac{1}{2LT} u_{LT}(t).$$

(continued)

Example 4.2 (continued)
Hence,

$$h_f(t, \mathbf{x}_n) = x_n h_{f,0}(t) + x_{n-1} h_{f,1}(t) + \cdots + x_{n-L+1} h_{f,L-1}(t),$$

where

$$h_{f,0}(t) = h_{f,1}(t) = \cdots = h_{f,L-1}(t) = \frac{1}{2LT} u_T(t).$$

Therefore,

$$h_f(t, \mathbf{x}_n) = (x_n + x_{n-1} + \cdots + x_{n-L+1}) \frac{1}{2LT} u_T(t).$$

Example 4.3. Consider a partial response CPM waveform with an LRC frequency shaping function. In this case

$$h_f(t) = \frac{1}{2LT} \left(1 - \cos\left(\frac{2\pi t}{LT}\right)\right) u_{LT}(t).$$

Hence,

$$h_f(t, \mathbf{x}_n) = x_n h_{f,0}(t) + x_{n-1} h_{f,1}(t) + \cdots + x_{n-L} h_{f,L-1}(t),$$

where

$$h_{f,k}(t) = \left(1 - \cos\left(\frac{2\pi(t + kT)}{LT}\right)\right) u_T(t).$$

4.8.1 Phase States

The excess phase of a partial response CPM waveform on the interval $nT \le t < (n+1)T$ is

$$\phi(t) = 2\pi h \int_0^t \sum_{k=0}^{n} x_k h_f(\tau - kT) \mathrm{d}\tau \tag{4.131}$$

$$= \pi h \sum_{k=0}^{n-L} x_k + 2\pi h \sum_{k=n-L+1}^{n} x_k \beta(t - kT) \tag{4.132}$$

$$= \theta_n + 2\pi h \sum_{k=n-L+1}^{n} x_k \beta(t - kT) \tag{4.133}$$

where

$$\theta_n = \pi h \sum_{k=0}^{n-L} x_k \qquad \text{modulo } 2\pi \tag{4.134}$$

is the accumulated phase. During the interval $nT \leq t < (n+1)T$, the excess phase depends on the input data symbol x_n, the vector of $L-1$ previous data symbols, $\{x_{n-1}, x_{n-2}, \ldots, x_{n-L+1}\}$, and the accumulated phase θ_n. The state of the CPM signal at time $t = nT$, is defined by the L-tuple

$$S_n = (\theta_n, x_{n-1}, x_{n-2}, \ldots, x_{n-L+1}). \tag{4.135}$$

Since the vector $(x_{n-1}, x_{n-2}, \ldots, x_{n-L+1})$ can take on M^{L-1} values, the number of states equals M^{L-1} times the number of values that θ_n can assume.

The modulation index is often restricted to be a rational number, $h = m/p$, where m and p are integers that have no common factors. This constraint ensures that the number of phase states is finite which is a useful property for the implementation CPM receivers. If m is even, then

$$\theta_n \in \left\{0, \frac{\pi m}{p}, \frac{2\pi m}{p}, \cdots, \frac{(p-1)\pi m}{p}\right\} \tag{4.136}$$

while if m is odd

$$\theta_n \in \left\{0, \frac{\pi m}{p}, \frac{2\pi m}{p}, \ldots, \frac{(2p-1)\pi m}{p}\right\}. \tag{4.137}$$

Hence, there are p phase states for even m, while there are $2p$ phase states for odd m. In conclusion, the number of CPM states is

$$|S_n| = \begin{cases} pM^{L-1}, & m \text{ even} \\ 2pM^{L-1}, & m \text{ odd} \end{cases}. \tag{4.138}$$

For example, if $h = 1/4$, $M = 4$, and $L = 2$, then

$$\theta_n \in \left\{0, \frac{\pi}{4}, \frac{\pi}{2}, \frac{3\pi}{4}, \pi, \frac{5\pi}{4}, \frac{3\pi}{2}, \frac{7\pi}{4}\right\} \tag{4.139}$$

and the number of CPM states is 32.

CPM waveforms cannot be described in terms of a signal-space diagram, like QAM and PSK waveforms. However, the CPM waveform can be described in terms of the trajectories from one phase state to another. Figures 4.18 and 4.19 show the phase state diagrams for MSK and binary CPM with $h = 1/4$, respectively. Since binary modulation is used, trajectories are only allowed between adjacent phase states as shown by the dotted lines in the figures. Since the CPM waveforms have constant envelope, the complex phaser trajectories will follow along the circle in Figs. 4.18 and 4.19.

4.8.2 Gaussian Minimum Shift Keying

Due to their non-linearity, CPM waveforms have a relatively complicated power spectrum as detailed in Sect. 4.9.7. However, the bandwidth of a CPM waveform can be approximated using Carson's rule developed for analog frequency modulation:

$$BW = (W + f_{\text{peak}}), \tag{4.140}$$

where W is the bandwidth of the frequency shaping pulse $h_f(t)$ and f_{peak} is the peak frequency deviation from the carrier. MSK waveforms have relatively poor spectral characteristics due to the large bandwidth W of the rectangular frequency pulse shaping $h_f(t) = \frac{1}{2T} u_T(t)$. A more compact power spectrum can be achieved by low-pass filtering the MSK modulating signal

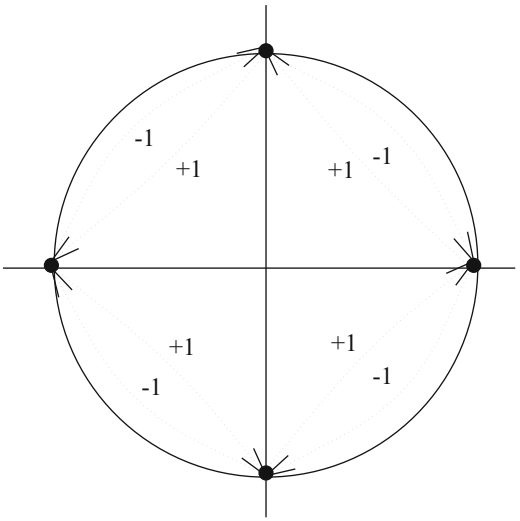

Fig. 4.18 Phase state diagram for MSK

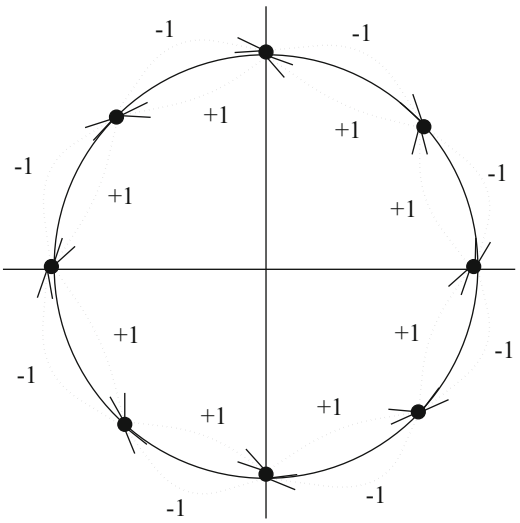

Fig. 4.19 Phase state diagram for binary CPM with $h = 1/4$

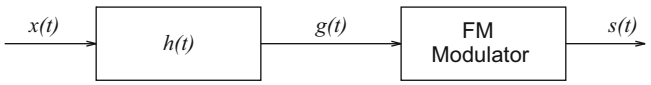

Fig. 4.20 Pre-modulation filtered MSK. The MSK modulating signal is low-pass filtered to remove the high frequency components prior to frequency modulation

$$x(t) = \sum_{n=-\infty}^{\infty} x_n h_f(t - nT) = \frac{1}{2T} \sum_{n=-\infty}^{\infty} x_n u_T(t - nT) \tag{4.141}$$

prior to frequency modulation as shown in Fig. 4.20. Such filtering suppresses the higher frequency components in $x(t)$ thus yielding a more compact power spectrum. Gaussian minimum shift keying (GMSK) is a special type of partial response CPM that uses a low-pass premodulation filter having the transfer function [234]

$$H(f) = \exp\left\{-\left(\frac{f}{B}\right)^2 \frac{\ln 2}{2}\right\}, \tag{4.142}$$

where B is the 3 dB bandwidth of the filter. It is apparent that $H(f)$ is shaped like a Gaussian probability density function with mean $f = 0$ and, hence, the name "Gaussian" MSK. Convolving the rectangular pulse

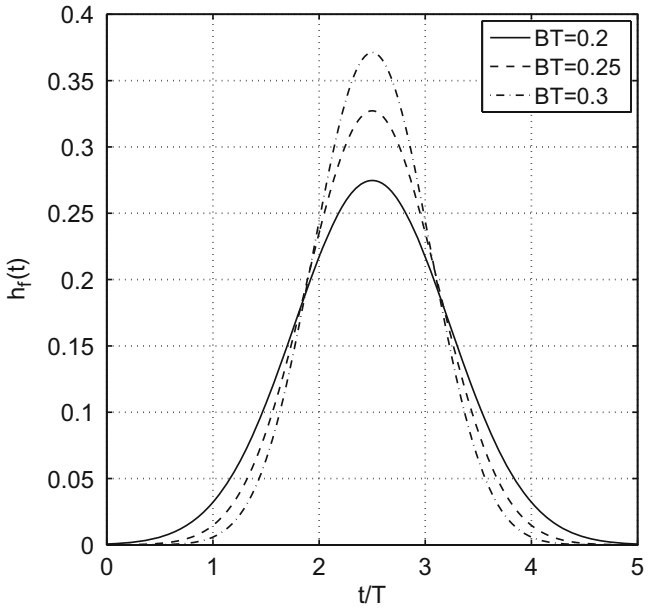

Fig. 4.21 GMSK frequency shaping pulse for various normalized premodulation filter bandwidths BT

$$\frac{1}{2T}\text{rect}(t/T) = \frac{1}{2T}u_T(t + T/2)$$

with the corresponding filter impulse response $h(t)$ yields the frequency shaping pulse

$$\begin{aligned} h_f(t) &= \frac{1}{2T}\sqrt{\frac{2\pi}{\ln 2}}(BT)\int_{t/T-1/2}^{t/T+1/2}\exp\left\{-\frac{2\pi^2(BT)^2x^2}{\ln 2}\right\}\,\mathrm{d}x \\ &= \frac{1}{2T}\left(Q\left(\frac{t/T-1/2}{\sigma}\right) - Q\left(\frac{t/T+1/2}{\sigma}\right)\right), \end{aligned} \tag{4.143}$$

where

$$Q(\alpha) = \int_{\alpha}^{\infty}\frac{1}{\sqrt{2\pi}}\mathrm{e}^{-x^2/2}\mathrm{d}x \tag{4.144}$$

$$\sigma^2 = \frac{\ln 2}{4\pi^2(BT)^2}. \tag{4.145}$$

Figure 4.21 plots the GMSK frequency shaping pulse (truncated to $5T$ and time shifted by $2.5T$ to yield a causal pulse) for various normalized premodulation filter bandwidths BT. The GSM cellular standard uses GMSK with $BT = 0.3$.

The phase shaping function is the integral of the frequency shaping function as defined in (4.105). Using $h_f(t)$ in (4.143), and integrating by parts, yields

$$\beta(t) = \int_{-\infty}^{t} h_f(t)\mathrm{d}t = \frac{1}{2}\left(G\left(\frac{t}{T}+\frac{1}{2}\right) - G\left(\frac{t}{T}-\frac{1}{2}\right)\right), \tag{4.146}$$

where

$$G(x) = x\,\Phi\left(\frac{x}{\sigma}\right) + \frac{\sigma}{\sqrt{2\pi}}\mathrm{e}^{-\frac{x^2}{2\sigma^2}}, \tag{4.147}$$

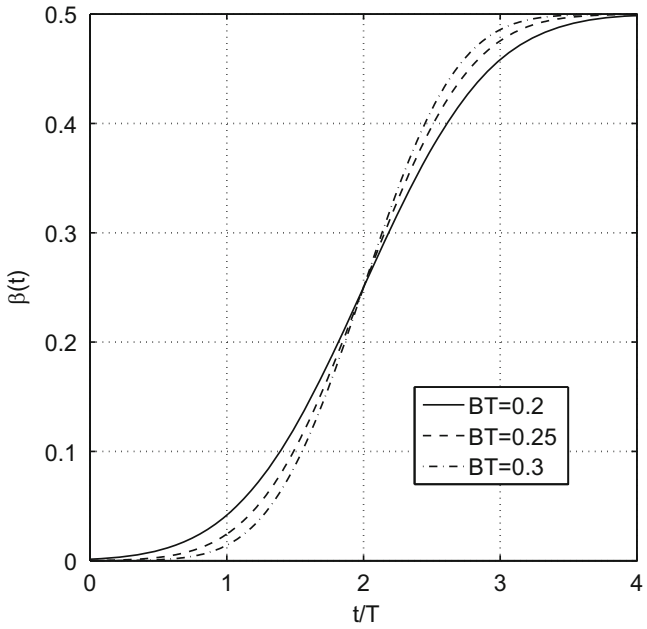

Fig. 4.22 GMSK phase shaping pulse for various normalized premodulation filter bandwidths BT

and

$$\Phi(\alpha) = \int_{-\infty}^{\alpha} \frac{1}{\sqrt{2\pi}} \mathrm{e}^{-x^2/2} \mathrm{d}x. \tag{4.148}$$

Figure 4.22 plots the GMSK phase shaping pulse (truncated to $4T$ and time shifted by $2T$ to yield a causal pulse) for $BT = 0.3$. Observe that $\beta(\infty) = 1/2$ and, therefore, the total contribution to the excess phase for each data symbol remains at $\pm\pi/2$.

The change in excess phase over the length-T baud interval from $-T/2$ to $T/2$ is

$$\phi(T/2) - \phi(-T/2) = \pi x_0 \beta_0(T) + \pi \sum_{\substack{n=-\infty \\ n\neq 0}}^{\infty} x_n \beta_n(T), \tag{4.149}$$

where

$$\beta_n(T) = \int_{-T/2-nT}^{T/2-nT} h_f(\tau) \mathrm{d}\tau. \tag{4.150}$$

The first term in (4.149) is the desired term, and the second term is the intersymbol interference (ISI) introduced by the Gaussian premodulation filter. While the premodulation filter will yield a more compact power spectrum, the induced ISI will degrade the bit error rate performance and may necessitate an equalizer in the receiver. However, the induced ISI is not severe and in many cases, including GSM cellular receivers, an equalizer is required anyway to combat the ISI due to channel delay spread.

4.8.3 Linearized GMSK (LGMSK)

Like all other CPM waveforms, GMSK is a nonlinear waveform. Similar to the linearized representation of MSK in Sect. 4.7.1.1, it is desirable to find a linearized representation for GMSK in order to simplify receiver processing. Several linear approximations have been suggested in the literature for GMSK. Here, an approximation based on Laurent's decomposition [193] is considered. Laurent showed that any binary partial response CPM signal can be represented exactly as a linear combination of 2^{L-1} partial-response pulse amplitude modulated (PAM) signals, viz.,

$$\tilde{s}(t) = \sum_{n=0}^{\infty} \sum_{p=0}^{2^{L-1}-1} \mathrm{e}^{j\pi h \alpha_{n,p}} c_p(t - nT), \tag{4.151}$$

where

$$c_p(t) = c(t) \prod_{n=1}^{L-1} c\left(t + (n + L\varepsilon_{n,p})T\right) \tag{4.152}$$

$$\alpha_{n,p} = \sum_{m=0}^{n} x_m - \sum_{m=1}^{L-1} x_{n-m}\varepsilon_{m,p} \tag{4.153}$$

and $\varepsilon_{n,p} \in \{0, 1\}$ are the coefficients of the binary representation of the index p, i.e.,

$$p = \varepsilon_{0,p} + 2\varepsilon_{1,p} + \cdots + 2^{L-2}\varepsilon_{L-2,p}. \tag{4.154}$$

The basic signal pulse $c(t)$ in (4.152) is

$$c(t) = \begin{cases} \frac{\sin(2\pi h\beta(t))}{\sin \pi h} & , \ 0 \le t < LT \\ \frac{\sin(\pi h - 2\pi h\beta(t-LT))}{\sin \pi h} & , \ LT \le t < 2LT \\ 0 & , \ \text{otherwise} \end{cases}, \tag{4.155}$$

where $\beta(t)$ is the CPM phase shaping function.

The above linear decomposition will yield an exact representation of the GMSK waveform. However, the fact that 2^{L-1} pulses are needed to represent the waveform means that the optimum coherent receiver will need 2^{L-1} filters that are matched to the set of 2^{L-1} pulses $\{c_p(t)\}$. Usually, the number of matched filters can be reduced to $K < 2^{L-1}$ when a good approximation to the CPM signal can be obtained with K of the set of 2^{L-1} pulses $\{c_p(t)\}$. Often the pulse $c_0(t)$ contains most of the signal energy, so the $p = 0$ term in (4.151) can provide a good approximation to the CPM signal. From Fig. 4.21, observe that the GMSK frequency shaping pulse spans approximately $L = 4$ symbol periods for practical values of BT. This means that the GMSK waveform can be constructed from the superposition of eight pulses, $c_p(t), p = 0, \ldots, 7$. Numerical analysis shows that, with $BT = 0.3$, the pulse $c_0(t)$ contains 99.83% of the energy and, therefore, a linearized GMSK waveform can be derived by using only $c_0(t)$ and neglecting the other pulses. This yields the waveform

$$\tilde{s}(t) = \sum_{n=0}^{\infty} \mathrm{e}^{j\pi h \alpha_{n,o}} c_0(t - nT), \tag{4.156}$$

where, with $L = 4$,

$$c_0(t) = \prod_{n=0}^{3} c\left(t + nT\right) \tag{4.157}$$

$$\alpha_{n,0} = \sum_{m=0}^{n} x_m. \tag{4.158}$$

Since the GMSK phase shaping pulse is non-causal, when evaluating $c(t)$ in (4.155) the truncated and time shifted GMSK phase shaping pulse

$$\hat{\beta}(t) = \beta(t - 2T) \tag{4.159}$$

is used with $L = 4$ as shown in Fig. 4.22, where $\beta(t)$ is defined in (4.146). Figure 4.23 plots the resulting LGMSK amplitude shaping pulse $c_0(t)$ obtained from (4.157).

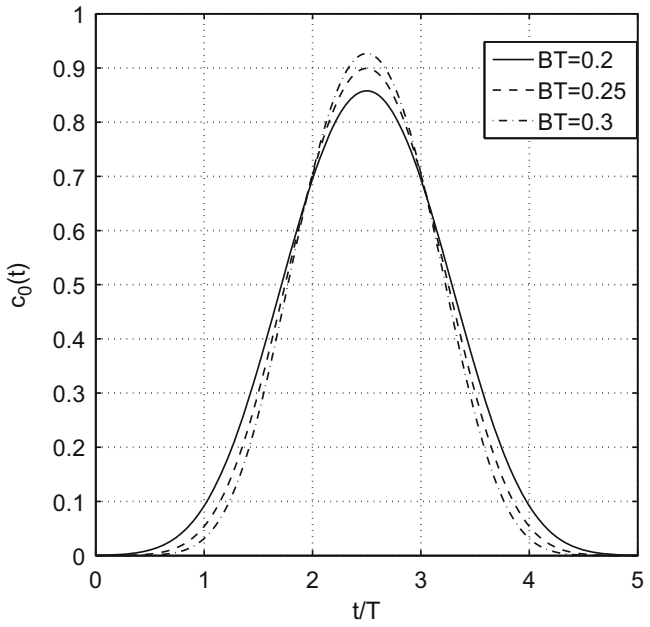

Fig. 4.23 LGMSK amplitude shaping pulse for various normalized premodulation filter bandwidths BT

For the modulation index $h = 1/2$ used in GMSK,

$$a_{n,0} = \mathrm{e}^{j\frac{\pi}{2}\alpha_{n,0}} \in \{\pm 1, \pm j\}, \tag{4.160}$$

and it follows that

$$\tilde{s}(t) = A \sum_n \left(\hat{x}_{2n+1} c_0(t - 2nT - T) + j\hat{x}_{2n} c_0(t - 2nT) \right), \tag{4.161}$$

where

$$\hat{x}_{2n} = \hat{x}_{2n-1} x_{2n} \tag{4.162}$$

$$\hat{x}_{2n+1} = -\hat{x}_{2n} x_{2n+1} \tag{4.163}$$

$$\hat{x}_{-1} = 1. \tag{4.164}$$

This is the same as the OQPSK representation for MSK in Sect. 4.7.1.1, except that the half-sinusoid amplitude pulse shaping function in (4.116) is replaced with the LGMSK amplitude pulse shaping function defined in (4.157). Note that the LGMSK pulse has length of approximately $4T$, while the pulses on the quadrature branches are transmitted every $2T$ seconds. Therefore, the LGMSK pulse will introduce ISI that must be corrected by an equalizer to avoid a performance degradation as mentioned earlier. However, as shown in Sect. 4.9.8, GMSK has excellent spectral properties.

4.8.4 Tamed Frequency Modulation

Tamed frequency modulation (TFM) is a special type of partial response binary CPM that was introduced by de Jager and Dekker [91]. TFM also has excellent spectral properties, similar to GMSK. To define TFM waveforms, recall that the MSK excess phase obeys the difference equation

$$\phi(nT + T) - \phi(nT) = \frac{\pi}{2} x_n. \tag{4.165}$$

The TFM excess phase trajectory is "smoothed" by imposing the constraint

$$\phi(nT+T)-\phi(nT)=\frac{\pi}{2}\left(\frac{x_{n-1}}{4}+\frac{x_n}{2}+\frac{x_{n+1}}{4}\right), \tag{4.166}$$

such that the maximum change in excess phase over any bit interval is $\pi/2$. To complete the definition of the TFM signal, an appropriate frequency shaping pulse $h_f(t)$ must be defined. The TFM excess phase can be written as

$$\phi(t)=\pi\sum_{k=0}^{\infty}x_k\beta(t-kT), \tag{4.167}$$

where

$$\beta(t)=\int_0^t h_f(t)\mathrm{d}t \tag{4.168}$$

and where a modulation index $h=1/2$ is assumed. The excess phase change over the time interval $[nT,(n+1)T]$ is

$$\begin{aligned}\phi((n+1)T)-\phi(nT)&=\pi\sum_{k=0}^{\infty}x_k\left(\beta(nT+T-kT)-\beta(nT-kT)\right)\\&=\pi\sum_{\ell=n}^{\infty}x_{n-\ell}\left(\beta(\ell T+T)-\beta(\ell T)\right).\end{aligned} \tag{4.169}$$

Expanding (4.166) in more detail gives

$$\phi(nT+T)-\phi(nT)=\frac{\pi}{2}\left(\cdots+x_{n-2}\cdot 0+\frac{x_{n-1}}{4}+\frac{x_n}{2}+\frac{x_{n+1}}{4}+x_{n+2}\cdot 0+\cdots\right). \tag{4.170}$$

Comparing (4.169) and (4.170) gives the condition

$$\beta((\ell+1)T)-\beta(\ell T)=\begin{cases}1/8\ , & |\ell|=1\\ 1/4\ , & \ell=0\\ 0\ , & \text{otherwise}\end{cases}. \tag{4.171}$$

From the definition of $\beta(t)$ in (4.168) the above equation leads to

$$\int_{\ell T}^{(\ell+1)T}h_f(t)\mathrm{d}t=\begin{cases}1/8\ , & |\ell|=1\\ 1/4\ , & \ell=0\\ 0\ , & \text{otherwise}\end{cases}. \tag{4.172}$$

One way of obtaining $h_f(t)$ is to use a pulse $h_N(t)$ that satisfies Nyquist's third criterion [244, 258]

$$\int_{(2\ell-1)T/2}^{(2\ell+1)T/2}h_N(t)\mathrm{d}t=\begin{cases}1\ , & \ell=0\\ 0\ , & \ell\neq 0\end{cases} \tag{4.173}$$

and generate $h_f(t)$ by using scaling and delay operations through the filter shown in Fig. 4.24. The transfer function of this filter is

$$\begin{aligned}H(f)&=\frac{1}{4}+\frac{1}{8}\mathrm{e}^{-j2\pi fT}+\frac{1}{8}\mathrm{e}^{j2\pi fT}\\&=\frac{1}{2}\cos^2(\pi fT).\end{aligned} \tag{4.174}$$

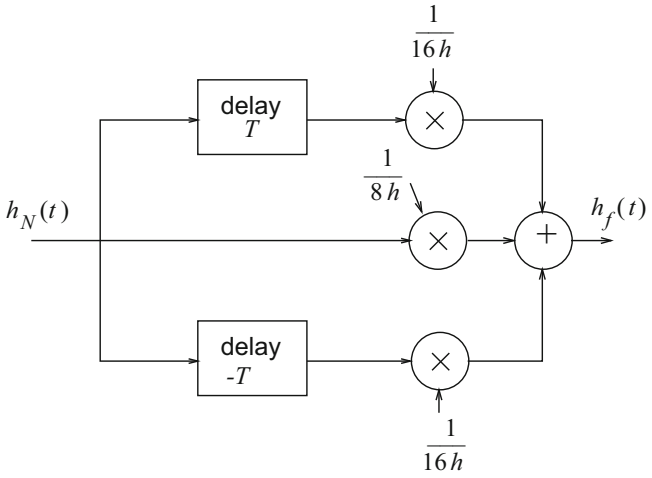

Fig. 4.24 Filter to generate a TFM frequency shaping pulse

The overall pulse $h_f(t)$ has the form

$$\begin{aligned} H_f(f) &= H_N(f)H(f) \\ &= H_N(f)\frac{1}{2}\cos^2(\pi fT). \end{aligned} \tag{4.175}$$

The filter $H(f)$ ensures that the phase constraint in (4.166) is satisfied. However, $H_N(f)$ determines the shape of the phase trajectories and can, therefore, influence the TFM power density spectrum. In general, $H_N(f)$ has the form

$$H_N(f) = \frac{\pi fT}{\sin(\pi fT)}N_1(f), \tag{4.176}$$

where $N_1(f)$ is the Fourier transform of a pulse that satisfies Nyquist's first criterion [244, 258]. One example of such a pulse is the raised cosine pulse $P(f)$ defined in (4.47). Consider, for example, the ideal Nyquist pulse (raised cosine pulse with $\beta = 0$)

$$N_1(f) = \begin{cases} 1\,, & 0 \le |f| \le 1/2T \\ 0\,, & \text{otherwise} \end{cases}. \tag{4.177}$$

Using (4.175)–(4.177) gives

$$H_f(f) = \begin{cases} \frac{1}{2}\frac{\pi fT}{\sin(\pi fT)}\cos^2(\pi fT)\,, & 0 \le |f| \le 1/2T \\ 0\,, & \text{otherwise} \end{cases}. \tag{4.178}$$

The corresponding frequency shaping pulse $h_f(t)$ is plotted in Fig. 4.25. Note the close similarity to the GMSK frequency shaping pulse in Fig. 4.21.

Generalized TFM (GTFM) is an extension of TFM where the phase difference has the form

$$\phi(nT+T) - \phi(nT) = \frac{\pi}{2}\left(ax_{n-1} + bx_n + ax_{n+1}\right). \tag{4.179}$$

The constants a and b satisfy the condition $2a + b = 1$ so that the maximum change in excess phase during one bit period is equal to $\pm\pi/2$. A large variety of waveforms can be constructed by varying the value of b and the pulse response $N_1(f)$ in (4.176). TFM is a special case of GTFM where $b = 0.5$.

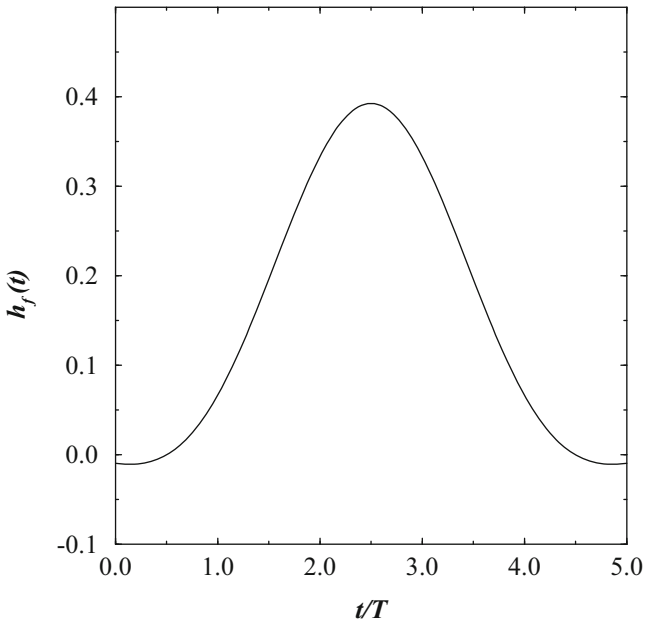

Fig. 4.25 TFM frequency shaping pulse

4.9 Power Spectrum

A digitally modulated bandpass waveform can be written in the generic form

$$\begin{aligned} s(t) &= \mathrm{Re}\left\{\tilde{s}(t)\mathrm{e}^{j2\pi f_c t}\right\} \\ &= \frac{1}{2}\left\{\tilde{s}(t)\mathrm{e}^{j2\pi f_c t} + \tilde{s}^*(t)\mathrm{e}^{-j2\pi f_c t}\right\}. \end{aligned} \tag{4.180}$$

Modulated waveforms belong to the class of cyclostationary or periodic wide-sense stationary random processes. The autocorrelation function of $s(t)$ is

$$\begin{aligned} \phi_{ss}(\tau) &= \mathrm{E}\left[s(t)s(t+\tau)\right] \\ &= \frac{1}{4}\mathrm{E}\left[\left(\tilde{s}(t)\mathrm{e}^{j2\pi f_c t} + \tilde{s}^*(t)\mathrm{e}^{-j2\pi f_c t}\right)\left(\tilde{s}(t+\tau)\mathrm{e}^{j(2\pi f_c t + 2\pi f_c \tau)} + \tilde{s}^*(t+\tau)\mathrm{e}^{-j(2\pi f_c t + 2\pi f_c \tau)}\right)\right] \\ &= \frac{1}{4}\left[\mathrm{E}[\tilde{s}(t)\tilde{s}(t+\tau)]\mathrm{e}^{j(4\pi f_c t + 2\pi f_c \tau)} + \mathrm{E}[\tilde{s}(t)\tilde{s}^*(t+\tau)]\mathrm{e}^{-j2\pi f_c \tau}\right. \\ &\quad \left. + \mathrm{E}[\tilde{s}^*(t)\tilde{s}(t+\tau)]\mathrm{e}^{j2\pi f_c \tau} + \mathrm{E}[\tilde{s}^*(t)\tilde{s}^*(t+\tau)]\mathrm{e}^{-j(4\pi f_c t + 2\pi f_c \tau)}\right]. \end{aligned} \tag{4.181}$$

If $s(t)$ is a wide-sense stationary random process, then the exponential terms that involve the time variable t must vanish, i.e., $\mathrm{E}[\tilde{s}(t)\tilde{s}(t+\tau)] = 0$ and $\mathrm{E}[\tilde{s}^*(t)\tilde{s}^*(t+\tau)] = 0$. Substituting $\tilde{s}(t) = \tilde{s}_I(t) + j\tilde{s}_Q(t)$ into these two expectations gives the requirement

$$\phi_{\tilde{s}_I\tilde{s}_I}(\tau) = \mathrm{E}[\tilde{s}_I(t)\tilde{s}_I(t+\tau)] = \mathrm{E}[\tilde{s}_Q(t)\tilde{s}_Q(t+\tau)] = \phi_{\tilde{s}_Q\tilde{s}_Q}(\tau) \tag{4.182}$$

$$\phi_{\tilde{s}_I\tilde{s}_Q}(\tau) = \mathrm{E}[\tilde{s}_I(t)\tilde{s}_Q(t+\tau)] = -\mathrm{E}[\tilde{s}_Q(t)\tilde{s}_I(t+\tau)] = -\phi_{\tilde{s}_Q\tilde{s}_I}(\tau). \tag{4.183}$$

Using these results,

$$\phi_{ss}(\tau) = \frac{1}{2}\phi_{\tilde{s}\tilde{s}}(\tau)\mathrm{e}^{j2\pi f_c \tau} + \frac{1}{2}\phi^*_{\tilde{s}\tilde{s}}(\tau)\mathrm{e}^{-j2\pi f_c \tau} \tag{4.184}$$

$$= \mathrm{Re}\left\{\phi_{\tilde{s}\tilde{s}}(\tau)\mathrm{e}^{j2\pi f_c \tau}\right\}, \tag{4.185}$$

where

$$\begin{aligned}\phi_{\tilde{s}\tilde{s}}(\tau) &= \frac{1}{2}\mathrm{E}\left[\tilde{s}^*(t)\tilde{s}(t+\tau)\right] \\ &= \phi_{\tilde{s}_I\tilde{s}_I}(\tau) + j\phi_{\tilde{s}_I\tilde{s}_Q}(\tau)\end{aligned} \tag{4.186}$$

Finally, the power density spectrum is the Fourier transform of $\phi_{ss}(\tau)$ in (4.184), i.e.,

$$S_{ss}(f) = \frac{1}{2}\Big(S_{\tilde{s}\tilde{s}}(f-f_c) + S^*_{\tilde{s}\tilde{s}}(-f-f_c)\Big) \tag{4.187}$$

where $S_{\tilde{s}\tilde{s}}(f)$ is the power density spectrum of the complex envelope $\tilde{s}(t)$. Note that $S_{\tilde{s}\tilde{s}}(f)$ is real though not necessarily even, although $\tilde{s}(t)$ and $\phi_{\tilde{s}\tilde{s}}(\tau)$ are complex-valued; this property follows from the fact that $\phi_{\tilde{s}\tilde{s}}(\tau) = \phi^*_{\tilde{s}\tilde{s}}(-\tau)$ as shown in Appendix A. It follows that

$$S_{ss}(f) = \frac{1}{2}\Big(S_{\tilde{s}\tilde{s}}(f-f_c) + S_{\tilde{s}\tilde{s}}(-f-f_c)\Big). \tag{4.188}$$

From the above expression, observe that the psd of the bandpass waveform $s(t)$ is real and even, and is completely determined by the psd of its complex envelope $\tilde{s}(t)$ and the carrier frequency f_c.

4.9.1 Psd of the Complex Envelope

The complex envelope of any digitally modulated signal can be expressed in the standard form

$$\tilde{s}(t) = A\sum_n b(t-nT, \mathbf{x}_n). \tag{4.189}$$

The autocorrelation of $\tilde{s}(t)$ is

$$\begin{aligned}\phi_{\tilde{s}\tilde{s}}(t, t+\tau) &= \frac{1}{2}\mathrm{E}\left[\tilde{s}^*(t)\tilde{s}(t+\tau)\right] \\ &= \frac{A^2}{2}\sum_i\sum_k \mathrm{E}\left[b^*(t-iT, \mathbf{x}_i)b(t+\tau-kT, \mathbf{x}_k)\right].\end{aligned} \tag{4.190}$$

Observe that $\tilde{s}(t)$ is a cyclostationary random process, meaning that the autocorrelation function $\phi_{\tilde{s}\tilde{s}}(t, t+\tau)$ is periodic in t with period T. To see this property, first note that

$$\begin{aligned}&\phi_{\tilde{s}\tilde{s}}(t+T, t+T+\tau) \\ &\quad= \frac{A^2}{2}\sum_i\sum_k \mathrm{E}\left[b^*(t+T-iT, \mathbf{x}_i)b(t+T+\tau-kT, \mathbf{x}_k)\right] \\ &\quad= \frac{A^2}{2}\sum_{i'}\sum_{k'} \mathrm{E}\left[b^*(t-i'T, \mathbf{x}_{i'+1})b(t+\tau-k'T, \mathbf{x}_{k'+1})\right].\end{aligned} \tag{4.191}$$

Under the assumption that the information sequence is a stationary random process it follows that

$$\begin{aligned}\phi_{\tilde{s}\tilde{s}}(t+T, t+T+\tau) &= \frac{A^2}{2}\sum_{i'}\sum_{k'} \mathrm{E}\left[b^*(t-i'T, \mathbf{x}_{i'})b(t+\tau-k'T, \mathbf{x}_{k'})\right] \\ &= \phi_{\tilde{s}\tilde{s}}(t, t+\tau).\end{aligned} \tag{4.192}$$

Therefore $\tilde{s}(t)$ is cyclostationary.

Since $\tilde{s}(t)$ is cyclostationary, the autocorrelation $\phi_{\tilde{s}\tilde{s}}(\tau)$ can be obtained by taking the time average of $\phi_{\tilde{s}\tilde{s}}(t+\tau, t)$, given by

$$\begin{aligned}
\phi_{\tilde{s}\tilde{s}}(\tau) &= \langle \phi_{\tilde{s}\tilde{s}}(t, t+\tau) \rangle \\
&= \frac{A^2}{2} \sum_i \sum_k \frac{1}{T} \int_0^T \mathrm{E}\left[b^*(t - iT, \mathbf{x}_i) b(t + \tau - kT, \mathbf{x}_k) \right] \mathrm{d}t \\
&= \frac{A^2}{2T} \sum_i \sum_k \int_{-iT}^{-iT+T} \mathrm{E}\left[b^*(z, \mathbf{x}_i) b(z + \tau - (k-i)T, \mathbf{x}_k) \right] \mathrm{d}z \\
&= \frac{A^2}{2T} \sum_i \sum_m \int_{-iT}^{-iT+T} \mathrm{E}\left[b^*(z, \mathbf{x}_i) b(z + \tau - mT, \mathbf{x}_{m+i}) \right] \mathrm{d}z \\
&= \frac{A^2}{2T} \sum_i \sum_m \int_{-iT}^{-iT+T} \mathrm{E}\left[b^*(z, \mathbf{x}_0) b(z + \tau - mT, \mathbf{x}_m) \right] \mathrm{d}z \\
&= \frac{A^2}{2T} \sum_m \int_{-\infty}^{\infty} \mathrm{E}\left[b^*(z, \mathbf{x}_0) b(z + \tau - mT, \mathbf{x}_m) \right] \mathrm{d}z,
\end{aligned} \tag{4.193}$$

where $\langle \cdot \rangle$ denotes time averaging and the second last equality used the stationary property of the data sequence $\{x_k\}$. The psd of $\tilde{s}(t)$ is obtained by taking the Fourier transform of $\phi_{\tilde{s}\tilde{s}}(\tau)$,[2]

$$\begin{aligned}
S_{\tilde{s}\tilde{s}}(f) &= \mathrm{E}\left[\frac{A^2}{2T} \sum_m \int_{-\infty}^{\infty} \int_{-\infty}^{\infty} b^*(z, \mathbf{x}_0) b(z + \tau - mT, \mathbf{x}_m) \mathrm{d}z \mathrm{e}^{-j2\pi f \tau} \mathrm{d}\tau \right] \\
&= \mathrm{E}\left[\frac{A^2}{2T} \sum_m \int_{-\infty}^{\infty} b^*(z, \mathbf{x}_0) \mathrm{e}^{j2\pi f z} \mathrm{d}z \int_{-\infty}^{\infty} b(z + \tau - mT, \mathbf{x}_m) \mathrm{e}^{-j2\pi f (z+\tau-mT)} \mathrm{d}\tau \mathrm{d}z \mathrm{e}^{-j2\pi f m T} \right] \\
&= \mathrm{E}\left[\frac{A^2}{2T} \sum_m \int_{-\infty}^{\infty} b^*(z, \mathbf{x}_0) \mathrm{e}^{j2\pi f z} \mathrm{d}z \int_{-\infty}^{\infty} b(\tau', \mathbf{x}_m) \mathrm{e}^{-j2\pi f \tau'} \mathrm{d}\tau' \mathrm{e}^{-j2\pi f m T} \right] \\
&= \frac{A^2}{2T} \sum_m \mathrm{E}\left[B^*(f, \mathbf{x}_0) B(f, \mathbf{x}_m) \right] \mathrm{e}^{-j2\pi f m T},
\end{aligned} \tag{4.194}$$

where $B(f, \mathbf{x}_m)$ is the Fourier transform of $b(t, \mathbf{x}_m)$. To express the power density spectrum in a more convenient form, let

$$S_{b,m}(f) = \frac{1}{2} \mathrm{E}\left[B^*(f, \mathbf{x}_0) B(f, \mathbf{x}_m) \right]. \tag{4.195}$$

Then

$$S_{\tilde{s}\tilde{s}}(f) = \frac{A^2}{T} \sum_m S_{b,m}(f) \mathrm{e}^{-j2\pi f m T}. \tag{4.196}$$

Note that the psd in (4.196) depends on the correlation properties of the information sequence $\mathbf{x}_m$ and the form of the generalized pulse shaping function $b(t, \mathbf{x}_m)$. Now suppose that the data characteristics are such that $\mathbf{x}_m$ and $\mathbf{x}_0$ are independent for $|m| \geq K$. Then

$$S_{b,m}(f) = S_{b,K}(f), \quad |m| \geq K, \tag{4.197}$$

[2]Note that expectation and integration are linear operations and their order can be exchanged.

where

$$\begin{aligned} S_{b,K}(f) &= \frac{1}{2}\mathrm{E}\left[B^*(f,\mathbf{x}_0)\right]\mathrm{E}\left[B(f,\mathbf{x}_m)\right] \\ &= \frac{1}{2}\mathrm{E}\left[B^*(f,\mathbf{x}_0)\right]\mathrm{E}\left[B(f,\mathbf{x}_0)\right] \\ &= \frac{1}{2}\left|\mathrm{E}\left[B(f,\mathbf{x}_0)\right]\right|^2 \ , \quad |m| \geq K. \end{aligned} \tag{4.198}$$

It follows that

$$S_{\widetilde{ss}}(f) = S^c_{\widetilde{ss}}(f) + S^d_{\widetilde{ss}}(f), \tag{4.199}$$

where

$$\begin{aligned} S^c_{\widetilde{ss}}(f) &= \frac{A^2}{T}\sum_{|m|<K}\Big(S_{b,m}(f) - S_{b,K}(f)\Big)\mathrm{e}^{-j2\pi fmT} \\ S^d_{\widetilde{ss}}(f) &= \frac{A^2}{T}S_{b,K}(f)\sum_m \mathrm{e}^{-j2\pi fmT}. \end{aligned} \tag{4.200}$$

The terms $S^c_{\widetilde{ss}}(f)$ and $S^d_{\widetilde{ss}}(f)$ represent the continuous and discrete (line) portions of the psd. The fact that $S^d_{\widetilde{ss}}(f)$ represents the discrete portion can be seen more clearly by using the identity

$$T\sum_m \mathrm{e}^{-j2\pi fmT} = \sum_n \delta\left(f - \frac{n}{T}\right) \tag{4.201}$$

to write

$$S^d_{\widetilde{ss}}(f) = \left(\frac{A}{T}\right)^2 S_{b,K}(f)\sum_n \delta\left(f - \frac{n}{T}\right). \tag{4.202}$$

Finally, by using the property $S_{b,-m}(f) = S^*_{b,m}(f)$, the continuous portion of the psd can be written as

$$\begin{aligned} S^c_{\widetilde{ss}}(f) &= \frac{A^2}{T}\Big(S_{b,0}(f) - S_{b,K}(f)\Big) + \frac{A^2}{T}\sum_{m=1}^{K}\Big(\left(S_{b,m}(f) - S_{b,K}(f)\right)\mathrm{e}^{-j2\pi fmT} + \left(S^*_{b,m}(f) - S_{b,K}(f)\right)\mathrm{e}^{j2\pi fmT}\Big) \\ &= \frac{A^2}{T}\Big(S_{b,0}(f) - S_{b,K}(f)\Big) + \frac{A^2}{T}2\mathrm{Re}\left\{\sum_{m=1}^{K}\Big(S_{b,m}(f) - S_{b,K}(f)\Big)\mathrm{e}^{-j2\pi fmT}\right\}. \end{aligned} \tag{4.203}$$

Note that the ensemble average and Fourier transform are interchangeable linear operators. Therefore, if the complex envelope $\tilde{s}(t)$ has zero mean, i.e., $\mathrm{E}[b(t,\mathbf{x}_0)] = 0$, then $\mathrm{E}[B(f,\mathbf{x}_0)] = 0$. Under this condition

$$S_{b,K}(f) = \frac{1}{2}\left|\mathrm{E}[B(f,\mathbf{x}_0)]\right|^2 = 0. \tag{4.204}$$

Hence, if $b(t,\mathbf{x}_0)$ has zero mean, then $S_{\widetilde{ss}}(f)$ contains no discrete components and $S_{\widetilde{ss}}(f) = S^c_{\widetilde{ss}}(f)$. Conversely, if $b(t,\mathbf{x}_0)$ has non-zero mean, then $S_{\widetilde{ss}}(f)$ will contain discrete (line) components. Another important case arises with uncorrelated zero-mean data, where $S_{b,K}(f) = 0$, $K = 1$. In this case, only the term $S_{b,0}(f)$ remains and

$$S_{\widetilde{ss}}(f) = \frac{A^2}{T}S_{b,0}(f) \tag{4.205}$$

where

$$S_{b,0}(f) = \frac{1}{2}\mathrm{E}\left[|B(f,\mathbf{x}_0)|^2\right]. \tag{4.206}$$

4.9.1.1 Alternative Method

An alternative method of computing the psd is as follows. From the first line in (4.194)

$$S_{\widetilde{s}\widetilde{s}}(f) = \mathrm{E}\left[\frac{A^2}{2T}\sum_m \int_{-\infty}^{\infty}\int_{-\infty}^{\infty} b(z,\mathbf{x}_0)b^*(z+\tau-mT,\mathbf{x}_m)\mathrm{d}z\mathrm{e}^{-j2\pi f\tau}\mathrm{d}\tau\right]$$
$$= \frac{A^2}{2T}\sum_m \int_{-\infty}^{\infty}\int_{-\infty}^{\infty} \mathrm{E}\left[b(z,\mathbf{x}_0)b^*(\tau',\mathbf{x}_m)\right]\mathrm{e}^{-j2\pi f(\tau'-z)}\mathrm{d}z\mathrm{d}\tau'\mathrm{e}^{-j2\pi fmT}. \tag{4.207}$$

Therefore, $S_{b,m}(f)$ is given by the double Fourier transform

$$S_{b,m}(f) = \int_{-\infty}^{\infty}\int_{-\infty}^{\infty} \phi_{b,m}(z,\tau')\mathrm{e}^{-j2\pi f(\tau'-z)}\mathrm{d}z\mathrm{d}\tau'. \tag{4.208}$$

where

$$\phi_{b,m}(z,\tau') = \frac{1}{2}\mathrm{E}\left[b(z,\mathbf{x}_0)b^*(\tau',\mathbf{x}_m)\right]. \tag{4.209}$$

4.9.1.2 Linear Full Response Modulation

Consider linear full response modulation schemes where $b(t,\mathbf{x}_n) = x_n h_a(t)$ and $B(f,\mathbf{x}_n) = x_n H_a(f)$. In general, the data sequence $\{x_n\}$ will be correlated with autocorrelation function $\phi_{xx}(m)$. From (4.195),

$$S_{b,m}(f) = \phi_{xx}(m)\left|H_a(f)\right|^2, \tag{4.210}$$

where

$$\phi_{xx}(m) = \frac{1}{2}\mathrm{E}[x_k^* x_{k+m}]. \tag{4.211}$$

Hence, from (4.196) the psd of the complex envelope is

$$S_{\widetilde{s}\widetilde{s}}(f) = \frac{A^2}{T}\left|H_a(f)\right|^2 S_{xx}(f), \tag{4.212}$$

where

$$S_{xx}(f) = \sum_m \phi_{xx}(m)\mathrm{e}^{-j2\pi fmT}. \tag{4.213}$$

Note that the psd is the product of two components; one depends on the squared magnitude of the amplitude shaping function and the other depends on the correlation of the data sequence. With uncorrelated data symbols

$$S_{b,0}(f) = \sigma_x^2\left|H_a(f)\right|^2 \tag{4.214}$$

$$S_{b,m}(f) = \frac{1}{2}\left|\mu_x\right|^2\left|H_a(f)\right|^2, \quad |m| \geq 1. \tag{4.215}$$

where $\mu_x = \mathrm{E}[x_m]$ and $\sigma_x^2 = \frac{1}{2}\mathrm{E}[|x_k|^2]$ are the mean and variance of the data symbols, respectively. The psd $S_{\widetilde{s}\widetilde{s}}(f)$ is then given by (4.199), where

$$S^d(f) = \frac{A^2}{T^2}S_{b,1}(f)\sum_n \delta\left(f-\frac{n}{T}\right) \tag{4.216}$$

$$S^c(f) = \frac{A^2}{T}\left(S_{b,0}(f) - S_{b,1}(f)\right). \tag{4.217}$$

If $\mu_x = 0$, then $S_{b,1}(f) = 0$ and the psd has the simple form

$$S_{\overline{ss}}(f) = \frac{A^2}{T}\sigma_x^2 \left|H_a(f)\right|^2. \tag{4.218}$$

In this case, the psd only depends on the amplitude shaping pulse $h_a(t)$.

4.9.1.3 Linear Partial Response Modulation

Consider linear partial response modulation schemes where $h_a(t)$ has duration LT. Following the development in Sect. 4.8 the generalized shaping function has the form

$$\begin{aligned} b(t, \mathbf{x}_m) &= h_a(t, \mathbf{x}_m) \\ &= \sum_{k=0}^{L-1} x_{m-k} h_{a,k}(t), \end{aligned} \tag{4.219}$$

where

$$h_{a,k}(t) = h_a(t + kT)u_T(t). \tag{4.220}$$

Taking the Fourier transform of (4.219) gives

$$B(f, \mathbf{x}_m) = \sum_{k=0}^{L-1} x_{m-k} H_{a,k}(f). \tag{4.221}$$

From (4.195),

$$\begin{aligned} S_{b,m}(f) &= \frac{1}{2}\mathrm{E}\left[\sum_{\ell=0}^{L-1} x_{-\ell}^* H_{a,\ell}^*(f) \sum_{k=0}^{L-1} x_{m-k} H_{a,k}(f)\right] \\ &= \sum_{k=0}^{L-1}\sum_{\ell=0}^{L-1} \phi_{xx}(m-k+\ell) H_{a,\ell}^*(f) H_{a,k}(f). \end{aligned} \tag{4.222}$$

For the special case of uncorrelated zero-mean data symbols, $\phi_{xx}(m-k+\ell) = \sigma_x^2 \delta(m-k+\ell)$. Hence,

$$S_{b,m}(f) = \sigma_x^2 \sum_{\ell=0}^{L-1} H_{a,\ell}^*(f) H_{a,m+\ell}(f) \tag{4.223}$$

where

$$\sigma_x^2 = \frac{1}{2}\mathrm{E}[|x_0|^2]$$

is the variance of the data symbols.

Example 4.4 (Duobinary Signaling). For duobinary signaling, $L = 2$ and $h_{a,0}(t) = h_{a,1}(t) = \text{sinc}(t/T)$ and $H_{a,0}(f) = H_{a,1}(f) = T\text{rect}(fT)$, where

$$\text{rect}(fT) = \begin{cases} 1\,, & |f| \le \frac{1}{2T} \\ 0\,, & \text{elsewhere} \end{cases}.$$

With uncorrelated zero-mean data symbols

$$\begin{aligned} S_{b,m}(f) &= \frac{1}{2}\text{E}\left[\left(x_0^* H_{a,0}^*(f) + x_{-1}^* H_{a,1}^*(f)\right)\left(x_m H_{a,0}(f) + x_{m-1} H_{a,1}(f)\right)\right] \\ &= \begin{cases} 2\sigma_x^2 T^2 \text{rect}(fT) & , \ m = 0 \\ \sigma_x^2 T^2 \text{rect}(fT) & , \ |m| = 1 \\ 0 & , \ \text{otherwise} \end{cases} \end{aligned}$$

and from (4.196)

$$S_{\tilde{s}\tilde{s}}(f) = 2A^2 T\sigma_x^2 \cos^2(\pi fT)\text{rect}(fT). \tag{4.224}$$

Example 4.5 (Modified Duobinary Signaling). For modified duobinary signaling, $L = 3$ and $h_{a,0}(t) = h_{a,2}(t) = \text{sinc}(t/T)$ and $h_{a,1}(t) = 0$. With uncorrelated zero-mean data symbols,

$$S_{b,m}(f) = \begin{cases} 2\sigma_x^2 T^2 \text{rect}(fT) & , \ m = 0 \\ -\sigma_x^2 T^2 \text{rect}(fT) & , \ |m| = 2 \\ 0 & , \ \text{otherwise} \end{cases}$$

and from (4.196)

$$S_{\tilde{s}\tilde{s}}(f) = 2A^2 T\sigma_x^2 \sin^2(2\pi fT)\text{rect}(fT).$$

4.9.2 Psd of QAM

The psd of QAM with uncorrelated zero-mean data symbols is given by (4.218). If $h_a(t) = u_T(t)$, then

$$S_{\tilde{s}\tilde{s}}(f) = A^2 T\sigma_x^2 \left(\frac{\sin(\pi fT)}{\pi fT}\right)^2. \tag{4.225}$$

With root-raised cosine pulse shaping, $|H_a(f)|^2 = P(f)$ has the form defined in (4.47) with $h_a(t)$ in (4.50). The root-raised cosine pulse is non-causal. When the pulse is implemented as a digital FIR filter, it must be truncated to a finite length $\tau = LT$. This truncation produces the new pulse $\tilde{h}_a(t) = h_a(t)\text{rect}(t/LT)$. The Fourier transform of the truncated pulse $\tilde{h}_a(t)$ is $\tilde{H}_a(f) = H_a(f) * LT\text{sinc}(\pi fLT)$, where $*$ denotes the operation of convolution taken over the frequency variable f. The psd of QAM with the pulse $\tilde{h}_a(t)$ can again be obtained from (4.218) by simply replacing $H_a(f)$ with $\tilde{H}_a(f)$. As shown in Fig. 4.26, pulse truncation can lead to significant side lobe regeneration.

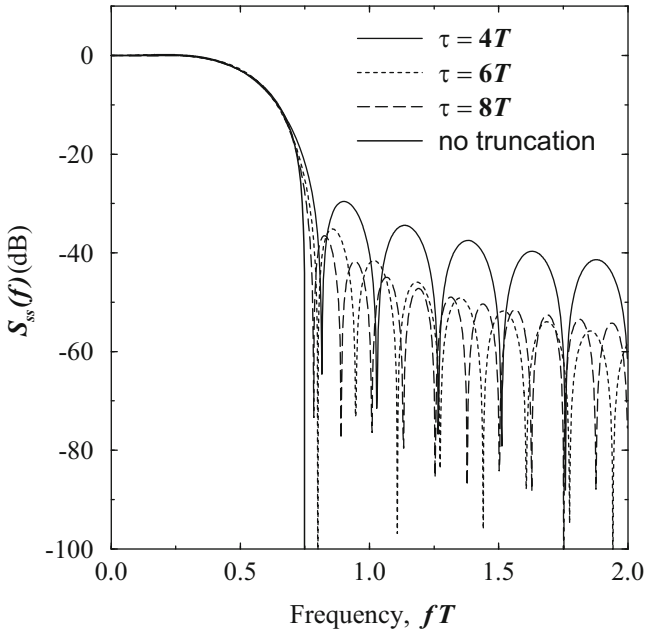

Fig. 4.26 Psd of QAM with a truncated square root-raised cosine amplitude shaping pulse with various truncation lengths; $\beta = 0.5$. Truncation of the amplitude shaping pulse leads to side lobe regeneration

4.9.3 Psd of PSK

For PSK signals with the uncorrelated data symbols and the generalized shaping function in (4.61), the psd is given by (4.218). Hence, PSK signals have the same psd as QAM signals. As such, the psd with truncated root-raised cosine amplitude pulse shaping is shown in Fig. 4.26.

4.9.4 Psd of OQPSK

For OQPSK, the generalized shaping function is

$$b(t, \mathbf{x}_n) = b(t, x_n) = x_{I,n} h_a(t) + j x_{Q,n} h_a(t - T/2) \tag{4.226}$$

where $x_{I,n}, x_{Q,n} \in \{-1/\sqrt{2}, +1/\sqrt{2}\}$. It follows that

$$B(f, \mathbf{x}_n) = \left(x_{I,n} + j x_{Q,n} \mathrm{e}^{-j2\pi f T/2}\right) H_a(f) \tag{4.227}$$

With uncorrelated data symbols,

$$\begin{aligned} S_{b,0}(f) &= \frac{1}{2} \mathrm{E}\left[|B(f, x_0)|^2\right] \\ &= \frac{1}{2} |H_a(f)|^2 \end{aligned} \tag{4.228}$$

Therefore,

$$S_{\widetilde{ss}}(f) = \frac{A^2}{2T} |H_a(f)|^2 \tag{4.229}$$

Hence, OQPSK has the same psd as QPSK. However, OQASK has a lower peak-to-average power ratio than QPSK.

4.9.5 Psd of $\pi/4$-DQPSK

To find the psd of $\pi/4$-DQPSK, the autocorrelation

$$\phi_{b,m}(z,\tau') = \frac{1}{2}\mathrm{E}\left[b^*(z,\mathbf{x}_0)b(\tau',\mathbf{x}_m)\right], \tag{4.230}$$

is first computed, where $b(t,\mathbf{x}_n)$ is defined in (4.70). For $m>0$,

$$\begin{aligned}\phi_{b,m}(z,\tau') &= \frac{1}{2}\mathrm{E}\left[h_a(z)\exp\left\{j\frac{\pi}{4}\sum_{k=1}^{m}x_k\right\}h_a(\tau')\right]\\ &= \frac{1}{2}\mathrm{E}\left[\exp\left\{j\frac{\pi}{4}\sum_{k=1}^{m}x_k\right\}\right]h_a(z)h_a(\tau')\\ &= 0.\end{aligned} \tag{4.231}$$

For $m=0$,

$$\phi_{b,0}(z,\tau') = \frac{1}{2}\mathrm{E}\left[h_a(z)h_a(\tau')\right] = \frac{1}{2}h_a(z)h_a(\tau'). \tag{4.232}$$

Taking the double Fourier transform gives

$$\begin{aligned}S_{b,0}(f) &= \int_{-\infty}^{\infty}\int_{-\infty}^{\infty}\phi_{b,0}(z,\tau')\mathrm{e}^{-j2\pi f(\tau'-z)}\mathrm{d}z\mathrm{d}\tau'\\ &= \frac{1}{2}\left|H_a(f)\right|^2.\end{aligned} \tag{4.233}$$

Finally, the psd is

$$S_{\widetilde{ss}}(f) = \frac{A^2}{2T}\left|H_a(f)\right|^2. \tag{4.234}$$

Just like OQPSK, $\pi/4$-DQPSK has the same psd as QPSK. However, as discussed earlier, $\pi/4$-DQPSK has a lower peak-to-average power ratio than QPSK.

4.9.6 Psd of OFDM

Recall that the OFDM waveform with guard interval is given by (4.88) and (4.89). The data symbols $x_{n,k}, k=0,\ldots,N-1$ that modulate the N subcarriers are assumed to have zero mean, variance $\sigma_x^2 = \frac{1}{2}\mathrm{E}[|x_{n,k}|^2]$, and they are mutually uncorrelated. In this case, the psd of the OFDM waveform is

$$S_{\widetilde{ss}}(f) = \frac{A^2}{T_g}S_{b,0}(f), \tag{4.235}$$

where

$$S_{b,0}(f) = \frac{1}{2}\mathrm{E}\left[\left|B(f,\mathbf{x}_0)\right|^2\right], \tag{4.236}$$

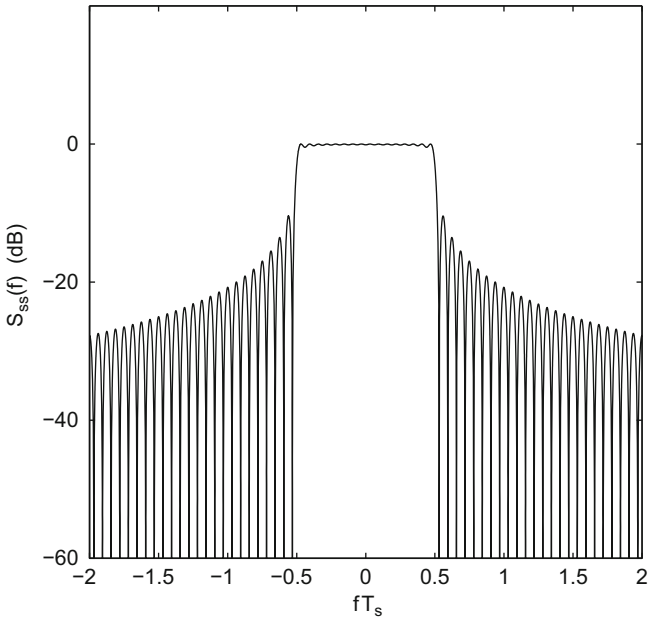

Fig. 4.27 Psd of OFDM with $N = 16, \alpha_g = 0$

and

$$B(f, \mathbf{x}_0) = \sum_{k=0}^{N-1} x_{0,k} T \text{sinc}(fT - k) + \sum_{k=0}^{N-1} x_{0,k} \alpha_g T \text{sinc}(\alpha_g (fT - k)) e^{j2\pi fT}. \tag{4.237}$$

Substituting (4.237) into (4.236) along with $T = NT_s$ and $T_g = (1 + \alpha_g)T$ yields the result

$$\begin{aligned} S_{\overline{ss}}(f) = \sigma_x^2 A^2 T \Bigg(& \frac{1}{1 + \alpha_g} \sum_{k=0}^{N-1} \text{sinc}^2(NfT_s - k) \\ & + \frac{\alpha_g^2}{1 + \alpha_g} \sum_{k=0}^{N-1} \text{sinc}^2(\alpha_g (NfT_s - k)) \\ & + \frac{2\alpha_g}{1 + \alpha_g} \cos(2\pi NfT_s) \sum_{k=0}^{N-1} \text{sinc}(NfT_s - k) \text{sinc}(\alpha_g (NfT_s - k)) \Bigg). \end{aligned} \tag{4.238}$$

The OFDM psd is plotted in Figs. 4.27 and 4.28 for $N = 16, \alpha_g = 0$ and $N = 16, \alpha_g = 0.25$, respectively. Observe the effect of the OFDM guard interval on the psd. Likewise, Figs. 4.29 and 4.30 plot the psd for $N = 1024, \alpha_g = 0$ and $N = 1024, \alpha_g = 0.25$, respectively, where the effect of increasing the block size N can be observed. When plotting the above figures, the index k was replaced with $k - (N - 1)/2$ in the argument of the sinc functions in (4.239) to center the spectrum around 0 Hz. Note that the psd is plotted against the normalized frequency fT_s. To avoid a reduction in data rate, the modulated symbol period with a cyclic extension is $T_s^g = T_s/(1 + \alpha_g)$. Hence, the Nyquist frequency in this case is $1/2T_s^g = (1 + \alpha_g)/2T_s$, which shows a bandwidth expansion due to the guard interval.

4.9.6.1 Psd of OFDM with IDFT Baseband Modulator

It is interesting to examine the OFDM power spectrum when the OFDM complex envelope is generated by using an IDFT baseband modulator followed by a balanced pair DACs as shown in Fig. 4.14. The output of the IDFT baseband modulator is given by $\{\mathbf{X}^g\} = \{X_{n,m}^g\}$, where m is the block index and

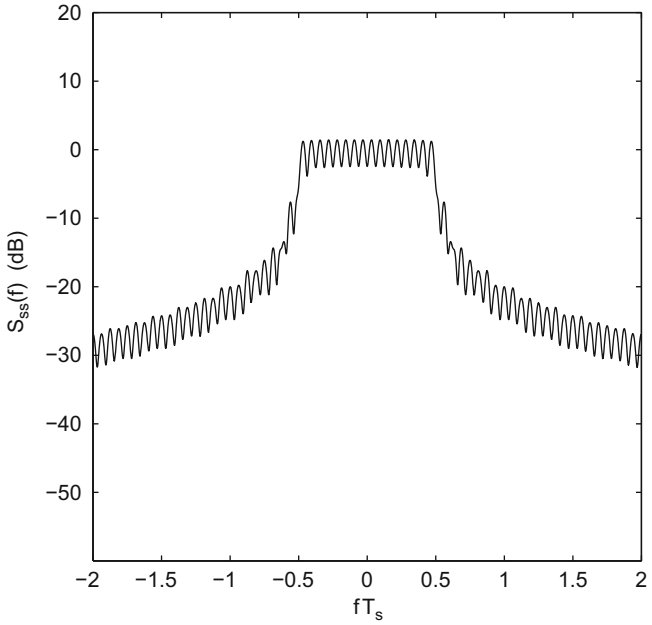

Fig. 4.28 Psd of OFDM with $N = 16, \alpha_g = 0.25$

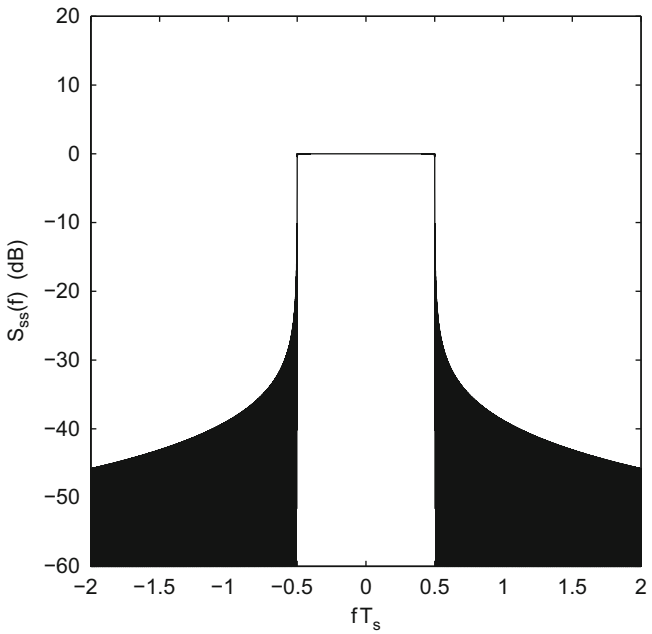

Fig. 4.29 Psd of OFDM with $N = 1024, \alpha_g = 0$

$$X_{n,m}^{g} = X_{n,(m)_N} \tag{4.239}$$

$$= A \sum_{k=0}^{N-1} x_{n,k} \mathrm{e}^{\frac{j2\pi km}{N}}, \quad m = 0,\ 1,\ \ldots,\ N + G - 1. \tag{4.240}$$

The power spectrum of the sequence $\{\mathbf{X}^g\}$ can be calculated by first determining the discrete-time autocorrelation function of the time domain sequence $\{\mathbf{X}^g\}$ and then taking a discrete-time Fourier transform of the discrete-time autocorrelation function. The psd of the OFDM complex envelope with ideal DACs can be obtained by applying the resulting power spectrum to an ideal low-pass filter with a cutoff frequency of $1/(2T_s^g)$ Hz.

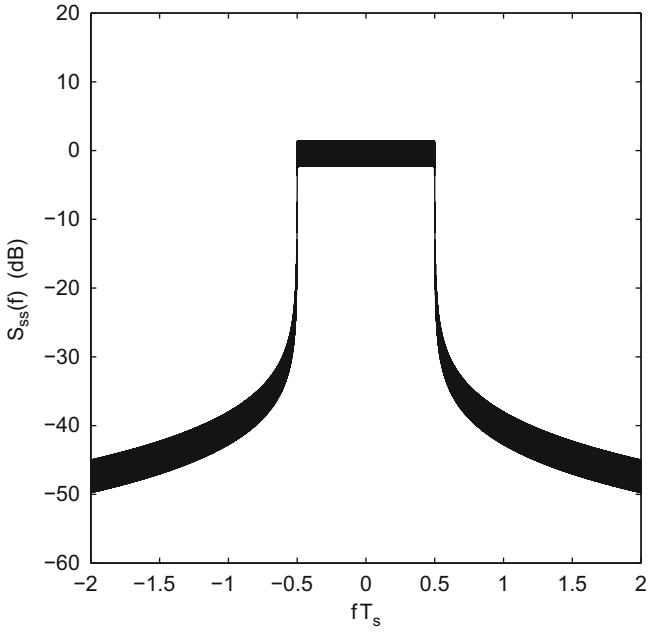

Fig. 4.30 Psd of OFDM with $N = 1024, \alpha_g = 0.25$

The time domain sequence $\{\mathbf{X}^g\}$ is a periodic wide-sense stationary sequence having the discrete-time autocorrelation function

$$\phi_{X^gX^g}(m,\ell) = \frac{1}{2}\mathrm{E}[(X^g_{n,m})^* X^g_{n,m+\ell}] \tag{4.241}$$

$$= A^2 \sum_{k=0}^{N-1}\sum_{i=0}^{N-1} \frac{1}{2}\mathrm{E}[x^*_{n,k}x_{n,i}]\mathrm{e}^{j\frac{2\pi}{N}(-km+im+i\ell)}\ , \tag{4.242}$$

$$\text{for } m = 0,\ldots,N+G-1. \tag{4.243}$$

The data symbols, $x_{n,k}$, are assumed to be mutually uncorrelated with zero mean and variance $\sigma_x^2 = \frac{1}{2}\mathrm{E}[|x_{n,k}|^2]$. Using the fact, that $X^g_{n,m} = X_{n,(m)_N}$, gives

$$\phi_{X^gX^g}(m,\ell) = \begin{cases} A\sigma_x^2 & m = 0,\ldots,G-1,\ \ell = 0,\ N \\ & m = G,\ldots,N-1,\ \ell = 0 \\ & m = N,\ldots,N+G-1,\ \ell = 0,\ -N \\ 0 & \text{otherwise} \end{cases}. \tag{4.244}$$

Averaging over all time indices m gives the time-averaged discrete-time autocorrelation function

$$\phi_{X^gX^g}(\ell) = \begin{cases} A\sigma_x^2 & \ell = 0 \\ \frac{G}{N+G}A\sigma_x^2 & \ell = -N,\ N \\ 0 & \text{otherwise} \end{cases}. \tag{4.245}$$

Taking the discrete-time Fourier transform of the discrete-time autocorrelation function in (4.245) gives

$$\begin{aligned} S_{X^gX^g}(f) &= \sum_{\ell=-\infty}^{\infty} \phi_{X^gX^g}(\ell)\mathrm{e}^{-j2\pi f\ell T_s^g} \\ &= A\sigma_x^2\left(1 + \frac{G}{N+G}\mathrm{e}^{j2\pi fNT_s^g} + \frac{G}{N+G}\mathrm{e}^{-j2\pi fNT_s^g}\right) \\ &= A\sigma_x^2\left(1 + \frac{2G}{N+G}\cos(2\pi fNT_s^g)\right). \end{aligned} \tag{4.246}$$

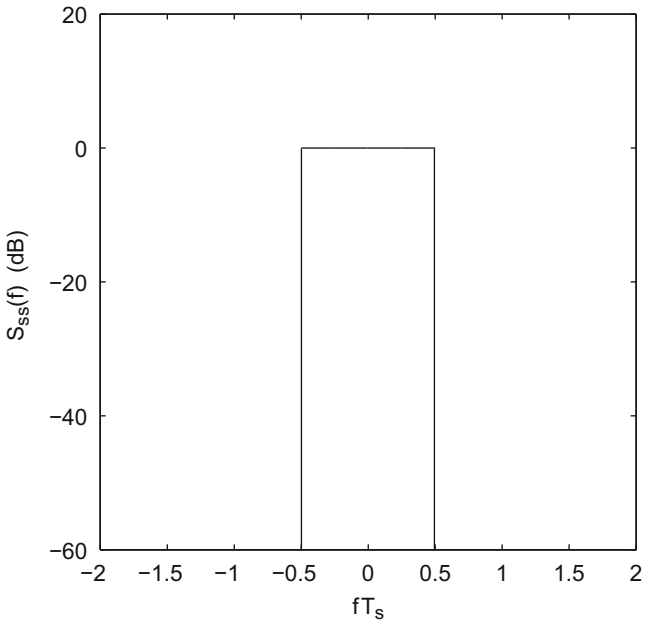

Fig. 4.31 Psd of IDFT-based OFDM with $N = 16, G = 0$. Note in this case that $T_s^g = T_s$

Finally, it is assumed here that the sequence $\{\mathbf{X}^g\} = \{X_{n,m}^g\}$ is passed through a pair of ideal DACs. The ideal DAC is a low-pass filter with cutoff frequency $1/(2T_s^g)$. Therefore, the OFDM complex envelope with an ideal DAC has the psd

$$S_{\tilde{s}\tilde{s}}(f) = A\sigma_x^2 \left(1 + \frac{2G}{N+G}\cos(2\pi f N T_s^g)\right) \text{rect}\left(fT_s^g\right). \tag{4.247}$$

The OFDM psd is plotted in Fig. 4.31 for $G = 0$, where it has the ideal rectangular form $\text{rect}(fT_s)$ for any block size N. Figures 4.32 and 4.33 plot the psd for $N = 16,\ G = 4$, and $N = 1024,\ G = 256$, respectively, where the effect of the cyclic guard interval and an increase in the block size N can be seen.

Finally, the psd plotted in Figs. 4.31, 4.32, and 4.33 assumes an ideal DAC. A practical DAC with a finite-length reconstruction filter will introduce side lobes into the spectrum. Side lobes are inherently present in the continuous-time OFDM waveform in (4.88) and (4.89) due to the use of rectangular amplitude pulse shaping on the subcarriers. However, they are introduced into the IDFT implementation by the non-ideal (practical) DAC.

4.9.7 Psd of Full Response CPM

Recall that the generalized shaping function for a CPM waveform is given by (4.103). To compute the psd, first define the auxiliary function

$$r(t, x_n) \triangleq \mathrm{e}^{j2\pi h x_n \beta(t)} u_T(t), \tag{4.248}$$

such that

$$b(t, \mathbf{x}_n) = \mathrm{e}^{j\pi h \sum_{k=0}^{n-1} x_k} r(t, x_n) \tag{4.249}$$

and calculate the mean and autocorrelation function of $r(t, x_n)$. If M-ary signaling is used with the values of x_k defined by

$$x_k \in \{2m - 1 - M : m = 1,\ 2,\ \cdots,\ M\} \tag{4.250}$$

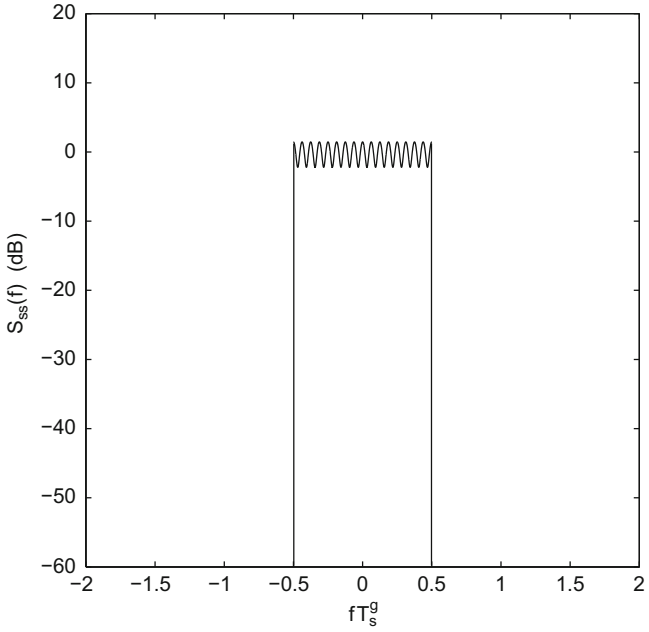

Fig. 4.32 Psd of IDFT-based OFDM with $N = 16, G = 4$

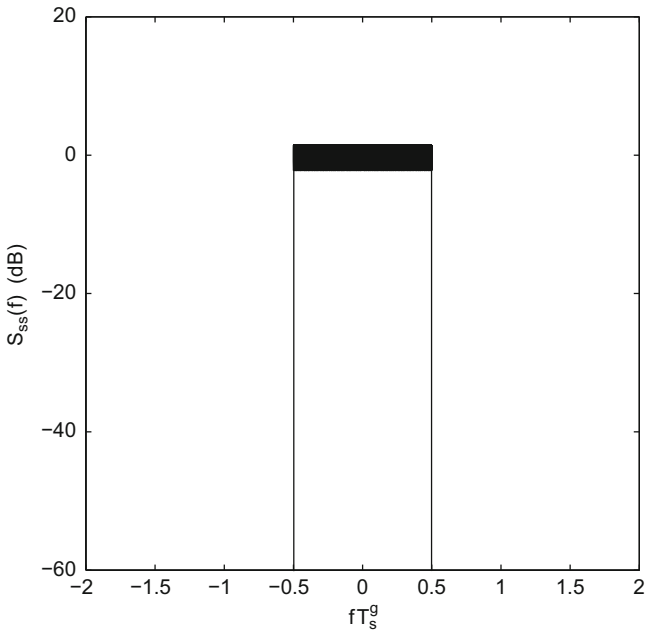

Fig. 4.33 Psd of IDFT-based OFDM with $N = 1024, G = 256$

then

$$\begin{aligned} m_r(t) &\triangleq \mathrm{E}[r(t, x_n)] \\ &= \frac{1}{M} \sum_{i=1}^{M} \mathrm{e}^{j2\pi h(2i-1-M)\beta(t)} u_T(t) \\ &= D_M(2\pi h \beta(t)) u_T(t). \end{aligned} \tag{4.251}$$

where

$$D_M(x) \triangleq \frac{\sin(Mx)}{M \sin x} \tag{4.252}$$

is the Dirichlet function. Also

$$\phi_{r,m}(t,t') = \frac{1}{2}\mathrm{E}\left[r^*(t,x_0)r(t',x_m)\right]. \tag{4.253}$$

Evaluating the above expression for $m = 0$ gives the following result which will be used later

$$\begin{aligned}
\phi_{r,0}(t,t') &= \frac{1}{2}\mathrm{E}\left[r^*(t,x_0)r(t',x_0)\right] \\
&= \frac{1}{2}\mathrm{E}\left[\mathrm{e}^{-j2\pi h x_0 \beta(t)}\mathrm{e}^{j2\pi h x_0 \beta(t')}\right] u_T(t)u_T(t') \\
&= \frac{1}{2}\mathrm{E}\left[\mathrm{e}^{-j2\pi h x_0 (\beta(t)-\beta(t'))}\right] u_T(t)u_T(t') \\
&= \frac{1}{2}D_M\Big(2\pi h(\beta(t)-\beta(t'))\Big) u_T(t)u_T(t').
\end{aligned} \tag{4.254}$$

To evaluate the psd, it is also necessary to compute the autocorrelation of $b(t,\mathbf{x}_m)$. This can be done as follows:

$$\begin{aligned}
\phi_{b,m}(t,t') &= \frac{1}{2}\mathrm{E}\left[b^*(t,\mathbf{x}_0)b(t',\mathbf{x}_m)\right] \\
&= \frac{1}{2}\mathrm{E}\left[\mathrm{e}^{-j\pi h\sum_{k=0}^{m-1} x_k}\; r^*(t,x_0)r(t',x_m)\right] \\
&= \frac{1}{2}\mathrm{E}\left[\left(\prod_{k=0}^{m-1} r^*(T,x_k)\right) r^*(t,x_0)r(t',x_m)\right] \\
&= \frac{1}{2}\mathrm{E}\left[\left(\prod_{k=1}^{m-1} r^*(T,x_k)\right) r^*(t,x_0)r^*(T,x_0)r(t',x_m)\right].
\end{aligned} \tag{4.255}$$

Now suppose that the data sequence is uncorrelated. Then for $m > 0$

$$\begin{aligned}
\phi_{b,m}(t,t') &= \frac{1}{2}\left[m_r(T)\right]^{m-1} m_r(t)\phi_{r,0}(T,t') \\
&= \frac{1}{2}\left[D_M(\pi h)\right]^{m-1} D_M(2\pi h\beta(t))D_M\Big(2\pi h(\beta(T)-\beta(t'))\Big) u_T(t)u_T(t'),
\end{aligned} \tag{4.256}$$

where (4.254) has been used. Likewise, for $m = 0$

$$\begin{aligned}
\phi_{b,0}(t,t') &= \frac{1}{2}\mathrm{E}\left[b^*(t,\mathbf{x}_0)b(t',\mathbf{x}_0)\right] \\
&= \frac{1}{2}\mathrm{E}\left[\mathrm{e}^{-j2\pi h x_0(\beta(t)-\beta(t'))}\right] u_T(t)u_T(t') \\
&= \frac{1}{2}D_M\Big(2\pi h(\beta(t)-\beta(t'))\Big) u_T(t)u_T(t') \\
&= \phi_{r,0}(t,t').
\end{aligned} \tag{4.257}$$

Finally, the psd is obtained by using (4.254) and (4.257) along with (4.196) and (4.208).

4.9.7.1 Alternative Method

There is an alternate method for obtaining the full response CPM psd that provides more insight. Using (4.196) along with the property $S_{b,-m}(f) = S^*_{b,m}(f)$ yields

$$S_{\widetilde{ss}}(f) = \frac{A^2}{T}\left(S_{b,0}(f) + 2\mathrm{Re}\left\{\sum_{m=1}^{\infty} S_{b,m}(f)\mathrm{e}^{-j2\pi fmT}\right\}\right). \tag{4.258}$$

Taking the double Fourier transform of (4.257) and (4.256) gives

$$S_{b,m}(f) = \begin{cases} S_{r,0}(f) & m = 0 \\ m_r^{m-1}(T)M_r(f)\hat{M}_r^*(f) & m > 0 \end{cases}, \tag{4.259}$$

where

$$\begin{aligned} m_r^{m-1}(T) &\triangleq [D_M(\pi h)]^{m-1} \\ M_r(f) &\triangleq \mathscr{F}[m_r(t)] = \mathscr{F}[D_M(2\pi h\beta(t)u_T(t)] \\ \hat{M}_r^*(f) &\triangleq \frac{1}{2}\mathrm{E}\left[r^*(T,x_0)R(f,x_0)\right] = \frac{1}{2}\mathrm{E}\left[\mathrm{e}^{-j\pi hx_0}R(f,x_0)\right] \end{aligned}$$

$\mathscr{F}[\,\cdot\,]$ denotes the Fourier transform and

$$R(f,x_0) = \mathscr{F}[r(t,x_0)] = \mathscr{F}\left[\mathrm{e}^{j2\pi hx_0\beta(t)}u_T(t)\right]. \tag{4.260}$$

Then,

$$\begin{aligned} S_{\widetilde{ss}}(f) &= \frac{A^2}{T}\left(S_{r,0}(f) + 2\mathrm{Re}\left\{M_r(f)\hat{M}_r^*(f)\sum_{m=1}^{\infty} m_r^{m-1}(T)\mathrm{e}^{-j2\pi fmT}\right\}\right) \\ &= \frac{A^2}{T}\left(S_{r,0}(f) + 2\mathrm{Re}\left\{M_r(f)\hat{M}_r^*(f)\sum_{n=0}^{\infty}\left[m_r(T)\mathrm{e}^{-j2\pi fT}\right]^n \mathrm{e}^{-j2\pi fT}\right\}\right). \end{aligned} \tag{4.261}$$

Observe that

$$\left|m_r(T)\mathrm{e}^{-j2\pi fT}\right| = |m_r(T)| = |D_M(\pi h)| \le 1. \tag{4.262}$$

The implication of equation (4.262) is that two separate cases must be considered when evaluating the psd.

Case 1: $|m_r(T)| < 1$

In this case the sum in (4.261) converges such that

$$S_{\widetilde{ss}}(f) = \frac{A^2}{T}\left(S_{r,0}(f) + 2\mathrm{Re}\left\{\frac{M_r(f)\hat{M}_r^*(f)}{\mathrm{e}^{j2\pi fT} - m_r(T)}\right\}\right). \tag{4.263}$$

and the psd has no discrete components.

Case 2: $|m_r(T)| = 1$

This case is possible only if

$$|m_r(T)| = \left|\mathrm{E}\left[\mathrm{e}^{j\pi h x_k}\right]\right| = 1. \tag{4.264}$$

For this condition to be true,

$$\mathrm{e}^{j\pi h x_k} = \mathrm{e}^{jc}\ , \quad \forall\ k, \tag{4.265}$$

where c is the same constant for all k. Since this must be true for $x_k = 1$, it follows that $c = \pi h$ and

$$x_k \pi h = \pi h \qquad \mod (2\pi)\ \ \forall k. \tag{4.266}$$

This means that h must be an integer, and when h is an integer

$$m_r(T) = \mathrm{E}[r(T, x_0)] = \mathrm{e}^{j\pi h} \tag{4.267}$$

and

$$\hat{M}_r^*(f) = M_r^*(f)\mathrm{e}^{j\pi h}. \tag{4.268}$$

Hence, the psd is

$$\begin{aligned}
S_{\overline{ss}}(f) &= \frac{A^2}{T}\left(S_{r,0}(f) + |M_r(f)|^2 2\mathrm{Re}\left\{\sum_{m=1}^{\infty}\mathrm{e}^{j2\pi\left(f-\frac{h}{2T}\right)mT}\right\}\right) \\
&= \frac{A^2}{T}\left(S_{r,0}(f) - |M_r(f)|^2 + |M_r(f)|^2\sum_{m=-\infty}^{\infty}\mathrm{e}^{-j2\pi\left(f-\frac{h}{2T}\right)mT}\right) \\
&= \frac{A^2}{T}\left(S_{r,0}(f) - |M_r(f)|^2 + \frac{1}{T}|M_r(f)|^2\sum_{n=-\infty}^{\infty}\delta\left(f-\frac{h}{2T}-\frac{n}{T}\right)\right) \\
&= \frac{A^2}{T}\left(S_{r,0}(f) - |M_r(f)|^2\right) + \left(\frac{A}{T}\right)^2\sum_{n=-\infty}^{\infty}\left|M_r\left(\frac{h}{2T}+\frac{n}{T}\right)\right|^2\delta\left(f-\frac{h}{2T}-\frac{n}{T}\right).
\end{aligned} \tag{4.269}$$

Clearly, the second term in the above expression is a discrete spectral component. Hence, integer values of h lead to discrete spectral components. Since discrete spectral components are generally undesirable, integer values of h are typically not used.

4.9.7.2 Psd of CPFSK

With CPFSK, the phase shaping pulse is given by (4.107). Hence,

$$\begin{aligned}
R(f, x_0) &= \int_0^T \mathrm{e}^{j\pi\frac{hx_0 t}{T}}\cdot\mathrm{e}^{-j2\pi ft}\mathrm{d}t \\
&= T\mathrm{e}^{-j\pi(fT-hx_0/2)}\mathrm{sinc}\left((fT - hx_0/2)\right),
\end{aligned} \tag{4.270}$$

where $x_0 \in \{\pm 1, \pm 3, \ldots, \pm(M-1)\}$. It follows that

$$\begin{aligned} M_r(f) &= \mathrm{E}\left[R(f, x_0)\right] \\ &= \frac{T}{M} \sum_{m=1}^{M} \mathrm{e}^{-j\pi(fT - hx_m/2)} \mathrm{sinc}\left((fT - hx_m/2)\right) \end{aligned} \tag{4.271}$$

$$\begin{aligned} S_{r,0}(f) &= \frac{1}{2}\mathrm{E}\left[|R(f, x_0)|^2\right] \\ &= \frac{T^2}{2M} \sum_{m=1}^{M} \mathrm{sinc}^2\left((fT - hx_m/2)\right) \end{aligned} \tag{4.272}$$

$$\hat{M}_r^*(f) = \frac{T}{2M} \sum_{m=1}^{M} \mathrm{e}^{j\pi(fT + x_m h/2)} \mathrm{sinc}\left(fT - x_m h/2\right). \tag{4.273}$$

These expressions are used in (4.263) to obtain the psd.

For binary $M = 2$ CPFSK,

$$S_{r,0}(f) = \frac{T^2}{4}\left(\mathrm{sinc}^2(fT - h/2) + \mathrm{sinc}^2(fT + h/2)\right) \tag{4.274}$$

$$M_r(f) = \frac{T}{2}\left(\mathrm{e}^{-j\pi(fT+h/2)}\mathrm{sinc}(fT + h/2) + \mathrm{e}^{-j\pi(fT-h/2)}\mathrm{sinc}(fT - h/2)\right) \tag{4.275}$$

$$\hat{M}_r^*(f) = \frac{T}{4}\left(\mathrm{e}^{j\pi(fT-h/2)}\mathrm{sinc}(fT + h/2) + \mathrm{e}^{j\pi(fT+h/2)}\mathrm{sinc}(fT - h/2)\right) \tag{4.276}$$

$$m_r(T) = D_2(h\pi). \tag{4.277}$$

When h is an integer, the psd has both continuous and discrete components

$$S_{\tilde{s}\tilde{s}}(f) = S^c_{\tilde{s}\tilde{s}}(f) + S^d_{\tilde{s}\tilde{s}}(f), \tag{4.278}$$

where

$$\begin{aligned} S^c_{\tilde{s}\tilde{s}}(f) &= \frac{A^2 T}{2}\mathrm{sinc}(fT + h/2)\mathrm{sinc}(fT - h/2) \\ S^d_{\tilde{s}\tilde{s}}(f) &= \frac{A^2}{T}\sum_{n=-\infty}^{\infty} \delta\left(f - \frac{h}{2T} - \frac{n}{T}\right)\left(\mathrm{sinc}^2(n + h) + \mathrm{sinc}^2(n) - 2\mathrm{sinc}(n + h)\mathrm{sinc}(n)\right) \end{aligned} \tag{4.279}$$

which clearly exhibits line components at frequencies $\left(\frac{h}{2T} + \frac{n}{T}\right)$. Further simplification may be possible for special cases, but otherwise the psd has an intractable form. Figures 4.34 and 4.35 plot the psd against the normalized frequency fT. MSK corresponds to the case $h = 0.5$. Observe that the CPFSK power spectrum becomes more compact for smaller h, while the converse is true for larger h. Figure 4.35 illustrates the appearance of discrete components at frequencies $\left(\frac{1}{2} + n\right)\frac{1}{T}$, n an integer, as $h \to 1$.

4.9.7.3 Psd of MSK

The psd of CPFSK is complicated for all but a few cases. By using Laurent's decomposition [193], MSK was shown equivalent to OQASK with half-sinusoid amplitude pulse shaping. From (4.112), the MSK baseband signal has the quadrature form

$$\tilde{s}(t) = A\sum_{n} b(t - 2nT, \mathbf{x}_n), \tag{4.280}$$

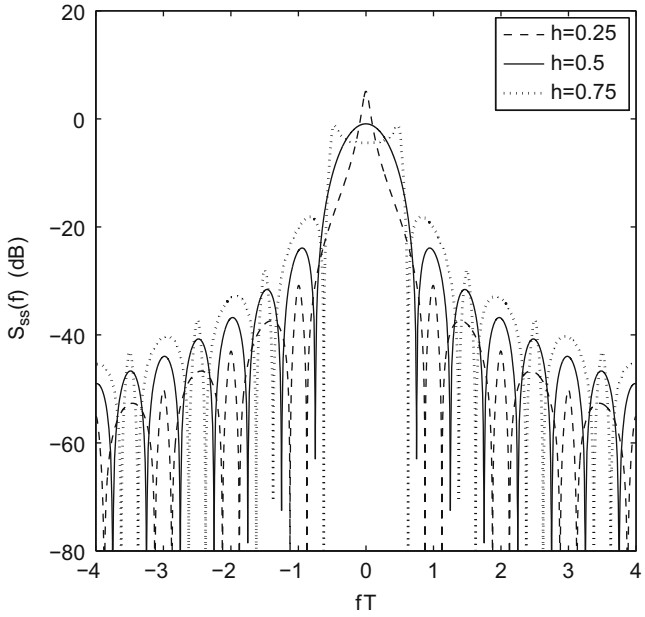

Fig. 4.34 Psd of binary CPFSK with various modulation indices. MSK corresponds to $h = 1/2$

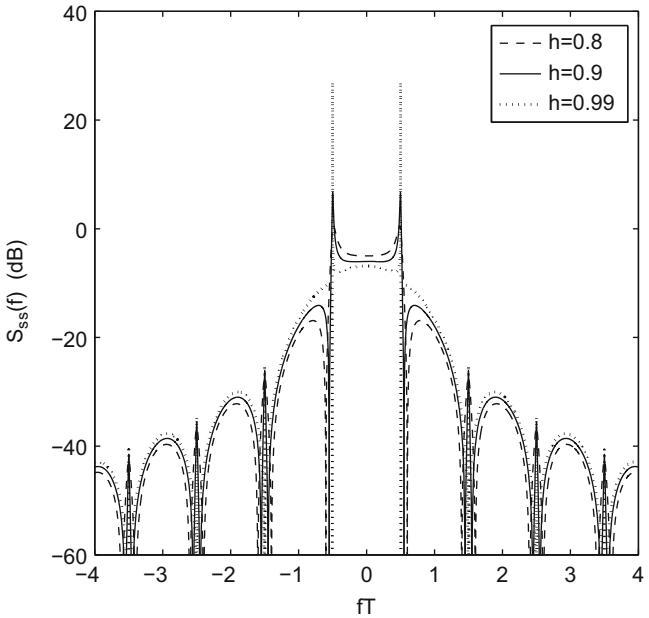

Fig. 4.35 Psd of binary CPFSK as the modulation index $h \to 1$

where

$$b(t, \mathbf{x}_n) = \hat{x}_{2n+1} h_a(t - T) + j\hat{x}_{2n} h_a(t) \tag{4.281}$$

$$h_a(t) = \sin\left(\frac{\pi t}{2T}\right) u_{2T}(t), \tag{4.282}$$

$\mathbf{x}_n = (\hat{x}_{2n+1}, \hat{x}_{2n})$ is a sequence of odd–even pairs assuming values from the set $\{\pm 1, \pm 1\}$, and T is the bit period. The Fourier transform of (4.281) is

$$B(f, \mathbf{x}_n) = \left(\hat{x}_{2n+1} \mathrm{e}^{-j2\pi fT} + j\hat{x}_{2n}\right) H_a(f). \tag{4.283}$$

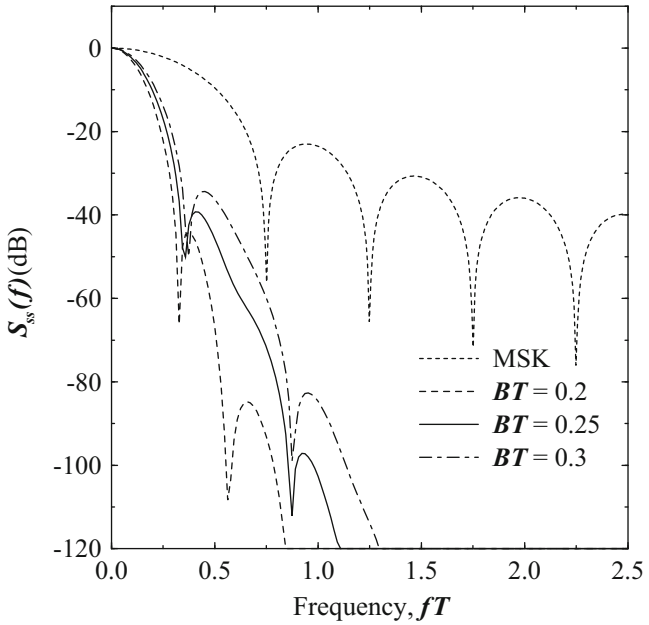

Fig. 4.36 Psd of GMSK with various normalized filter bandwidths BT

Since the data sequence is zero mean and uncorrelated, the MSK psd is

$$\begin{aligned} S_{b,0}(f) &= \frac{1}{2}\mathrm{E}\left[|B(f,\mathbf{x}_0)|^2\right] \\ &= \frac{1}{2}\mathrm{E}\left[\hat{x}_1^2 + \hat{x}_0^2\right]|H_a(f)|^2 \\ &= |H_a(f)|^2. \end{aligned} \tag{4.284}$$

The Fourier transform of the half-sinusoid pulse in (4.282) is

$$H_a(f) = \frac{2T}{\pi(1-(4fT)^2)}\left(1+\mathrm{e}^{-j4\pi fT}\right). \tag{4.285}$$

Hence, the power spectrum becomes

$$S_{\widetilde{ss}}(f) = \frac{A^2}{T}|H_a(f)|^2 = \frac{16A^2T}{\pi^2}\left(\frac{\cos^2(2\pi fT)}{1-(4fT)^2}\right)^2. \tag{4.286}$$

The psd of MSK is plotted in Fig. 4.34.

4.9.8 Psd of GMSK and TFM

GSMK and TFM are special cases of partial response CPM. In general, the psd of partial response CPM is difficult to obtain except for a rectangular shaping function. One solution has been suggested by Garrison [135], where the modulating pulses are approximated by using a large number of rectangular sub-pulses with properly chosen amplitudes.

Figure 4.36 plots the psd of GMSK with various normalized filter bandwidths BT. Note that a smaller BT results in a more compact psd. Likewise, Fig. 4.37 plots the psd of TFM and GMSK with $BT = 0.25$. Observe that the psd of TFM compares well with that of GMSK. This is not surprising since their corresponding frequency shaping pulses are quite similar as seen from Figs. 4.21 and 4.25.

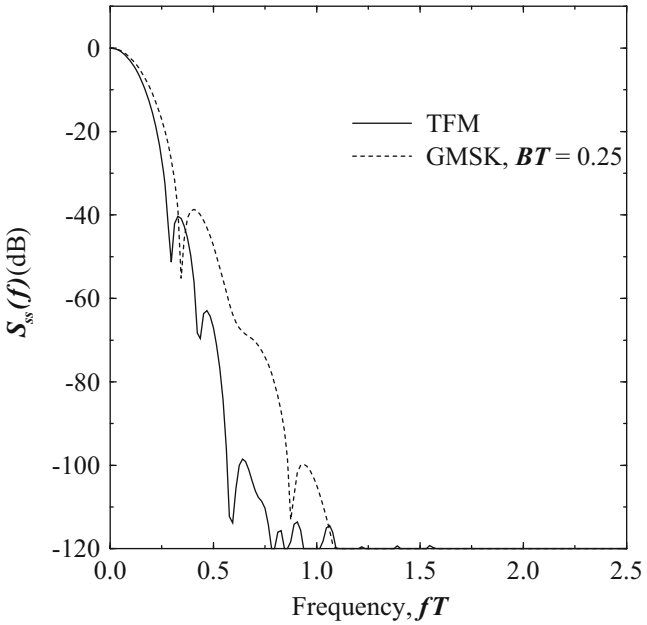

Fig. 4.37 Psd of TFM and GMSK with $BT = 0.25$

Finally, it is interesting to compare the spectral characteristics of GMSK and $\pi/4$-DQPSK. To make a fair comparison, it must be remembered that GMSK transmits 1 bit/baud while $\pi/4$-DQPSK transmits 2 bits/baud. If $\pi/4$-DQPSK uses root-raised cosine pulse shaping, then the spectral occupancy normalized to a bit duration is obtained by dividing the elements on the horizontal axis of Fig. 4.26 by a factor of 2. For example, at $f = 1/(2T_b)$ (corresponding to $fT = 1.0$) the side lobes are about 44 dB down from the main lobe ($f = 0$) when $\tau = 6T$. From Fig. 4.36, with $f = 1/(2T)$, almost the same side lobe roll-off is obtained. However, for larger values of f, the GMSK pulse side lobes are seen to decay faster in frequency than those of $\pi/4$-DQPSK.

Problems

4.1. Assume that a received signal is given by

$$\tilde{y}(t) = A \sum_{n=-\infty}^{\infty} x_n p(t - nT),$$

where $x_k = \pm 1$, and $p(t)$ is the ideal Nyquist pulse

$$p(t) = \text{sinc}(t/T)$$
$$P(f) = T\text{rect}(fT).$$

Due to a slight timing error, the received signal is sampled with a timing offset t_o, resulting in the sample sequence $\{\tilde{y}_k\}$ shown in (4.46). Show that

$$\tilde{y}_k = Aa_k \text{sinc}(t_o/T) + A\frac{\sin(\pi t_o/T)}{\pi} \sum_{n \neq k} \frac{a_n(-1)^n}{t_o/T - n}.$$

4.2. Show that 16-QAM can be represented as a superposition of two four-phase constant envelope signals where each component is amplified separately before summing, i.e.,

$$s(t) = G\Big(A_n \cos(2\pi f_c t) + B_n \sin(2\pi f_c t)\Big) + \Big(C_n \cos(2\pi f_c t) + D_n \sin(2\pi f_c t)\Big),$$

where G is a gain constant and $\{A_n\}$, $\{B_n\}$, $\{C_n\}$, and $\{D_n\}$ are statistically independent binary sequences with elements from the set $\{-1, +1\}$. Thus, show that the resulting signal is equivalent to

$$s(t) = I_n \cos(2\pi f_c t) + Q_n \sin(2\pi f_c t)$$

and determine I_n and Q_n in terms of A_n, B_n, C_n, and D_n.

4.3. Consider the two 8-QAM signals constellations shown in Fig. 4.8. Suppose that the distance between nearest-neighbor signal points in each constellation is equal to A.

(a) For the constellation on the left, determine the cartesian coordinates of the constellation points.
(b) For the constellation on the right, determine the radii a and b of the inner and outer circles.
(c) Find the average energy per symbol for each of the two signal constellations in terms of A assuming that each signal point is used with equal probability. Which constellation is more power efficient?

4.4. Two data streams, $\{x_{n,1}\}$ and $\{x_{n,2}\}$, are to be transmitted using *unbalanced* QPSK with rectangular amplitude pulse shaping, such that the data rate for $\{x_{n,1}\}$ is 10 kbps and that for $\{x_{n,1}\}$ is 1 Mbps.

(a) Relate the amplitudes of the waveforms, A_1 and A_2, such that both bit sequences have equal energies per bit.
(b) With A_1 and A_2 so related, find the possible phase shifts for the carrier, where the $x_{n,1}$ and $x_{n,2}$ take on all possible combinations of $+1$ and -1.

4.5. An important parameter for digital modulation schemes is the peak-to-average power ratio (PAPR), defined by

$$\text{PAPR} = \lim_{T\to\infty} \frac{\max_{0\le t\le T} |\tilde{s}(t)|^2}{T^{-1}\int_0^T |\tilde{s}(t)|^2 dt}.$$

When nonlinear power amplifiers are used it is desirable to keep the PAPR as small as possible.

(a) Plot the PAPR for $\pi/4$-DQPSK with root-raised cosine pulse shaping, as a function of the roll-off factor β.
(b) Repeat part (a) for QPSK. What conclusions can you draw?

4.6. Two new modulation schemes have been proposed called Q-O-QAM and B-O-QAM. Q-O-QAM transmits 2 bits/symbol, while B-O-QAM transmits 1 bit/symbol. The mapping of Q-O-QAM data bits (a_{2k}, a_{2k+1}) to symbols b_k is as follows: The symbols b_k are used to generate the symbols x_k which are given by

(a_{2k}, a_{2k+1})	b_k
0,0	$+3$
0,1	$+1$
1,0	-3
1,1	-1

$$x_k = b_k e^{jk\frac{\pi}{2}}.$$

For B-O-QAM the mapping of data bits a_k to symbols b_k is as follows: The symbols a_k are also used to generate the symbols

a_k	b_k
0	$+3$
1	-3

x_k which are given by

$$x_k = b_k e^{jk\frac{\pi}{2}}.$$

(a) Plot the signal space diagram for Q-O-QAM and B-O-QAM and show the allowable transitions between the signal points in the signal constellation. Why would these modulation schemes be useful for radio transmitters that use nonlinear power amplifiers.
(b) Assuming an AWGN channel and coherent detection, write down an expression for the probability of *symbol* error for Q-O-QAM and B-O-QAM in terms of the bit energy to noise ratio γ_b.

4.7. Consider two sinusoids waveforms

$$s_1(t) = A\cos(2\pi f_c t)$$
$$s_2(t) = A\cos(2\pi(f_c + \Delta_f)t).$$

(a) Determine the minimum value of Δ_f such that the inner product $(s_1, s_2) = 0$ over the interval $0 \le t \le T$. Assume that $f_c T \gg 1$.
(b) Repeat part (a) for the two sinusoids

$$s_1(t) = A\cos(2\pi f_c t + \phi_1)$$
$$s_2(t) = A\cos(2\pi(f_c + \Delta_f)t + \phi_2),$$

where ϕ_1 and ϕ_2 are arbitrary phases.

4.8. A guard interval consisting of a cyclic prefix or cyclic suffix is used in OFDM systems to mitigate the effects of channel time dispersion.

(a) Assess the cost of the cyclic prefix in terms of
  (i) bandwidth and/or data rate.
  (ii) transmitter power.
(b) Suppose a guard interval of 500 ns is used. The data rate with 64-QAM modulation is 54 Mb/s. The power penalty due to the guard interval is to be kept less than 1 dB. What is the required value of G (constrained to an integer) and minimum possible OFDM block size (constrained to 2^k for some k)?

4.9. Consider the time-domain sample sequence for the nth OFDM block

$$X_{n,m} = \sum_{k=0}^{N-1} x_{n,k} e^{j\frac{2\pi km}{N}}.$$

The data symbols $x_{n,k},\ k = 0, \ldots, N-1$, are independent and each is chosen with equal probability from a BPSK symbol alphabet, such that $x_{n,k} \in \{-1, +1\}$. The PAPR of the sample sequence for block n can be defined as follows:

$$\text{PAPR} = \frac{\max_m |X_{n,m}|^2}{N^{-1}\sum_{m=0}^{N-1} |X_{n,m}|^2}.$$

By using the triangle inequality, show that PAPR $\le N$.

4.10. Consider an OFDM time-domain sequence (without cyclic guard interval)

$$\begin{aligned} X_{n,m} &= \sum_{k=0}^{N-1} x_{n,k} e^{j\frac{2\pi km}{N}} \\ &= \sum_{k=0}^{N-1} x_{n,k}\cos\left(\frac{2\pi km}{N}\right) + j\sum_{n=0}^{N-1} x_{n,k}\sin\left(\frac{2\pi km}{N}\right), \quad m = 0,\ 1,\ \ldots,\ N-1, \end{aligned}$$

where the $x_{n,k}$ are symbols are i.i.d. symbols chosen from the binary alphabet $\{-1, +1\}$.

(a) Invoke the central limit theorem for large N and treat the $X_{n,m} = X^I_{n,m} + jX^Q_{n,m}$ as independent complex Gaussian random variables. What are the means, variances, and cross-correlation of the quadrature components $X^I_{n,m}$ and $X^Q_{n,m}$?
(b) Suppose that the $X_{n,m}$ can be treated as complex Gaussian random variables with the parameters in part (a). What is the probability density function of the peak power

$$\mathrm{P}_{\max} = |X_{\max}|^2 = \max_{0\le m\le N-1}|X_{n,m}|^2?$$

(c) What is the probability density function of the peak-to-average power ratio

$$\mathrm{PAPR} = \frac{\mathrm{P}_{\max}}{\mathrm{P}_{\mathrm{av}}}$$

in terms of the block size N?

4.11. Let $\{X_m\}_{m=0}^{N-1}$ be a finite duration time domain sequence of length N and let $\{x_k\}_{k=0}^{N-1}$ be its N-point DFT. Suppose that $\{X_m\}_{m=0}^{N-1}$ is padded with L zeroes and the $(N+L)$-point DFT is computed, denoted by $\{\hat{x}_k\}_{k=0}^{N+L-1}$.

(a) What is the relationship between x_0 and $\hat{x}_0$?
(b) If $|x_k|,\ k = 0,\ldots,N-1$ and $|\hat{x}_k|,\ k = 0,\ldots,N+L-1$ are plotted on the same graph, explain the relationships between the two graphs.

4.12. (**Computer Exercise**) Consider the time-domain sample sequence for the nth OFDM block $\{X_{n,m}\}_{m=0}^{N-1}$. The peak-to-average power ratio (PAPR) for the nth data block can be defined as follows:

$$\mathrm{PAPR}_n = \frac{\max_m |X_{n,m}|^2}{N^{-1}\sum_{m=0}^{N-1}|X_{n,m}|^2},$$

Note that the PAPR for the nth data block, PAPR_n, depends on the random data vector $\{x_{n,0}, x_{n,1}, \ldots, x_{n,N-1}\}$.

By averaging over many randomly generated data vectors, determine the mean of the PAPR and the variance of the PAPR. Do this for 16-QAM modulation with block sizes $N = 256$, 512, and 1024. Assume in all cases that no guard interval is used, i.e., $G = 0$.

4.13. (**Computer Exercise**) Consider a selective mapping scheme to reduce the PAPR of an OFDM waveform. The technique begins by generating L different random phase vectors of length N, i.e., first generate

$$\boldsymbol{\phi}_\ell = (\phi_{\ell,0}, \phi_{\ell,1}, \ldots, \phi_{\ell,N-1})\ ,\ \ \ell = 1, 2, \ldots, L,$$

where the $\phi_{\ell,i}$ are independent uniformly distributed random variables on the interval $(-\pi, \pi]$. Then for each $\boldsymbol{\phi}_\ell, \ell = 1,\ldots,L$, compute the PAPR of the OFDM sample sequence

$$X^\ell_{n,m} = \sum_{k=0}^{N-1} x_{n,k} e^{j\phi_{\ell,k}} e^{j\frac{2\pi km}{N}}\ ,\ \ m = 0, 1, \ldots, N-1,$$

and select the waveform having the smallest PAPR for transmission.

Consider $N = 256$ and 16-QAM symbols, and assume that no guard interval is used, i.e., $G = 0$. Compute the mean PAPR and the variance of the PAPR of the transmitted OFDM waveform for $L = 1, 2, 4$.

4.14. An OFDM signal with a large number of subcarriers N and no guard interval ($G = 0$) has a complex envelope that can be approximated as a zero-mean complex Gaussian random process. Assume an "ideal" OFDM signal spectrum, where the modulated power spectrum is

$$S_{\tilde{s}\tilde{s}}(f) = \begin{cases} S_0 & ,\ |f| \le 1/2T_s \\ 0 & ,\ \text{elsewhere} \end{cases}$$

where $T = NT_s$.

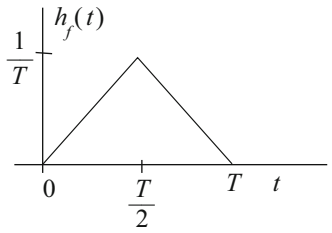

Fig. 4.38 Frequency shaping pulse for Problem 4.16

(a) Using the above Gaussian approximation, what is the distribution of the magnitude of the complex envelope, $|\tilde{s}(t)|$, at any time t.
(b) Suppose that the RF power amplifier will clip the OFDM waveform if the magnitude of the complex envelope $|\tilde{s}(t)|$ exceeds the level ΘR_{rms}, where R_{rms} is the rms envelope level $\sqrt{E[|\tilde{s}(t)|^2]}$. What is the probability that the OFDM waveform will be clipped at any time t?
(c) Suppose that a continuous stream of OFDM symbols is transmitted. How many times per second on average will the OFDM waveform be clipped?

4.15. The following problem requires you to design a length $N = 256$ phase vector

$$\boldsymbol{\phi} = (\phi_0, \phi_1, \ldots, \phi_{N-1})$$

such that the corresponding OFDM sample sequence

$$X_m = \sum_{k=0}^{N-1} e^{j\phi_k} e^{j\frac{2\pi km}{N}}, \quad m = 0, 1, \ldots, N-1,$$

has a PAPR that is no bigger than 3 dB and preferably as small as possible. Using any and all techniques at your disposal, such as analysis and/or computer search, find such a phase vector $\boldsymbol{\phi}$.

4.16. Consider a CPM signal that is generated by using a triangular frequency shaping pulse shown in Fig. 4.38.

(a) If $h = 1/2$, find the peak frequency deviation from the carrier, where frequency deviation is

$$f_{\text{dev}} = \frac{1}{2\pi}\frac{d\phi(t)}{dt}.$$

(b) Sketch the phase tree and phase trellis for the binary source symbol sequence

$$\mathbf{x} = (+1, +1, +1, -1, -1, +1, -1, -1)$$

4.17. A CPM signal is generated from a baseband signal with a half-sinusoid frequency shaping function $h_f(t)$.

(a) If $h = 1/2$, find the peak frequency deviation from the carrier frequency, where frequency deviation is

$$f_{\text{dev}} = \frac{1}{2\pi}\frac{d\phi(t)}{dt}.$$

(b) Sketch the phase tree and phase trellis if the data symbol sequence is

$$\mathbf{x} = \{+3, -1, +1, +3, -3, +1, -1\}.$$

4.18. Sketch the phase tree, the phase trellis, and phase state diagram for partial response CPM with $h = 1/2$ and

$$h_f(t) = \frac{1}{4T}u_{2T}(t).$$

4.19. Consider a partial response CPM signal

(a) Generate a frequency shaping function of duration $3T$ by convolving two rectangular shaping functions of duration T and $2T$.
(b) Define and sketch the three segments of the shaping function, $h_{f,k}(t)$, $k = 0, 1, 2$.
(c) Sketch the baseband signal if the symbol sequence is

$$\mathbf{x} = \{+1, -1, +1, -1, -1\}.$$

4.20. What are the phase states and states for the following CPM signals:

(a) Full response binary CPFSK with either $h = 2/3$ or $h = 3/4$.
(b) Partial response $L = 3$ binary CPFSK with either $h = 2/3$ or $h = 3/4$.

4.21. Equation 4.142 defines the transfer function $H(f)$ of the Gaussian low pass filter that is used to generate the GMSK waveform.

(a) Obtain the impulse response $h(t)$ and show that it satisfies the properties of a probability density function (pdf).
(b) Expanding on the interpretation of $h(t)$ as a pdf, determine the variance of the distribution. What is the significance of this interpretation?

4.22. Design a Gaussian pulse-shaping filter with $BT = 0.5$ for a symbol rate of 19.2 kbps. Write expressions for and plot (i) the impulse response and frequency response of the filter and (ii) the frequency shaping pulse $h_f(t)$. Repeat for the case of $BT = 0.2$ and $BT = 0.75$.

4.23. Consider TFM with the frequency shaping pulse

$$H_f(f) = \frac{\pi}{4h} \frac{\pi fT}{\sin(\pi fT)} \cos^2(\pi fT).$$

Suppose that this pulse is obtained by exciting a filter $\tilde{h}(t)$ with a gate function $\text{rect}(t/T)$. Find and sketch the impulse response of the filter $\tilde{h}(t)$.

4.24. Prove the identity

$$T \sum_m \mathrm{e}^{-j2\pi fmT} = \sum_n \delta\left(f - \frac{n}{T}\right).$$

4.25. Consider the case of uncorrelated data symbols.

(a) Show that if the symbols are equiprobable, then

$$\mathrm{E}\left[|B(f, x_0)|^2\right] - \left|\mathrm{E}\left[B(f, x_0)\right]\right|^2 = \frac{1}{2M^2} \sum_{i=1}^{M} \sum_{k=1}^{M} \left|B(f, x_i) - B(f, x_k)\right|^2.$$

(b) Compute the value of part (a) for $M = 2$.

4.26. Consider the complex low-pass binary modulated signal

$$\tilde{s}(t) = A \sum_n x_n h_a(t - nT),$$

where $x_n \in \{-1, +1\}$. The data sequence $\{x_n\}$ is correlated such that

$$\phi_{xx}(n) = \frac{1}{2}\mathrm{E}[x_k^* x_{k+n}] = \rho^{|n|}.$$

Compute the power density spectrum of $\tilde{s}(t)$.

4.27. Suppose that a binary data sequence $\{x_n\}$, $x_i \in \{-1, +1\}$ is correlated such that $P(x_n = x_{n+1}) = 3/4$, i.e., adjacent data bits are the same with probability 3/4 and different with probability 1/4.

(a) Compute the autocorrelation function $\phi_{xx}(m)$ for this data sequence.
(b) Compute the power spectrum $S_{xx}(f)$.

4.28. Suppose that an uncorrelated binary data sequence is transmitted by using binary PAM with a root-Gaussian amplitude shaping pulse

$$H_a(f) = \left(\tau \mathrm{e}^{-\pi(f\tau)^2}\right)^{1/2}$$

(a) What is the transmitted power density spectrum?
(b) Find the value of τ so that the power density spectrum is 20 dB below its peak value at frequency $1/T$, where T is the baud duration.
(c) What is the corresponding time domain pulse $h_a(t)$?

4.29. Consider the M-ary orthogonal FSK waveform defined by (4.71) and (4.72). Assuming equally likely messages, determine the psd of the transmitted complex envelope $S_{\tilde{s}\tilde{s}}(f)$.

4.30. Consider a system that uses a set of $M = 16$ bi-orthogonal signals that are derived from the Hadamard matrix $\mathbf{H}_8$ in (4.76). The set of 16 signals is constructed according to

$$\tilde{s}_i(t) = \begin{cases} A\sum_{k=0}^{7} h_{ik} h_c(t - kT_c)\,, & k = 1, \ldots, 8 \\ -\tilde{s}_i(t)\,, & k = 9, \ldots, 16 \end{cases}, \tag{4.287}$$

where $T = 8T_c$ is the baud period. Note that 4 bits are transmitted per baud. Assume an uncorrelated data sequence and assume that all 16 waveforms are used with equal probability.

(a) If $h_c(t) = u_{T_c}(t)$, find the psd of the transmitted complex envelope $S_{\tilde{s}\tilde{s}}(f)$.
(b) Plot the power spectrum $S_{\tilde{s}\tilde{s}}(f)$ against the normalized frequency fT_b, where $T_b = T/4$ is the bit duration.